Dirk de Bruyn Ouboter

RATIONAL DESIGN OF PURELY PEPTIDIC AMPHIPHILES FOR DRUG DELIVERY APPLICATIONS

hydrophilic

hydrophobic

50 nm

1 µm
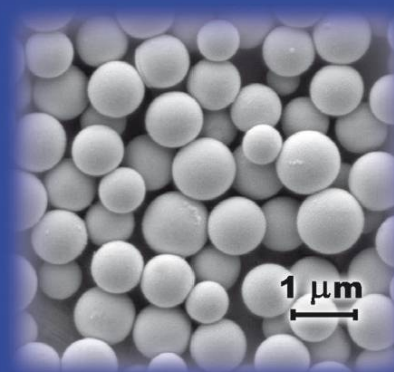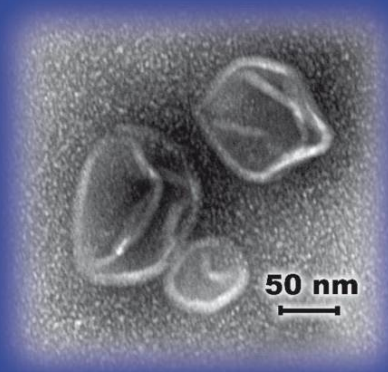
UNI BASEL

Cuvillier Verlag Göttingen
Internationaler wissenschaftlicher Fachverlag

Rational Design of Purely Peptidic Amphiphiles for Drug Delivery Applications

Inauguraldissertation

zur

Erlangung der Würde eines Doktors der Philosophie

vorgelegt der Philosophisch-Naturwissenschaftlichen Fakultät der Universität Basel

von

Dirk de Bruyn Ouboter

aus Ettingen, Schweiz

UNI
BASEL

Basel 2011

Genehmigt von der Philosophisch-Naturwissenschaftlichen Fakultät der Universität Basel

auf Antrag von

Prof. Dr. Wolfgang Meier und

Prof. Dr. Thomas Pfohl

Basel, den 26. April 2011

Prof. Dr. Martin Spiess

Dekan

Table of contents

Impact of the work

Publications:

Th. B. Schuster, D. de Bruyn Ouboter, E. Bordignon, G. Jeschke, W. Meier; *Reversible peptide particle formation using a mini amino acid sequence*; Soft Matter, **2010**, 6, 5596-5604

D. de Bruyn Ouboter, Th. B. Schuster, Ch. Dittrich, W. Meier; *Self-Assembled Peptide Microspheres*; eCells & Materials Journal, **2010**, 20, 3, 51

T. Schuster, D. de Bruyn Ouboter, W. Meier, *Vesicular Structures Using Short Amphiphilic Peptides*; eCells & Materials Journal, **2010**, 20, 3, 232

T. Schuster, D. de Bruyn Ouboter, W. Meier; *Access to Controlled Self-Assembly form Fibers to Micelles of a Lysine Rich Amphiphilic Peptide via Point Mutation*; Chimia, **2010,** 64, (7/8), 594

T. Schuster, D. de Bruyn Ouboter, C. G. Palivan, W. Meier; *From fibers to micelles using point mutated amphiphilic peptides*; Langmuir, **2011**, 10.1021/la200443p

T. Schuster, D. de Bruyn Ouboter, N. Bruns, W. Meier; *Exploiting dimerization of amphiphilic peptides to form vesicles*; Small, **2011**, 10.1002/smll.201100701

D. de Bruyn Ouboter, T. Schuster, A. Mantion, W. Meier; *Hierarchical organization of purely peptidic amphiphiles into peptide beads*; The Journal of Physical Chemistry C, **2011**, 10.1021/jp203048h

D. de Bruyn Ouboter, T. Schuster, V. Shanker, M. Heim, W. Meier; *Multicompartmentized peptide beads as biocompatible drug delivery tool*; **2011**, in preparation

T. Schuster, D. de Bruyn Ouboter, W. Meier; *Molecular thin films produced by short amphiphilic peptides*; **2011**, in preparation

Patents:

Pat. Pend. USPPA61328198 *"Self-Assembly of Short Peptides to Supramolecular Aggregates"*

European patent application EP11172558 *"Peptide Beads"*

Oral presentations:

D. de Bruyn Ouboter, Th. B. Schuster, W. Meier; *Self-Assembled Peptide Microspheres*; 3rd International NanoBio Conference, ETH Zürich, Switzerland, **2010**

D. de Bruyn Ouboter, Th. B. Schuster, V. Shanker, M. Heim, W. Meier; *Self-assembled peptide microspheres for drug delivery applications*; 4th Swiss Soft Days, Nestlé Research Center, Lausanne, Switzerland, **2011**

Poster presentations:

D. de Bruyn, Ch. Dittrich, W. Meier; *Purpose and Adaptability: Induced Self-Assembly of a Biological Peptide Motif*; SONS Polymers, Amphiphiles and Nanostructured Materials Workshop, Bristol, United Kingdom*, **2007***

Ch. Dittrich, D. de Bruyn, W. Meier; *Purpose and Adaptability: Induced Self-Assembly of a Biological Peptide Motif*; ESF-EMBO Symposium on BIOLOGICAL SURFACES AND INTERFACES, Sant Feliu de Guixols, Spain, **2007**

Th. Schuster, D. de Bruyn Ouboter, Ch. Dittrich, W. Meier; *Short Helical D, L - Peptides in Solution and on Surfaces*; Polymers in Life Science, Basel, Switzerland*, **2008***

D. de Bruyn Ouboter, Th. Schuster, Ch. Dittrich, W. Meier; *Amphiphilic Helical D,L-Peptides as Building-Block for Self-Assembled Peptide Beads*; 8th PSI Summer School on Condense Matter Research, Zuoz/Villigen, Switzerland, **2009**

Th. Schuster, D. de Bruyn Ouboter, Ch. Dittrich, W. Meier; *Controlling the Assembly of Short Helical D, L- Peptides*; Swiss Chemical Society, Workshop on Nanoscience and the NCCR Nanoscience Annual Meeting, Basel, Switzerland*, **2009***

Th. Schuster, D. de Bruyn Ouboter, Ch. Dittrich, W. Meier; *Insights in the Self-Assembly of Helical Peptides;* 40th CUSO Summer School, Villars, Switzerland*, **2009***

D. de Bruyn Ouboter, Th. Schuster, Ch. Dittrich, W. Meier; *Suitable Applications for Self-Assembled Peptide Beads;* 40th CUSO Summer School, Villars, Switzerland*, **2009***

D. de Bruyn Ouboter, Th. Schuster, Ch. Dittrich, W. Meier; *Applications for Self-Assembled Peptide Beads;* NCCR Nanoscience Annual Meeting, Basel, Switzerland, **2010**

Th. Schuster, D. de Bruyn Ouboter, W. Meier; *Vesicular Structures from Short Amphiphilic Peptides;* 3rd International NanoBio Conference, ETH Zürich, Switzerland*, **2010***

Summary of the PhD-thesis

A broad range of new properties is emerging from supramolecular aggregates. Self-assembled structures of purely peptidic amphiphiles exploit these properties to produce biocompatible, biodegradable, smart materials for drug administration. This thesis explores the design, synthesis, purification, characterization of purely peptidic amphiphiles, and the evaluation of potential applications.

The first chapter provides a general introduction to the field of self-assembly and drug delivery as compared to nature's delivery mechanisms. Further, the advantage of amino acid based molecules in producing smart materials for drug delivery applications is highlighted via biocompatibility and biodegradability considerations. Next, synthetic strategies and purification methods are discussed. Finally gramicidin A (gA) – a naturally occurring, short, hydrophobic, membrane-integrating peptide used to produce the amphiphilic peptides presented here – is introduced.

Chapter two presents an initial approach to produce self-assembled structures by purely peptidic amphiphiles. The undecamer used features a repetitive L-tryptophan and D-leucine [$_L$W-$_D$L] motif representing the hydrophobic block, and an N-terminally attached hydrophilic (lysine or acetylated lysine) section. Besides solid-phase peptide synthesis and purification, the process that self-assembles micelles and spherical peptide particles, termed "peptide beads", was characterized as a function of temperature and solvent composition by means of electron paramagnetic resonance (EPR), dynamic and static light scattering, fluorimetry and electron microscopy. An equilibrium process between single peptide molecules, micelles and peptide beads is then presented.

Chapter three examines the structure of self-assembled peptide beads of diameters between 200 to 1500 nm. The beads were analyzed by electron and atomic force microscopy (AFM), static and dynamic light-, and small angle X-ray scattering. The beads are seen to result from hierarchical organization of micellar-like subunits and confirm the concept of multicompartment micelles. An improved understanding of the beads' capacity to embed hydrophobic and hydrophilic payloads and provide perspectives for drug delivery applications emerges.

Chapter four presents a library of longer peptides, based on the full sequence of gA. The peptide design includes three parts: (a) a charged lysine part, (b) an acetylated lysine part and (c) a constant hydrophobic rod-like helix, based on gA. Stepwise replacement of free lysine (K) with acetylated lysine (X) generated the ten peptides Ac-X_8-gA and K_mX_{8-m}-gA (m ranging from 0 to 8). With the change in the primary sequence, a change in secondary structure was observed. The transition reflected a change in the self-assembled structures from fibers to micelles. This demonstrates how even small point mutations influence the supramolecular outcome and serve as an important step to understanding and controlling self-assembly.

In chapter five, the knowledge gained on gA-based peptides is applied to produce purely peptidic vesicles. The work here demonstrated that, to form such structures with short amphiphiles, additional stabilizing factors were necessary. Thus, we exploited different dimerization strategies

to form stable peptide membranes and developed a general recipe to form purely peptidic vesicles. The vesicles demonstrated pH responsiveness as well as the capacity to embed hydrophilic and hydrophobic payloads in their structure.

Chapter six presents the potential of self-assembled peptide beads in drug delivery applications. The hydrophobic and hydrophilic payload-filled peptide beads are shown to be internalized by human cells. Further, a method to increase embedding efficiency for RNA/DNA to 99% due to charge-driven complexation and embedding is presented. The internalization of the gene delivery vehicle into cells led to gene silencing through delivered siRNA and to antibiotic resistance, and siRNA production followed by gene silencing through a delivered plasmid. The delivery of co-embedded paclitaxel and doxorubicin was then probed and proven effective. The results also demonstrate that the new class of drug delivery material caused no measurable toxicity during the experiments. Therefore, the material is suggested as a biocompatible drug delivery vehicle for gene therapy and multi-drug delivery.

In chapter 7, the self-assembly capacity of the peptide is used to template the dense packing of gold nanoparticles. The C-terminally cysteinated peptide Ac-X_3-gT-C was used to coat gold nanoparticles and form gold core micelles. These micelles then aggregate to composite peptide-gold nanoparticles in which the individual gold nanoparticles remain separated from another. The dense packing of the gold nanoparticles offers opportunities for exceptional optical- and electronic properties as well as the use of composite material for a potential, triggered destruction of the peptide beads by the typical radiation absorption effect of gold nanoparticles. The latter could, in particular, be useful to control the release of embedded payloads.

The final chapter summarizes and discusses the achievements of this work. Further, it gives an overview of ongoing work and an outlook for worthwhile research from the present point of view. This includes *e.g.* the development of drug delivery applications, the use of the presented peptidic self-assembly system as template material in nanosciences, as well as the use of the material to investigate cellular uptake pathways of nano-sized objects.

1 Introduction

The first chapter provides a general introduction to the field covered by this PhD thesis. First, a view of the *nanometer-sized world* is afforded by means of a variety of structures that are obtained using the method of self-assembly. The *basic principles of self-assembly* are then explained and compared to *self-assembly mechanisms as they appear in nature*. Next, we switch to the topic of *drug-delivery* and compare the *classical drug delivery* – as is common for most medications – to *payload delivery as designed by nature*. This gives us the opportunity to combine drug delivery and self-assembly within new *concepts to design novel smart materials* for drug delivery applications, and to show their possible use. Subsequently, we will come to see that these novel materials also need to be *biocompatible* in order to engender as little harm to a patient as possible. This requirement will lead us to the *synthesis of amino acid-based amphiphiles* and I will highlight different synthetic strategies to obtain the molecular building blocks needed to produce self-assembled supramolecular structures. Finally, I will introduce *gramicidin A,* a naturally occurring, short and hydrophobic, membrane-integrating peptide that was used as a basis to produce the amphiphilic peptides that are presented in this thesis. The definition of the *scope of the thesis* closes the chapter.

1.1 Self-assembly

From our daily experiences we know that organization and construction requires considerable effort. Therefore, it would be expedient to use pre-existing building blocks that arrange autonomously to build a desired construct. Such a phenomenon, termed *self-assembly*, actually does exist, exemplified by a variety of different dimensions that range from the organization of galaxies and solar systems down to the organization of small molecules as they assemble into larger aggregates. In this fundamental principle, the organization of pre-existing parts or disordered components forms larger structures or patterns, while the process itself is reversible. Molecular self-assembly is the topic of this thesis and is – as the term implies – an assembly of molecules that leads to the formation of a variety of structures in the nanometer and micrometer scale, while being an important tool for the bottom-up construction in nanotechnology and material science.[1]

1.1.1 The variety of self-assembled structures
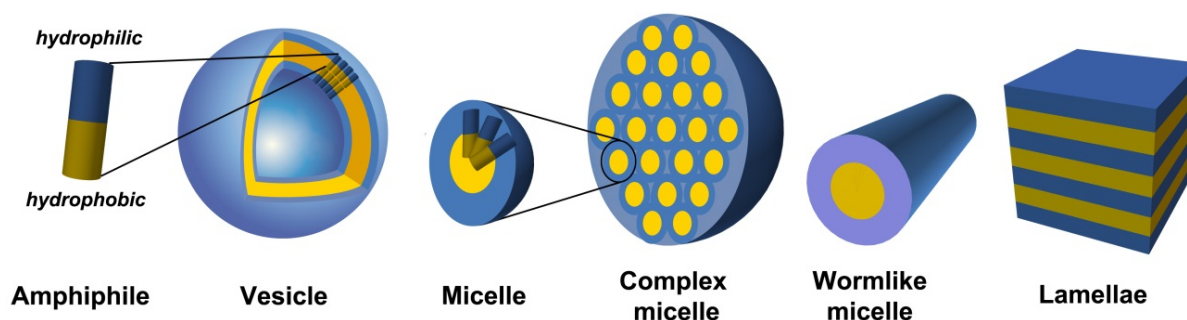
Figure 1-1: A selection of common, self-assembled morphologies and their amphiphilic subunit.

Molecular self-assembly, hereinafter referred to simply as self-assembly, produces a variety of structures of higher order, ranging from the nanometer to the micrometer scale. To obtain such structures, non-covalent intermolecular as well as intramolecular interactions take place. The simplest example is the intermolecular self-assembly of surfactant molecules into micelles in aqueous solution. However, varying the molecular properties (*e.g.* length, mass, shape) can lead to more complex supramolecular assemblies such as, for example, worm-like micelles, complex micelles, lamellae, vesicles, and tubes (see Figure 1-1).[2]

1.1.2 Self-assembly of amphiphilic molecules

Most self-assembly is enabled by using *amphiphilic* molecules. The amphiphilic (*amphi:* of both kinds; *philic:* having an affinity) properties are produced by combining at least two subunits, one possessing hydrophilic properties, the other having a hydrophobic character. The self-assembly occurring in aqueous solution is mainly driven by the low solubility of the hydrophobic part. Aggregation of the hydrophobic parts, and thus their shielding from the aqueous environment, leads to a hydrophobic surface minimization of the aggregate and results in minimized free energy. The structures of the thereby obtained supramolecular aggregates strongly depend on the position and availability of non-covalent interactions (van der Waals forces, electrostatic-, and π-π interactions) as well as the shape and flexibility of the molecules.[3]

Described in more detail, the aggregation of an amphiphilic molecule can be separated into three terms influencing the free energy of an amphiphilic self-assembly in dilute, aqueous solutions: (1) the hydrophobic contribution from the hydrophobic parts that aggregate inside the structure; (2) the surface contribution of the hydrophilic parts, reflecting the tendency to arrange so as to minimize the effect of the surrounding water on the hydrophobic parts enabled by hydration, electrostatic repulsion, and steric hindrance and (3) a packing term, describing the geometrical shape of the molecule and the possibility of their spatial arrangement. Surface and packing contribution are expressed in the surfactant parameter N_s, defined as $v_0/l_0 a_e$ with v_0 for the volume of the hydrophobic part of the molecule, l_0 being the length and a_e the equilibrium area per molecule at the aggregate surface, which is in fact the effective area of the hydrophilic group. The surfactant parameter is often used to explain and predict the curvature of the assemblies and

the resulting structure, e.g. for spherical micelles (N_s = 0.33), infinite cylinders (N_s = 0.5), planar bilayers and vesicles (N_s = 1), bicontinuous structures (N_s ≥ 1) and inverted micelles (N_s >1).[3-4]

Another attempt to predict resulting structures is the hydrophilic to hydrophobic ratio ($f_{hydrophilic}$), which expresses the tendency to form vesicles ($f_{hydrophilic}$ = 35% ± 10%), inverted microstructures $f_{hydrophilic}$ < 25%) and micelles ($f_{hydrophilic}$ > 45%).[5]

As mentioned above, the low solubility of the hydrophobic part is a major driving force for the self-assembly. Being referred to as attractive forces among apolar solutes in water, the important factor is actually the increase in entropy due to the liberation of water from the hydration shell during aggregation. However, the thermodynamic factors giving rise to this phenomenon, commonly referred to as the hydrophobic effect [6], are complex and still not fully understood.

As derived from the above driving forces, the structures can also be influenced by environmental stimuli, *e.g.* pH[7], ionic strength[7d-f, 8], temperature[9], counter ions[9c, 10], light[9b, 11], and oxidative stress[12], which all influence either the stabilizing interactions, the shape of the molecule, or the molecular composition itself. This fact can either be used to control or to trigger the destruction of the self-assembled structures[13]. The latter, in particular, is of interest in the triggered release of encapsulated payloads (*e.g.* in drugs delivery). Due to the so produced capability of the resulting materials to react to environmental stimuli, the materials are often referred to as "smart". The versatile variables thereby obtained enable manifold possibilities to control the self-assembly, but, on the other hand also make it hard to rationally predict self-assembled morphologies from scratch.

1.1.3 Hierarchically organized structures in nature

Hierarchical organization, as is often the case in self-assembly, also occurs in nature, where, for example, spider silks are produced by salt- and shear force-triggered self-assembly of proteins[10b]. But also the production of functional enzymes and of molecular machines in each cell are most often constructs of hierarchical organization and the key parameter for life[14]. Surprisingly, the variety of functions is mostly enabled by proteins and peptides that consist of only 20 natural amino acids (AA). These serve multiple functions as acids, bases, thiols, aromatic rings, etc., while spanning the wide range from hydrophilic to hydrophobic, resulting in almost endless possibilities of combinations in linear sequences. However, these linear sequences (primary structures) do not, in such state, allow for the broad functions of molecular machines. Only the folding of the sequence into a three-dimensional secondary structure – which is, in fact, self-assembly – imparts a functional structure to the biopolymers. The necessary rotations of the molecules happen on the N-C_α-bonds and the C_α-C-bonds, the related angles of rotation are expressed as Φ and Ψ, respectively. Other rotations are impossible, due to the specific electronic structure of the peptide bond. Steric hindrance also limits remaining possibilities to about 25%, reflected in the Ramachandran plot (Figure 1-2). With natural occurring L-amino acids, three secondary structures are possible: α-helix, β-sheet, and random coil. The alternation of L- and D-amino acids (rare) also enables wider β-helical confirmations, in which all residues point to the outside of the helix.[15]
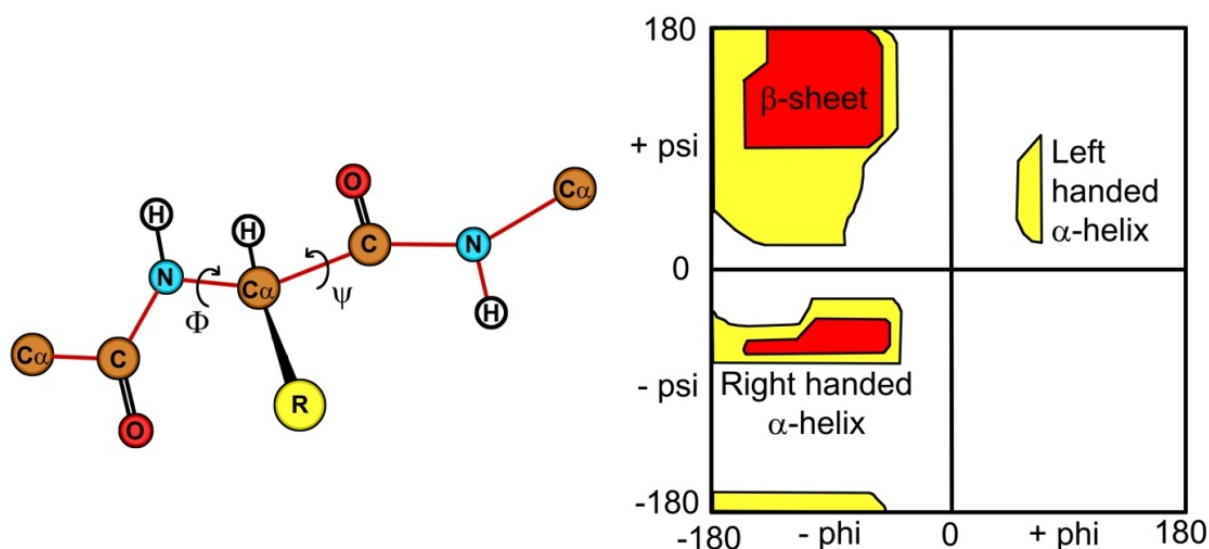
Figure 1-2: Illustration of the peptides phi- and psi-angles with the red line forming the repeating backbone of the peptide (left). The Ramachandran plot representing the possible angel combinations and the resulting secondary structures (right).

The complete folding of a protein – comprising several regions of different secondary structures – is called the tertiary structure and forms three-dimensional building blocks, which can further assemble into more complex tertiary structures.

The oxygen transporter, hemoglobin, is a good example of an assembly consisting of four subunits. Another more complex example is the hierarchically organized thermosome, a chaperonin from the thermophilic organism *Thermoplasma acidophilum*. It is a spherical assembly, consisting of two stacked, eight-membered rings, where each member is built of alternating α and β subunits.[16] Ironically, this self-assembled construct of two half-spheres assists proteins in folding.

Further examples are viruses, which are also the product of hierarchical organization, their sole task being the protection of their own DNA/RNA in the interior and delivering it into other cells. Recently, a self-assembled protective capsule of a virus (capsid) was produced by a synthetic 24-mer peptide[17]. This is a good example of how nature's self-assembly strategies can be understood and used in designing self-assembled structures.

1.2   Drug delivery

Drug delivery is commonly known as the process of administering a pharmaceutical compound to humans or animals in order to obtain a therapeutic effect.

1.2.1   The classical drug delivery approach

Classical drug delivery uses drug molecules that are generally dissolved in and distributed by the blood stream. Uptake by individual cells and transport to the final place of effect is rarely a targeted or specific process but rather controlled by the well-known dependence on the amount of blood circulating as well as the hydrophilic and hydrophobic character of the bodies' organs. Therefore, weak control over the final destination and the delivery pathways causes the molecules to also enter healthy cells or cells of different types, which leads to side-effects. Classical drug delivery approaches therefore rely instead on the formulation of the drug (the mixture of the dosage form, e.g. a pill), which, for instance, enables the active pharmaceutical ingredient (API) to pass through the acidic conditions of the stomach and to be liberated in the intestine. Nevertheless, enzymes can still decompose the API on its way to its final destination. Thus, a nano-sized protection of the drug, that still allows or even improves the uptake by the target tissue/cells, would be preferred and might allow new therapies with less side-effects.

1.2.2   Payload delivery in nature

Nature developed a variety of ways to deliver payloads to other cells or organisms. Reproduction uses the sperm, an example of a complex architecture of a whole cell[18], to deliver the genome to the ovum. Pollen performs the same task in the life of plants, while representing a diversity of shapes and sizes in the micrometer range (Figure 1-3). Not only protection from environmental factors, but also targeted delivery and release of precious payloads are performed by such complex carriers.
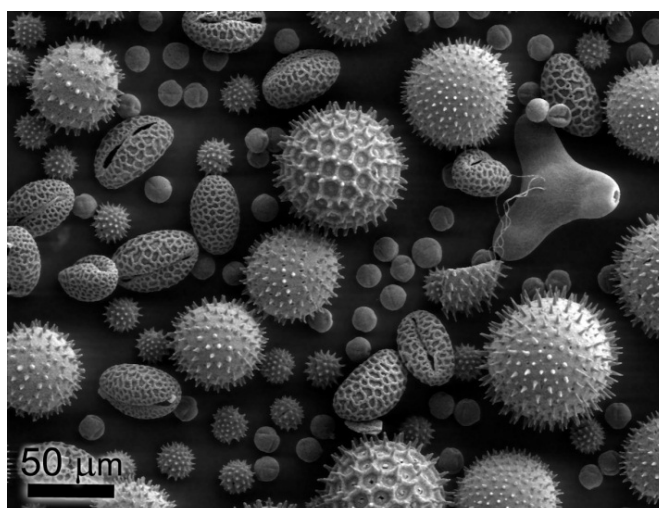
Figure 1-3: Scanning electron microscopy (SEM) of pollen from a variety of plants. *Reproduced by general permission of the Dartmouth Electron Microscope Facility, Dartmouth College[21].*

A less appreciated form of payload delivery is performed by viruses. Their DNA/RNA-carrying virus capsids are produced by the self-assembly of peptide or protein subunits, and understanding their architecture has recently also gained attention[19] (*cf. section 1.1.2*). Equipped with target recognition features (e.g. sugars or channel protein recognition sites), active release mechanisms, and cellular uptake enhancing factors on the surface, these nano-sized constructs perform very specific and efficient payload delivery of their own recipe for reproduction. Good examples of high efficiency are the approx. 35 nm-sized noroviruses that deliver a single stranded RNA. A low amount of only 10 – 100 viruses is enough to infect a human[20].

1.2.3 Smart material drug delivery concepts

Inspired by nature's sophisticated delivery systems, an eagerness to minimize side-effects and even mere solubility problems encountered by potential drugs, several concepts for drug delivery using self-assembled smart materials have been developed. A good overview of these is provided by recent reviews[22]. In order to decrease degradation by metabolic enzymes, reduce immunogenicity, and to prolong persistence in the body, the covalent modification of drugs with poly(ethylene glycol) (PEG) has led to several new therapeutic agents. The non-immunogenic, non-antigenic, non-toxic – and therefore biocompatible – hydrophilic polymer has recently also achieved FDA approval[23]. However, the covalent binding of such a large polymer is not always favorable when reaching the final point of action. As a result, the scientific community developed non-covalent shielding methods that exploit the method of self-assembly to achieve similar properties.

The fact that a large fraction of APIs are hydrophobic necessitates envelops that are able to incorporate such a payload while presenting a hydrophilic surface to the environment. A straight forward approach – which does not bind the payload covalently – is micellization of hydrophobic payloads with amphiphilic molecules. In such a case the hydrophobic, core forming part of an amphiphile can be tailored to fit the needs of the payload, while the hydrophilic part can still present a suitable surface to the environment.

For hydrophilic payloads, a segregated hydrophilic cavity is required. Vesicles can perform this task by providing cavities with sizes ranging from a few nanometers to a few micrometers. The stability and robustness of these nano-carriers varies depending on the materials from which they are built. Vesicles made of lipids (liposomes) may be integrated more easily into existing cell membranes; block-co-polymer vesicles, on the other hand, can adapt the thickness of the membrane to fit the demands of membrane proteins, which can be integrated in order to enable a selective release function. Variation in the molecular weight of the block-co-polymers can further control the thickness of the vesicular membrane, which goes along with enhanced membrane stability and robustness[24]. In contrast to liposomes, polymersomes offer better opportunities for chemical modifications that can be used to tailor their interaction with environmental factors. Such modifications can be a response to adhesion (used for targeting), integration into biological membranes, but also the reaction to environmental stimuli[13, 24-25] (*cf. section 1.1.2*). For example, nitrilotriacetic acid (NTA) functionalized block-co-polymer vesicles were recently shown[26] to

complex nickel to build coordination sites that bind to his-tagged proteins. But also the functionalization of vesicles already formed can be performed with polymersomes, as long as the functional groups are selected properly[27]. Including a photocleavable linker, on the other hand, can lead to light-triggered destruction of the polymersomes and a release of encapsulated payloads, as e.g. shown by Cabane et al.[28]. Recently, also the incorporation of metal nanoparticles into the membranes was demonstrated and may allow new possibilities in functionalization but also in heat- and radiation-triggered release of payloads[29].

Medical applications often need simultaneous treatment with several APIs of different solubilities and/or different release profiles[30]. Nature often provides diverse properties to different molecules in segregated compartments. The concept of multicompartmentization as a crucial factor to enable the delivery and staged release of payloads depending on different demands was therefore identified by Ringsdorf[31] in the late nineties. Since then, various approaches have been under investigation to produce micro- to nano-sized vehicles that have segregated hydrophobic as well as hydrophilic cavities to incorporate multiple guest molecules with different properties. Such concepts can use top-down strategies such as, for example, the sputtering of big compartments with small compartments to build raspberry-like structures[32] as well as bottom-up strategies such as self-assembly[31, 33].

The combination of several of the above mentioned functionalities might finally lead to nano-sized sensors or drug delivery vehicles that fulfill qualitatively similar tasks as their natural paradigms with regard to targeted as well as triggered release of payloads. Thereby, the comparably easier synthesis of artificial systems may allow cost effective large scale production.

1.3   The need for smart materials and their potential for drug delivery

The great interest in "smart materials" is reflected in the steadily increasing number of publications contributing to this field of research (2005:*285*, 2010:*467*). The properties of the investigated materials promote various beneficial applications comprising the fields of tissue engineering, sensors, nanoreactors, as well as drug delivery. All of the mentioned applications have one main topic in common: the wish to have materials that are no longer just static, but rather interact with the surrounding by adapting the properties instantly when necessary, imitating a "smart" behavior. Such functions can be programmed at a molecular level and are reflected in the responsive properties of the self-assembled materials. An example is the pH triggered release of encapsulated payloads in vesicles formed by poly(ethylene oxide)-*block*-poly(N,N-diethylamino ethylmethacrylate) diblock copolymer (PEO-PDEAMA)[34]. Due to its cationic character, the PDEAMA block is hydrophilic below pH 7.3; at high pH, the block is deprotonated, becomes hydrophobic and enables self-assembly. Further working principles and functions are presented in *chapter 1.1.2 and 1.2.3*. Such systems would deliver and liberate drugs only to a specific target (when equipped with a recognition pattern), or when a symptom traced back to the molecular level is recognized (*e.g.* oxidative stress due to inflammation).

It has been known that targeting leads to more efficiency and less side effects, since humans being have been using bows and arrows. Therefore, the same is also expected of novel smart material drug delivery systems and thus, highly aspired by academia and industry. Besides tedious development and optimization of new drugs with incalculable outcome, new formulations of existing drug molecules in smart drug delivery systems also lead to increased competitiveness and extended patent lifetimes, which dramatically increases market values[35].

1.3.1 Biocompatibility & biodegradability

A major concern in the development of smart material drug delivery systems should be their biocompatibility and biodegradability. The most sophisticated, targeted, and triggered-release enabled system has only hypothetical value if it causes immunogenic, antigenic, or even toxic reactions in the body (need for *biocompatibility*[23, 36]) and if it accumulates in the body during long-term use (need for *biodegradability*[37]). Unfortunately, orientation towards these specifications is rarely done at early stages of new material research.

Amino acid based materials, especially peptides and proteins – due to their natural origin, the similarity to the biological machinery, and the fact that they are subjects to natural degradation pathways – are generally seen as biocompatible and biodegradable. The potential unwanted interaction with other enzymes or functions in the body still exists, but in contrast to non-natural building blocks it is reduced to a very small probability. Therefore, the use of amino acid based materials, from a pragmatic point of view, is a smart choice. Further, degradation pathways of peptides and proteins can even be used to control a release from amino acid based materials[38].

1.3.2 Market demand for nano-sized drug delivery systems

Controlled release polymer systems were previously estimated to have an annual worldwide market of $60 billion. Further, it has been estimated that novel drug delivery methods (*cf. section 1.1.2 and 1.2.3*) will play a crucial role in approximately 40% of all pharmaceutical sales in the near future, due to the above mentioned advantages.[39] A good introduction of nano-sized drug delivery systems to the marked has already been shown for two oncology drugs, Abraxane and Doxil, which deliver paclitaxel and doxorubicin, respectively. In 2006 they generated sales of $184 million (Abraxane) and $177 million (Doxil) and are preferred in oncology due to enhanced solubility and reduced side-effects.[40] These examples show the great potential for nano-sized drug delivery systems also from the point of view of profit. Table 1-1 provides an overview of potential targets for nano-sized drug delivery systems.

Table 1-1: Nano-sized drug delivery systems, information taken from [40].

Type and diameter (nm)	Indication	Advantages
Polymeric nanoparticles (10-10 000)	Brain tumors, bone healing, restenosis, diabetes	Sustain localized drug therapeutic agent for weeks
Ceramic nanoparticles (<100)	Photodynamic therapy, liver therapy, diabetes	Easily prepared, water-soluble, very stable
Polymeric micelles (<100)	Solid tumors, anti-fungal	Hydrophobic core, suitable for water-insoluble drugs
Liposomes (50-100)	Tumors, HIV, vaccines	Reduces toxicity and long lasting in targeted tissue
Metallic nanoparticles (<50)	Cancer	Extremely small size, vast surface area
Dendrimers (<19)	Tumors, HIV, bacterial infection treatment	Can carry hydrophobic or hydrophilic content

1.4 Synthesis of amino acid based amphiphilic materials

Amino acids are small molecules with a carboxylic acid and an amine function connected through a carbon (α-carbon), holding the residue of the amino acid (AA) that gives the unique properties to each of the 22 standard AAs (*cf.* Figure 1-2). In nature, the genetic code defines 20 stereochemical L-isomers; however, for synthesis, each chirality of the standard AAs as well as a large variety of artificial AAs can be used. The covalent connection of AAs to form peptides, proteins, and poly(amino acids) is enabled by an amide bond, also referred to as peptide bond, due to its origin.[41] To form amphiphilic materials that are based on amino acids, several methods can be used, comprising polymerization, the joining of peptidic and non-peptidic materials into hybrid materials, solid phase peptide synthesis (SPPS), and recombinant protein expression.

1.4.1 Polymerization

Polymerization can produce large molecules from small monomers in a very effective way. Sequential ring-opening polymerization of N-carboxy anhydrides (NCAs) can be used to synthesize a variety of AA-based block-co-polymers without racemization of chiral centers, with good yields[7e, 42]. Among others, Deming et al. improved the rather high polydispersity index (PD.I.) of the method by using organo-nickel initiators to obtain well-defined block-co-polymers or polypeptides[43]. Nevertheless, polymerization produces a certain molecular weight distribution that often varies from batch to batch; furthermore, it cannot produce precisely defined sequences of amino acids, as would be the case in proteins and peptides.

1.4.2 Hybrid materials

For certain functions (*e.g.* targeting, triggering of cell function, secondary/tertiary structure formation, etc., *cf. chapter 1.1.2*) precise sequences are needed. Hybrid materials have been created in order to combine this precision with the efficient production method to make polymers. The covalent connection of polymers with peptides or proteins can be made with the fully available knowledge of organic chemistry. Often used methods are esterification, amide bond formation, or the attachment to thiols. Bioconjugates produced in this way have been shown to be effective in self-assembly to produce new materials in, e.g. bio-medical applications[44].

1.4.3 Solid phase peptide synthesis

The production of a defined AA sequence requires advanced protective group chemistry as well as several reaction and intermediate purification steps. Solid phase peptide synthesis (SPPS) – affectionately referred to by peptide chemists as "the supreme protective group chemistry" – combines these tasks in a straight forward synthesis strategy.

In general, a single AA is linked to a functionalized solid phase (resin), followed by a stepwise elongation with AAs and several washing (filtering) steps until the final up to ~ 50 AAs long peptide is cleaved from the resin. In the original Boc-strategy, protection of the single AA was performed with a Boc-protective group that had to be removed prior to the next coupling with trifluoro acetic acid (TFA). The final cleavage from the resin was then performed with HF. After about 15 years, the strategy was replaced by the less dangerous Fmoc-strategy, which uses piperidine in deprotection and TFA as the cleavage agent. A general scheme for SPPS is shown in Figure 1-4. Due to the coupling to a solid support, intermediate by-products can easily be removed by washing and filtration with appropriate solvents, which is the mayor advantage of SPPS. The high solvent consumption and the repetitive steps are often seen as acceptable drawbacks.[45]

Figure 1-4: General scheme for SPPS.

The variety of available resins for SPPS is large (e.g. Merrifield, Wang, SASRIN, and Rink Amide). Most often beaded polystyrene, cross-linked with a low amount of m/p-divinylbenzene, is used as a support and functionalized with different AA linkers. The latter define the initial AA coupling as well as the cleavage conditions and the outcome of the peptides' C-terminus. The low amount of cross-linking facilitates swelling of the beads during synthesis and, in this way, allows the reagents to enter into the polymer network to grow the peptide. The typical loading capacity of resins is between 0.1 –1.5 mmol/g and might be adjusted to fit the need of side-chain cyclization, sequences with intrinsic difficulties, or synthesis of long peptides.[45]

The attachment of the initial AA is often an overall yield determining, crucial step, which requires conditions that differ from the elongation steps. As a result, several pre-coupled amino acid resins are available on the market. However, resins that use the same conditions for the initial coupling as for the elongation are also available (*e.g.* Rink Amide).

Growing the peptide is performed with stepwise elongation of the solid-support-bound peptide. First, the Fmoc-protected amine is liberated using the specific deprotection agent, piperidine. After washing, the C-terminally activated amino acid is coupled to the free amine of the peptide, while the Fmoc-protection on the N-terminus of the AA prevents multiple coupling. To capture the liberated proton and to keep the reaction conditions above pH 9, an organic base (*e.g.* N,N-diisopropylethylamine) is used. To prevent sequential errors, unreacted, free N-termini of the bound peptide are acetylated with acetic anhydride, which leads to growth stoppage at this stage, and allows easy separation from the final product. Derived from the original activation N,N'-dicyclohexylcarbodiimide (DCC), several faster, more soluble, racemization insensitive, and less irritating activation agents have been developed and are being used today. HOBt, TBTU, HCTU, and PyBOP are some common examples. For the protection of the AA residues, several orthogonal protective groups are used. The Boc protective group is commonly used for amines and tryptophan, and tBu for thiols, due to its easy removal during the final cleavage step. However, a large variety of differently protected AAs is available on the market and also allow intermediate deprotection.[45]

Cleavage of the final peptide from the resin depends on the resin-linker used. Often used cleavage cocktails utilize concentrated TFA (95% aqueous TFA). Due to the production of highly reactive carbocations, scavengers to trap them are used and they depend on the used amino acids. Typical scavengers, besides water, are silane derivatives (triethylsilane, triisopropylsilane), or the malodorous ethanedithiol if sulfur containing AAs are in the sequence. Good starting conditions for cocktail preparation are available in literature [45] or from chemical providers. The dissolved peptide in the cleavage cocktail is filtered from the solid support and precipitated in organic solvents (e.g. diethylether, diisopropylether, tert.-buthylmethylether) and washed by filtration or centrifugation to obtain the crude peptide.

1.4.4 Recombinant protein expression

Recombinant protein expression is a common way to produce proteins that are larger than the maximal available length obtained by SPPS (~ 50 AAs). The method uses genetically modified cells to overexpress the desired protein. To engineer such little factories, host cells – either *bacteria, yeast, insect* or *mammalian* – are transformed or transfected with the expression vector (plasmid) containing the protein's gene and adequate antibiotic-resistance genes (e.g. ampicillin, chloramphenicol, tetracycline, kanamycin, etc.).

The cells are then exposed to the antibiotic(s) and only the ones with copies of the plasmid survive since the plasmid provides the resistance to the antibiotic. After selection, the protein, encoded by the gene inserted in the host cells, can be produced in a defined medium. Depending on the chosen expression system, the protein can be expressed either intra- or extracellularly.

The method is a convenient way of protein production, once the expression organism is engineered. However, for large-scale production, the low yield/space ratio of the reactors is costly if compared to chemical reactors. Nevertheless the method represents the only way to produce large proteins under controlled conditions and has been used to produce self-assembling peptides for new materials.[10b, 46]

1.4.5 Purification of amphiphilic peptides

Crude peptides/proteins as produced by SPPS or expression are usually purified by size exclusion or reversed phase high pressure/performance liquid chromatography (RP HPLC). The latter is preferred, because it provides good yields, high purities, and easily adjustable purification protocols, as well as a high separating capacity for crude products containing several impurities with molecular masses in the same range as the target molecule. However, amphiphilic molecules and hydrophobic peptides in particular are difficult to purify, due to exactly these wanted properties. Because the products have low solubility in pure aqueous or organic solvents but are soluble in mixtures thereof, problems are often already encountered during dissolving. However, often these can be handled with sophisticated solubility trials[47].

If the crude product is dissolved in a compatible solvent for RP HPLC, it can be separated on, e.g. endcapped C18 reversed-phase materials, using one of the established eluent systems. Common eluent systems are shown in Table 1-2.

After the separation, the pure peptide/protein carries the counter ion of the corresponding buffer used. These can be replaced/removed using ion exchange chromatography or, in case of volatile components, lyophilization (ammonium acetate) to obtain the final product.

Table 1-2: Common eluent systems for RP HPLC purification of peptides

ACN / H_2O (0.1%TFA)

ACN / H_2O (2% acetic acid)

ACN / H_2O (0.5% formic acid)

ACN / H_2O (1% triethyl ammonium phosphate, pH 2.3 or pH 7)

ACN / H_2O (0.4% NH_4OAc, pH 6.5)
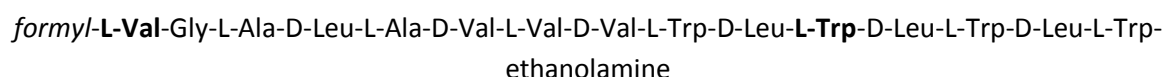
ACN / H_2O (0.3% H_3PO_4-$NaClO_4$, pH 2.8)

ACN = acetonitrile; alternatively methanol, isopropanol, or tetrahydrofuran can be used

1.5   Gramicidin – a short, hydrophobic, and membrane-integrating peptide

Gramicidin is a pentadecapeptide, consisting of alternating and completely hydrophobic D- and L-amino acids. Its origin is the soil bacterial species *Bacillus brevis*, which is still used to produce gramicidin in a biotechnological way. The sequence of 15 amino acids is N-terminally modified with a formyl residue and C-terminally functionalized with an ethanolamine residue:

formyl-**L-Val**-Gly-L-Ala-D-Leu-L-Ala-D-Val-L-Val-D-Val-L-Trp-D-Leu-**L-Trp**-D-Leu-L-Trp-D-Leu-L-Trp-ethanolamine

Originally occurring gramicidin D is a mixture of gramicidin A, B, and C, that interchanges the tryptophan at position 11 with either phenylalanine or tyrosine, respectively. Isomers with isoleucine in position one also exist. The gramicidin K family is an esterified variation with different fatty acids on the ethanolamine terminus. Gramicidin S, in contrast to its analogues, is not a linear but a cyclic peptide. However, gramicidin A, at a fraction of 80%, remains the most frequently occurring isomer.[48]

Gramicidin is known for its antibiotic effect on gram positive bacteria, caused by its ion channel formation for monovalent cations, and also owes its name to this feature. Ion channel formation is enabled by a β-helical-like secondary structure, causing two molecules to dimerize and span a present lipid bilayer. Several states of dimerization exist: double helical dimers, helical dimers, in parallel and antiparallel fashion, as well as in left- and right-handed orientations. The degree of dimerization as well as the dimerization itself depend on the polarity of the surrounding, and can be influenced by the presence of ions (see Figure 1-5).[48]

In the present thesis, gramicidin A plays an important role in the formation of a purely peptidic amphiphile, because the unique structure hides the hydrophilic backbone in the interior of the helix while presenting the hydrophobic residues to the exterior, making it an ideal sequence for the hydrophobic part of an amphiphile.

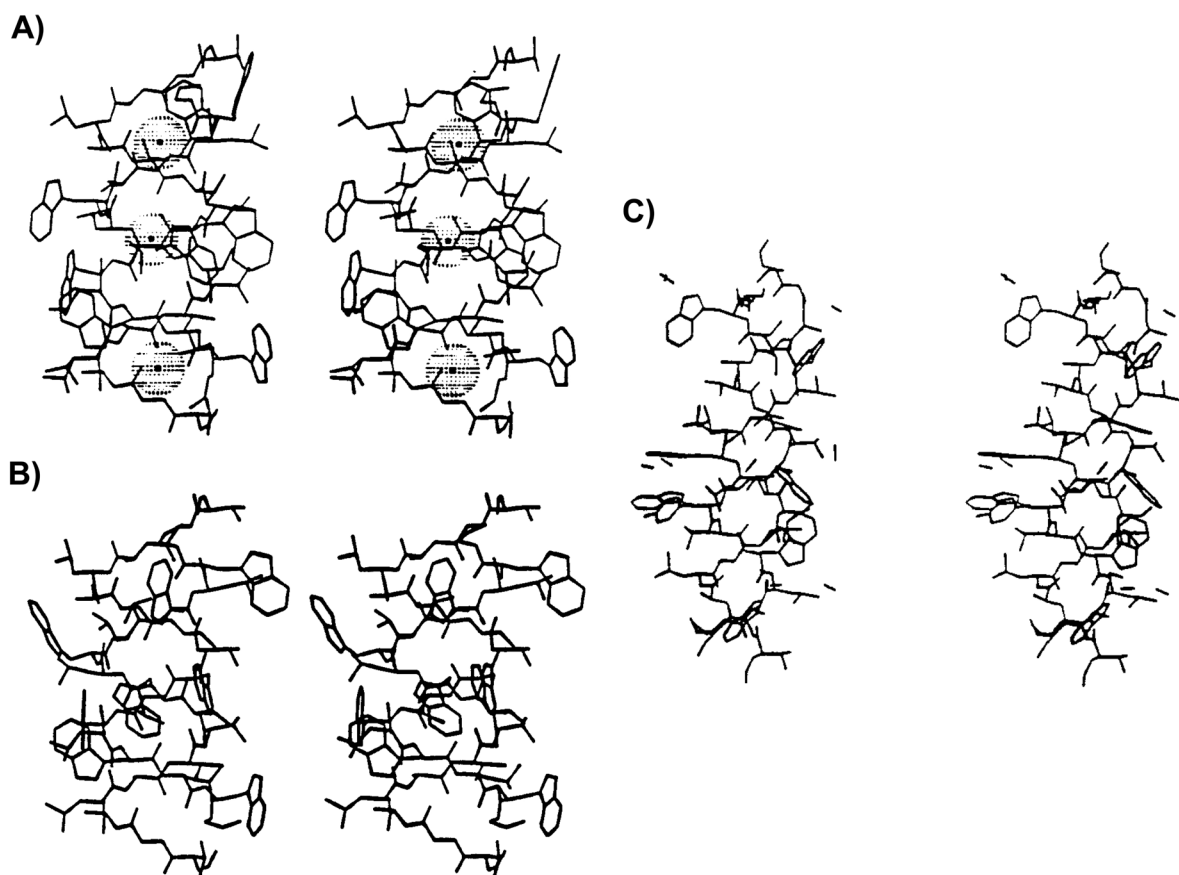Figure 1-5: Stereographic illustrations of gramicidin a) structure of Cs$^+$ complexed, right-handed antiparallel double stranded double helical (DSDH$_R$) dimer crystal structure, b) H$^+$ complexed DSDH$_R$ dimer from glacial acetic acid crystal structure, c) methanol solvated DSDH$_L$ gramicidin structure as major conformer in polar solvents. *From Burkhart et al.*[49] *reprinted by permission of John Wiley and Sons.*

1.6 Scope of the thesis

The aim of the present thesis is the generation of new, nano-sized materials that are produced by the delicate method of self-assembly. In order to interact with biological systems in a most effective way, the underlying chemically designed building blocks should be based on purely peptidic amphiphiles.

The first task is to find a peptide system in which a peptide is segregated into an hydrophilic and a hydrophobic region to enable self-assembly, as is known from other amphiphilic but rarely biocompatible/biodegradable systems. These conceptual steps will need to be transferred into practice by finding an adequate synthesis route as well as purification steps, which can then be used to produce different peptides, based on this new class of self-assembly materials.

The variation of the sequence – representing designed point mutations of the molecular building block's architecture – combined with the characterization of the resulting nanostructures in solution will lead to an iteratively understanding of the hierarchical, purely peptidic self-assembly. Furthermore, the use of defined amino acids will induce possible molecular anchor points for environmental stimuli such as, for example, the pH-dependence of the nanostructures. This will finally lead to a tunable, purely peptidic self-assembly system, and result in new "smart" materials. These are then tested for potential applications in the field of drug delivery, but might also be useful as templates to produce three-dimensional, nano-patterned materials with new optical and electronic properties.

1.7 References

[1] G. M. Whitesides and M. Boncheva, *Proceedings of the National Academy of Sciences of the United States of America* **2002**, *99*, 4769-4774.

[2] a) A. Katsuhiko and et al., *Science and Technology of Advanced Materials* **2008**, *9*, 014109; b) I. W. Hamley, *Introduction to Block Copolymers*, John Wiley & Sons, Ltd, **2004**, p. 1-29.

[3] D. F. Evans, *The Colloidal Domain: Where Physics, Chemistry, Biology, and Technology Meet, 2nd*, **1998**, p. 640 pp.

[4] a) R. Nagarajan, *Langmuir* **2001**, *18*, 31-38; b) M. Antonietti and S. Förster, *Advanced Materials (Weinheim, Germany)* **2003**, *15*, 1323-1333.

[5] G. Srinivas, J. C. Shelley, S. O. Nielsen, D. E. Discher and M. L. Klein, *The Journal of Physical Chemistry B* **2004**, *108*, 8153-8160.

[6] a) L. R. Pratt, *Annual Review of Physical Chemistry* **1985**, *36*, 433-449; b) C. Tanford, *Science* **1978**, *200*, 1012-1018.

[7] a) U. Borchert, U. Lipprandt, M. Bilang, A. Kimpfler, A. Rank, R. Peschka-Suess, R. Schubert, P. Lindner and S. Foerster, *Langmuir* **2006**, *22*, 5843-5847; b) J. Du, Y. Tang, A. L. Lewis and S. P. Armes, *Journal of the American Chemical Society* **2005**, *127*, 17982-17983; c) E. G. Bellomo, M. D. Wyrsta, L. Pakstis, D. J. Pochan and T. J. Deming, *Nature Materials* **2004**, *3*, 244-248; d) F. Checot, A. Brulet, J. Oberdisse, Y. Gnanou, O. Mondain-Monval and S. Lecommandoux, *Langmuir* **2005**, *21*, 4308-4315; e) J. Rodriguez-Hernandez and S. Lecommandoux, *J. Am. Chem. Soc.* **2005**, *127*, 2026-2027; f) F. Checot, J. Rodriguez-Hernandez, Y. Gnanou and S. Lecommandoux, *Biomolecular Engineering* **2007**, *24*, 81-85.

[8] M. Sauer, D. Streich and W. Meier, *Advanced Materials* **2001**, *13*, 1649-1651.

[9] a) I. Dimitrov, B. Trzebicka, A. H. E. Mueller, A. Dworak and C. B. Tsvetanov, *Progress in Polymer Science* **2007**, *32*, 1275-1343; b) C. J. F. Rijcken, O. Soga, W. E. Hennink and C. F. van Nostrum, *J Control Release* **2007**, *120*, 131-148; c) Y. Li, B. S. Lokitz and C. L. McCormick, *Angewandte Chemie, International Edition* **2006**, *45*, 5792-5795; d) X. Chen, X. Ding, Z. Zheng and Y. Peng, *New Journal of Chemistry* **2006**, *30*, 577-582; e) S. Qin, Y. Geng, D. E. Discher and S. Yang, *Advanced Materials (Weinheim, Germany)* **2006**, *18*, 2905-2909.

[10] a) L. Eisoldt, J. G. Hardy, M. Heim and T. R. Scheibel, *Journal of Structural Biology* **2010**, *170*, 413-419; b) F. Hagn, L. Eisoldt, J. G. Hardy, C. Vendrely, M. Coles, T. Scheibel and H. Kessler, *Nature (London, United Kingdom)* **2010**, *465*, 239-242; c) M. Heim, D. Keerl and T. Scheibel, *Angewandte Chemie, International Edition* **2009**, *48*, 3584-3596; d) M. Heim, L. Roemer and T. Scheibel, *Chemical Society Reviews* **2010**, *39*, 156-164; e) U. K. Slotta, S. Rammensee, S. Gorb and T. Scheibel, *Angewandte Chemie, International Edition* **2008**, *47*, 4592-4594.

[11] a) X. Tong, G. Wang, A. Soldera and Y. Zhao, *Journal of Physical Chemistry B* **2005**, *109*, 20281-20287; b) Y. Zhao, *Chemical Record* **2007**, *7*, 286-294; c) W. Su, K. Han, Y. Luo, Z. Wang, Y. Li and Q. Zhang, *Macromolecular Chemistry and Physics* **2007**, *208*, 955-963; d) W. Su, Y. Luo, Q. Yan, S. Wu, K. Han, Q. Zhang, Y. Gu and Y. Li, *Macromolecular Rapid Communications* **2007**, *28*, 1251-1256.

[12] a) A. Napoli, M. Valentini, N. Tirelli, M. Mueller and J. A. Hubbell, *Nature Materials* **2004**, *3*, 183-189; b) S. Cerritelli, D. Velluto and J. A. Hubbell, *Biomacromolecules* **2007**, *8*, 1966-1972.

[13] K. Kita-Tokarczyk, J. Grumelard, T. Haefele and W. Meier, *Polymer* **2005**, *46*, 3540-3563.

[14] B. Alberts, J. Alexander, J. Lewis, M. Raff, K. Roberts and P. Walter, *Molecular Biology of the Cell, 4th Edition*, Wiley, **2004**, p. 2000 pp.

[15] S. Durani, *Accounts of Chemical Research* **2008**, *41*, 1301-1308.

[16] N. Bruns, K. Pustelny, L. M. Bergeron, T. A. Whitehead and D. S. Clark, *Angewandte Chemie, International Edition* **2009**, *48*, 5666-5669, S5666/5661-S5666/5617.

[17] K. Matsuura, K. Watanabe, T. Matsuzaki, K. Sakurai and N. Kimizuka, *Angewandte Chemie* **2010**, *122*, 9856-9859.

[18] K. Toshimori and C. Ito, *Arch Histol Cytol* **2003**, *66*, 383-396.

[19] a) D. G. Angelescu and P. Linse, *Soft Matter* **2008**, *4*, 1981-1990; b) S. Andersson, *Zeitschrift fuer Anorganische und Allgemeine Chemie* **2008**, *634*, 2161-2170.

[20] a) B. V. Venkataram Prasad, S. Crawford, J. A. Lawton, J. Pesavento, M. Hardy and M. K. Estes, *Structural Studies on Gastroenteritis Viruses*, John Wiley & Sons, Ltd, **2008**, p. 26-46; b) K. Mattison, A. Shukla, A. Cook, F. Pollari, R. Friendship, D. Kelton, S. Bidawid and J. M. Farber, *Emerg Infect Dis* **2007**, *13*, 1184-1188.

[21] L. Howard and C. Daghlian in *Pollen from a variety of common plants*, *Vol.* (Ed. Misc_pollen.jpg), Dartmouth Electron Microscope Facility, Dartmouth College, Hanover, New Hampshire.

[22] a) Y. Malam, M. Loizidou and A. M. Seifalian, *Trends in Pharmacological Sciences* **2009**, *30*, 592-599; b) O. Onaca, R. Enea, D. W. Hughes and W. Meier, *Macromolecular Bioscience* **2009**, *9*, 129-139.

[23] F. M. Veronese and G. Pasut, *Drug Discovery Today* **2005**, *10*, 1451-1458.

[24] V. Malinova, S. Belegrinou, D. de Bruyn Ouboter and W. P. Meier, *Adv. Polym. Sci.* **2010**, *224*, 113-165.

[25] K. Kita-Tokarczyk, F. Itel, M. Grzelakowski, S. Egli, P. Rossbach and W. Meier, *Langmuir* **2009**, *25*, 9847-9856.

[26] R. Nehring, C. G. Palivan, S. Moreno-Flores, A. Mantion, P. Tanner, J. L. Toca-Herrera, A. Thunemann and W. Meier, *Soft Matter* **2010**, *6*, 2815-2824.

[27] a) S. Egli, B. Fischer, S. Hartmann, P. Hunziker, W. Meier and P. Rigler, *Macromolecular Symposia* **2010**, *296*, 278-285; b) S. Egli, H. Schlaad, N. Bruns and W. Meier, *Polymers* **2011**, *3*, 252-280.

[28] E. Cabane, V. Malinova and W. Meier, *Macromolecular Chemistry and Physics* **2010**, *211*, 1847-1856.

[29] a) R. Sachsenhofer, W. H. Binder, D. Farnik and R. Zirbs, *Macromolecular Symposia* **2007**, *254*, 375-377; b) Y. Li, A. E. Smith, B. S. Lokitz and C. L. McCormick, *Macromolecules (Washington, DC, United States)* **2007**, *40*, 8524-8526; c) G. S. Cleveland Eugene Rayford II, Kevin Shuford, *Nanoscape* **2005**, *2*, 27-33; d) M. K. Corbierre, N. S. Cameron, M. Sutton, K. Laaziri and R. B. Lennox, *Langmuir* **2005**, *21*, 6063-6072.

[30] F. Xie, M. Woodle and P. Lu, *Drug Discovery Today* **2006**, *11*, 67-73.

[31] H. Ringsdorf, P. Lehmann and R. Weberskirch, **1999**, pp. BTEC-001.

[32] a) M. Delcea, N. Madaboosi, A. M. Yashchenok, P. Subedi, D. V. Volodkin, G. B. G. De, H. Moehwald and A. G. Skirtach, *Chemical Communications (Cambridge, United Kingdom)* **2011**, *47*, 2098-2100; b) M. Delcea, A. Yashchenok, K. Videnova, O. Kreft, H. Mohwald and A. G. Skirtach, *Macromolecular Bioscience* **2010**, *10*, 465-474.

[33] a) S. Kubowicz, J.-F. Baussard, J.-F. Lutz, A. F. Thuenemann, H. von Berlepsch and A. Laschewsky, *Angewandte Chemie, International Edition* **2005**, *44*, 5262-5265; b) J.-F. Lutz and A. Laschewsky, *Macromolecular Chemistry and Physics* **2005**, *206*, 813-817; c) H. von Berlepsch, C. Boettcher, K. Skrabania and A. Laschewsky, *Chemical Communications (Cambridge, United Kingdom)* **2009**, 2290-2292; d) C. Zhong and D. Liu, *Macromolecular Theory and Simulations* **2007**, *16*, 141-157; e) K. Skrabania, H. von Berlepsch, C. Boettcher and A. Laschewsky, *Macromolecules (Washington, DC, United States)* **2010**, *43*, 271-281.

[34] D. J. Adams, S. Adams, D. Atkins, M. F. Butler and S. Furzeland, *Journal of Controlled Release* **2008**, *128*, 165-170.

[35] K. V. Rajan and G. Sanjay, *Pharmaceutical Technology* **2001**, *25*, 1-14.

[36] a) D. Williams, *Medical Device Technology* **2003**, *14*, 10; b) F. M. Veronese, *Biomaterials* **2001**, *22*, 405-417.

[37] a) J. F. Kennedy and M. M. He, *Carbohydrate Polymers* **2005**, *60*, 127; b) D. F. Carmignac, *Cell Biochemistry and Function* **2003**, *21*, 298-298.

[38] a) P. D. Thornton and A. Heise, *J. Am. Chem. Soc.* **2010**, *132*, 2024-2028; b) B. Romberg, F. M. Flesch, W. E. Hennink and G. Storm, *Int. J. Pharm.* **2008**, *355*, 108-113; c) B. Law, R. Weissleder and C.-H. Tung, *Biomacromolecules* **2006**, *7*, 1261-1265.

[39] J. Venugopal, M. P. Prabhakaran, S. Low, A. T. Choon, G. Deepika, V. R. G. Dev and S. Ramakrishna, *Current Pharmaceutical Design* **2009**, *15*, 1799-1808.

[40] a) B. I. Ltd. in *Next Generation Protein Engineering and Drug Design*, *Vol. BI00020-004* Business Insights Ltd., **2007**; b) B. I. Ltd. in *Innovation in Drug Delivery*, *Vol. BI00019-004* Business Insights Ltd., **2006**.

[41] a) P. J. Halling, *Journal of Chemical Technology and Biotechnology* **1995**, *62*, 105; b) K. P. C. Vollhardt and N. E. Schore, *Organische Chemie 3. Auflage*, Wiley-VCH, Weinheim, Germany, **2000**, p. 1445 pp.

[42] J. Sun, X. Chen, C. Deng, H. Yu, Z. Xie and X. Jing, *Langmuir* **2007**, *23*, 8308-8315.

[43] a) T. J. Deming, *Nature* **1997**, *390*, 386-389; b) K. T. Kim, M. A. Winnik and I. Manners, *Soft Matter* **2006**, *2*, 957-965; c) C. Schatz, S. Louguet, J.-F. Le Meins and S. Lecommandoux, *Angew. Chem., Int. Ed.* **2009**, *48*, 2572-2575.

[44] a) J.-F. Lutz and H. G. Boerner, *Progress in Polymer Science* **2008**, *33*, 1-39; b) J. Sun, C. Deng, X. Chen, H. Yu, H. Tian, J. Sun and X. Jing, *Biomacromolecules* **2007**, *8*, 1013-1017; c) J. Lin, J. Zhu, T. Chen, S. Lin, C. Cai, L. Zhang, Y. Zhuang and X.-S. Wang, *Biomaterials* **2009**, *30*, 108-117; d) F. Checot, S. Lecommandoux, Y. Gnanou and H.-A. Klok, *Angewandte Chemie, International Edition* **2002**, *41*, 1339-1343; e) H. Kukula, H. Schlaad, M. Antonietti and S. Forster, *Journal Of The American Chemical Society* **2002**, *124*, 1658-1663; f) S. Kimura, D.-H. Kim, J. Sugiyama and Y. Imanishi, *Langmuir* **1999**, *15*, 4461-4463.

[45] M. Mergler and J. P. Durieux, *The Bachem Practice of SPPS*, Bachem AG, Bubendorf, Switzerland, **2000**, p. 1-83.

[46] S. Kyle, A. Aggeli, E. Ingham and M. J. McPherson, *Trends in Biotechnology* **2009**, *27*, 423-433.

[47] a) Vydac in *Designing Purification Methods for Hydrophobic Peptides*, *Vol. AN #9802* Vydac, The Separations Group, Hesperia, CA, USA, **1998**; b) C. T. Choma, G. T. Robillard and D. R. Englebretsen, *Tetrahedron Letters* **1998**, *39*, 2417-2420; c) R. Bollhagen, M. Schmiedberger and E. Grell, *Journal of Chromatography A* **1995**, *711*, 181-186.

[48] a) K. Bauer, R. Roskoski, Jr., H. Kleinkauf and F. Lipmann, *Biochemistry* **1972**, *11*, 3266-3271; b) B. A. Wallace, *Biophys. J* **1986**, *49*, 295-306; c) B. A. Wallace, *Advances in experimental medicine and biology* **1996**, *398*, 607-614; d) B. M. Burkhart, R. M. Gassman, D. A. Langs, W. A. Pangborn and W. L. Duax, *Biophysical Journal* **1998**, *75*, 2135-2146; e) B. A. Wallace, *Journal of Structural Biology* **1998**, *121*, 123-141; f) D. Voet and J. Voet, *Biochemistry*, John Wiley and Sons New York, **1995**, p. 519-520.

[49] B. M. Burkhart, R. M. Gassman, D. A. Langs, W. A. Pangborn, W. L. Duax and V. Pletnev, *Biopolymers* **1999**, *51*, 129-144.

2   Reversible peptide particle formation using a mini amino acid sequence

Thomas B. Schuster[a], Dirk de Bruyn Ouboter[a], Enrica Bordignon[b], Gunnar Jeschke[b], and Wolfgang Meier[a]

[a]Department of Chemistry, University of Basel, Klingelbergstrasse 80, CH-4056 Basel, Switzerland.
[b]Laboratory for Physical Chemistry, ETH Zurich, Wolfgang-Pauli-Str.10, CH-8093 Zürich, Switzerland
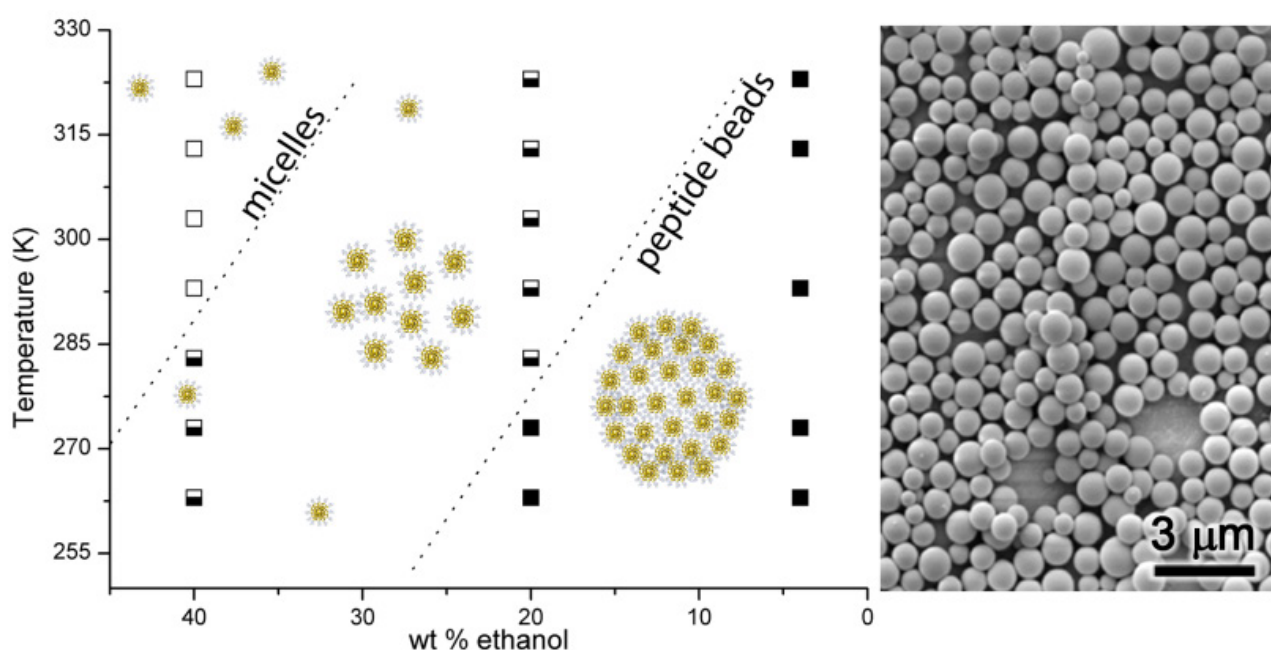
Phase diagram of the self-assembly process of the short peptides Ac-X$_3$-gT and AcC-X$_3$-gT into micelles and spherical peptide particles, termed "peptide beads" (left). SEM of the formed peptide beads (right).

Parts of this chapter were published in:

2.1 Abstract

This chapter focuses on the formation of self-assembled peptide particles using an amphiphilic amino acid (AA) sequence derived using solid-phase peptide synthesis (SPPS) and describes the purification and characterization thereof. The prepared undecamer features a repetitive L-tryptophan and D-leucine [LW-DL] motif representing the hydrophobic block, and an N-terminally attached hydrophilic (lysine or acetylated lysine) section. This chapter also shows the first approach used in this thesis to produce self-assembled structures that are based on a purely peptidic amphiphile.

Peptides that contain charged lysine were observed to aggregate into micelles and a minor fraction of peptide particles. Charge shielding with anionic counter ions shifted the equilibrium towards the larger peptide aggregates, their size depending on counter ion positioning as found in the Hofmeister series. Similarly, the corresponding uncharged (acetylated) peptide was also demonstrated to assemble into micelles and subsequently into spherical peptide particles, termed "peptide beads", which are hypothesized to be multicompartment micelles. The formation of peptide beads was studied as a function of temperature and solvent composition by means of electron paramagnetic resonance (EPR), dynamic and static light scattering, fluorimetry and electron microscopy. The results suggest an equilibrium among single peptide molecules, micelles, and peptide beads. Interestingly, once formed, the peptide beads show high mechanical stability and preserve their shape and dimensions even after isolation from solution.

2.2 Introduction

The increased efforts and interest in self-assembled nanostructures in recent decades, especially in aqueous solutions, have led to manifold morphologies as exhibited by micelles, cylindrical micelles and vesicles. Block copolymers have been explored to tailor-make micelles for the encapsulation of hydrophobic compounds[1]. Inspired by nature and imitating lipid membranes, block copolymer vesicles are now being used to create nanocompartments that encapsulate dyes[2] and active enzymes[3], insert active proteins[4], perform molecular recognition[5] and form stimuli-responsive nanoreactors and drug delivery systems (DDSs)[6]. Vesicular structures are interesting candidates for DDSs because they permit the simultaneous encapsulation of hydrophobic and hydrophilic compounds in their membranes and aqueous cores, respectively[7]. Other self-assembled structures that could serve as DDSs are large compound micelles[8] (LCM) or multicompartment micelles[9] (MCM). These nano-sized systems have a hydrosoluble shell and are characterized by segregated, incompatible subdomains that entrap drugs as a function of hydrophobicity, potentially followed by controlled release. MCM and LCM consist of micellar and inverse micellar-type subunits, respectively.

Hybrid materials composed of polypeptides and polymers combine the advantages of the two, *e.g.* solubility and processability[10]. Polypeptides contribute positive aspects in terms of chemical functionality due to a diversity of amino acid (AA) side chains, combined with specific AA sequences that act, *e.g.* as a specific recognition site[11] (RGD sequence for cell adhesion or

arginine rich sequences for cell penetration[12]). Another characteristic feature of polypeptides is their secondary structure, which permits exploiting their geometry[13]. The primary sequence, along with environmental conditions (pH, ionic strength, temperature, solvent), *i.e.* intrinsic and external factors respectively, determine the secondary structure and therefore also control the overall morphology of the assembly.

Peptide-based materials can respond to environmental triggers with sensitivity and specificity. In the biological context this smartness makes a multitude of applications possible, including triggered drug release, biosensors, tissue repair, and also patterning[14]. For example, applying changes in pH and temperature triggered the inversion of a micellar structure based on the properties of the two blocks used in a peptide-containing block copolymer[15]. In another system the release of a drug was controlled by the presence of poly(L-glutamic acid) within the block copolymer micelle's corona, leading to a pH-triggered increase in permeability[16].

The importance of charges was also demonstrated by the charge-driven complexation of oppositely charged peptide-based blocks, yielding vesicles with a semipermeable membrane[17].

Recently, also amphiphilic biopolymers have been reported that comprise only natural amino acids and hence are expected to display enhanced biocompatibility. For example, Deming et al.[12, 18] and Rodriguez-Hernandez et al.[19] designed block copolypeptides that self-assemble into vesicular structures. It should be noted that the systems described so far were generated by conventional polymerization techniques. Despite the fact that rather narrow molar mass distributions can be reached[12, 18] the resulting polymers are not monodisperse and allow only a limited control over the sequence.

These problems are overcome by genetic engineering techniques that result in excellent control of sequence and length[20]. In this regard, Scheibel et al. reported the use of a natural 47.7 kDa spider silk protein to form microspheres[21].

Solid phase synthesis also offers optimal tuning of properties by point mutation, but is limited to oligo and polypeptides (up to maximal 50 AA).

Santoso et al. reported the self-assembly of small amphiphilic peptides having no defined secondary structure into well-defined superstructures[22] which, however, proved to be highly sensitive to the purity of the peptides[23]. The continued search for an essential amyloid-forming sequence, led to still smaller molecules containing just two amino acids capable of forming superstructures, *i.e.* nanotubes [24].

In summary, manifold architectures of self-assembled nanostructures exist. All are intrinsically very interesting and have potential application not only in medicine and nanobiotechnology but also in solar cells and optical and electronic devices. Naturally occurring amino acids, as hydrophobic or hydrophilic components, contribute to the self-assembly and can respond to external stimuli. After performing their mission they degrade to prevent accumulation in the body.

Here we report the synthesis and characterization of amphiphilic oligopeptides while focusing on the self-assembly process. Inspired by gramicidin A (gA), the C-terminal sequence of the peptides consists of a truncated gA (gT) – a repetitive L-tryptophan – D-leucine [$_L$W-$_D$L] motif. The motif results in distinct *phi* and *psi* angles of the peptide backbone, whereas similarities in sequence between gramicidin and the amphiphilic peptides also suggest similarities in secondary structure[25]. Overall, the peptide is amphiphilic due to the N-terminal attached lysines (K) or acetylated lysines (X).

An overview of the synthesized peptides is given in Table 2-1 (for details, see Table S 2-1). We investigated the amphiphilic mini (11 AA) peptides by EPR, dynamic (DLS) and static light scattering (SLS) as well as transmission (TEM) and scanning electron microscopy (SEM). The focus was centered on the process that forms the superstructures as a function of temperature and solvent composition. To investigate the effect of electrostatic interactions on the self-assembly, charges on the molecule were removed by acetylation, while shielding by the addition of counter ions also proved effective.

Table 2-1: Code and sequence of charged (K) and uncharged (X = $_L$K(Ac)) amphiphilic peptides

Code	Sequence
K$_3$-gT	*H*-$_L$K$_3$-[$_L$W-$_D$L]$_3$-$_L$W-*NH$_2$*
C-K$_3$-gT	*H*-$_L$C-$_L$K$_3$-[$_L$W-$_D$L]$_3$-$_L$W-*NH$_2$*
Ac-X$_3$-gT	*Ac*-[$_L$K(Ac)]$_3$-[$_L$W-$_D$L]$_3$-$_L$W-*NH$_2$*
AcC-X$_3$-gT	*Ac*-$_L$C-[$_L$K(Ac)]$_3$-[$_L$W-$_D$L]$_3$-$_L$W-*NH$_2$*
AcC(sl)-X$_3$-gT	*Ac*-$_L$C(acetamidoproxyl)-[$_L$K(Ac)]$_3$-[$_L$W-$_D$L]$_3$-$_L$W-*NH$_2$*

2.3   Results and discussion

Similar to other amphiphiles, amphiphilic peptides are also expected to self-assemble into well-defined superstructures in aqueous solution. Here, we focused on peptides with a given hydrophobic [$_L$W-$_D$L]$_3$-$_L$W-*NH$_2$* sequence that was coupled to a hydrophilic tripeptide either based on a positively charged $_L$K$_3$ sequence or the corresponding, electrically neutral [$_L$K(Ac)]$_3$.

2.3.1   Dimerization capacity

The repetitive [$_L$W-$_D$L] sequence of our model peptides derives from gA, which is known to form dimers in apolar environment[26]. Hence, we expected that the C-terminus of our peptides would also be accessible for such intermolecular organization. The nature of the building blocks (monomeric vs. dimeric peptides) is expected to directly influence the structure of the resulting self-assemblies in aqueous media. Therefore we performed model experiments in organic solvents to probe the dimerization capacity of the peptides by GPC and EPR. The GPC elution profile for

gramicidin shows separation into mono- and dimers in different solvents[27] (THF, ethanol,Figure S 2-1). The elution profile of the amphiphilic peptide was characterized by a slightly broader peak with no indication of distinct dimerization.

EPR was used to further verify possible dimerization in solution. The spin-labeled amphiphilic peptide AcC(sl)-X$_3$-gT was dissolved in ethanol, in which gA is known to lead to dimerization[27]. Dimerization of the molecule can occur by association of the hydrophobic component in a head-to-head or in an intertwining configuration, both well-established forms for gA[28]. Either means of dimerization is expected to bring the two spin labels at the hydrophilic ends of the peptide into close proximity (2 – 3 nm range). Dzikovski[29] et al. found direct evidence of a head-to-head gA dimer in the dimyristoylphosphatidylcholine (DMPC) membrane with an interspin distance of 3.1 nm by double-quantum coherence (DQC) EPR.
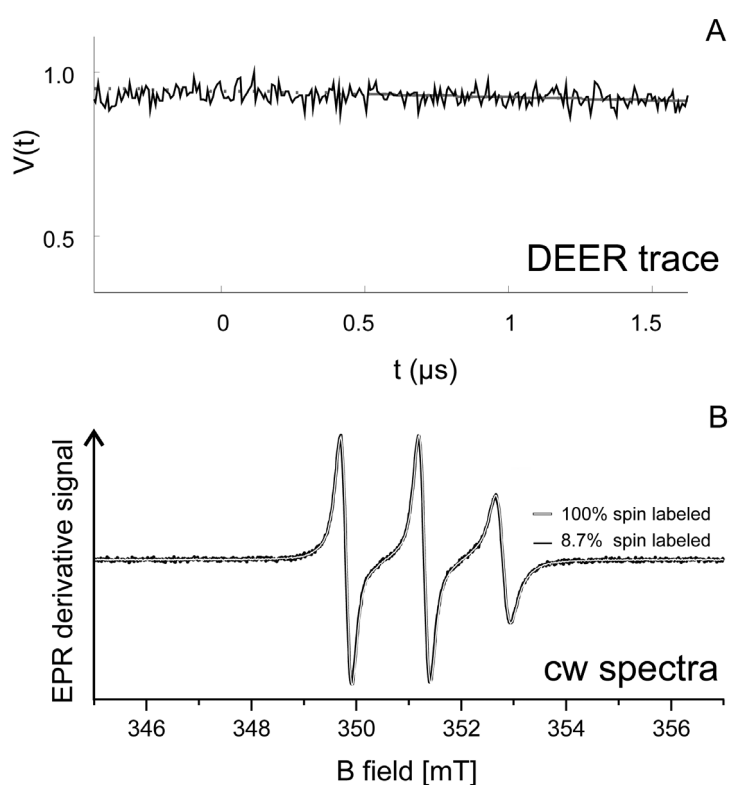
Figure 2-1: (A) Pulse double electron-electron resonance on 150 µM AcC(sl)-X$_3$-gT in ethanol in the presence of 50 v % deuterated glycerol and (B) cw EPR spectra on AcC(sl)-X$_3$-gT (300 µM, white line) as well as a AcC(sl)-X$_3$-gT/AcC-X$_3$-gT mixture (100 µM, black line) in ethanol.

Here, double electron-electron resonance (DEER), which is sensitive in the 1.7 – 8 nm range[30], was performed on AcC(sl)-X$_3$-gT in dd water. No DEER signal modulation from dipole-dipole interaction between electron spins was detected. Therefore, the trace clearly confirmed that no dimerization occurred (Figure 2-1A). To verify the possible presence of short interspin distances (< 2 nm), the spin labeled AcC(sl)-X$_3$-gT was spin-diluted with unlabeled AcC-X$_3$-gT. The continuous wave (cw) EPR spectra of AcC(sl)-X$_3$-gT at 100 wt % and 8.7 wt % (2:23 dilution with unlabeled AcC-X$_3$-gT) in ethanol are superimposed in Figure 2-1B. The identical spectral shapes at room temperature ruled-out the presence of short interspin distances.

In conclusion, both GPC and EPR showed that the amphiphilic peptides are monomeric in ethanol.

2.3.2 Charged amphiphilic peptide – C-K$_3$-gT

The hydrophilic building block C-K$_3$-gT possesses free amine functionalities on the lysine residues as well as a free N-terminus. Therefore, at neutral pH (pK of 10.2) the peptide is charged and self-assembly is constrained by electrostatic repulsion.

The peptide can be directly dissolved in an aqueous environment. In such, it exhibited a confined critical micelle concentration of cmc (C-K$_3$-gT) = 0.23 mmol/L (*cf.* Figure S 2-2), thus suggesting assembly into micelles and conventional surfactant behavior.

This is confirmed by DLS, indicating spherical micelles with a hydrodynamic radius of R$_h$ ≈ 10 nm. In addition – particularly at higher peptide concentrations – DLS indicated the presence of a minor fraction of larger aggregates with a hydrodynamic radius of approximately 160 nm. Indeed, TEM micrographs also showed that, besides the dominant micelle fraction, spherical objects of the mentioned dimension were occasionally found (Figure S 2-3). We hypothesize that these structures are formed by the aggregation of individual micelles into "multicompartment micelles", herein termed "peptide beads". Since the assembly of C-K$_3$-gT is strongly influenced by electrostatic interactions of the positively charged oligolysine groups, we expected that an equilibrium between micelles and peptide beads would be directly influenced by shielding the charges with appropriate counter ions. The Hofmeister series orders such ions according to their properties at interfaces [21b, 31]. Chaotropic ions, for example, increase surface tension and protein stability, in contrast to cosmotropic ions having the opposite effects.

Indeed, stepwise addition of small aliquots of concentrated salt solution to C-K$_3$-gT increased the fraction and size of the beads as monitored by DLS. The growth in size was similar for the different ions. The size of the peptide beads increased up to a salt concentration of 0.3 mol/L. Beyond that value only minor size changes were observed, indicating saturation and maximum shielding.

The final radii of the formed particles at salt concentrations of 0.6 mol/L essentially followed the Hofmeister series (Figure 2-2). Cosmotropic and chaotropic ions influenced the size and the relative fraction of the corresponding aggregates while "neutral" ions led to a minor response in the peptide assemblies. For chaotropic ions, we monitored salting out due to a decrease in solubility of the peptide, and therefore the amplification of the tendency to agglomerate.

Chaotropic ions lowered the interfacial tension and therefore affected the curvatures and dimensions of the peptide beads. Exemplary SEM of peptide particles in the presence of PO$_4^{3-}$ and SCN$^-$ are given in Figure S 2-4.

We found only one exception to the Hofmeister series. Despite their chaotropic nature, SCN$^-$ ions (Figure 2-2) still led to particles with relatively small radii. This is possibly due to a specific interaction that stabilizes the structure[32].
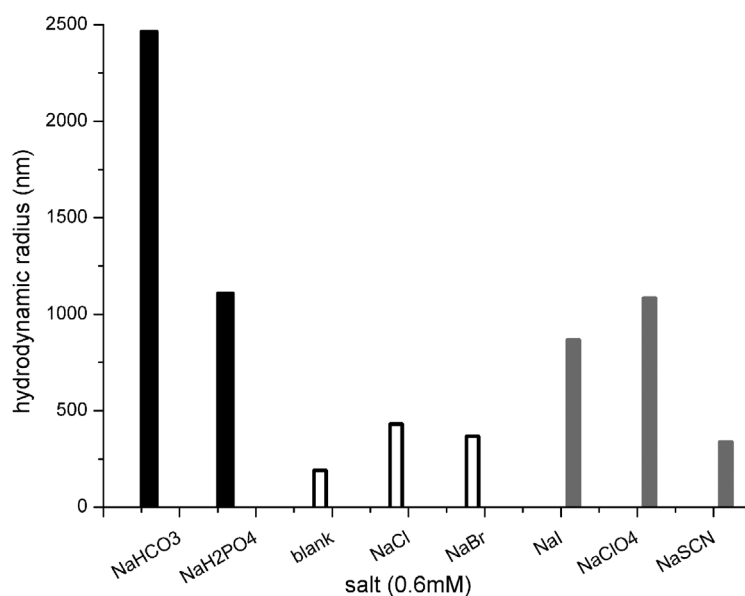
Figure 2-2: Effect of cosmotropic (black), neutral (white), and chaotropic anions (grey) on the self-assembly (radius).

2.3.3 Electrically neutral amphiphilic peptide – acetylated AcC-X$_3$-gT

It is obviously possible to manipulate self-assembly of the charged amphiphile by external factors (correct choice of counter ions). Therefore, we expected that a similar or even stronger effect could be induced by acetylation of the lysine residues, thus eliminating the electrostatic interactions. Consequently, the only difference between C-K$_3$-gT and AcC-X$_3$-gT is a lack of charges due to the acetylation of the primary amine functions. It should be noted, however, that acetylation to AcC-X$_3$-gT reduces hydrophilicity to the extent that the entire amphiphilic molecule does not dissolve directly in dd water. Therefore, the self-assembly process is induced by dissolving the peptide in ethanol and changing the surrounding polarity by exchanging the ethanol with dd water.

The self-assemblies formed by AcC-X$_3$-gT were characterized by SEM and TEM (Figure 2-3A and B). Indeed, this peptide also assembled into micelles and larger peptide beads. Interestingly in TEM the spherical particles display an indentation as shown in Figure 2-3 for AcC(sl)-X$_3$-gT. This phenomenon might be caused by solvent evaporating from the assembly during the sample preparation (drying). The self-assembly behavior proved to be insensitive to minor structural changes of the peptides. For example, for Ac-X$_3$-gT, AcC-X$_3$-gT (with an additional acetylated cysteine) or AcC(sl)-X$_3$-gT (carrying a spin label at the hydrophilic end), no difference was observed with any of the methods used (Figure 2-3 and Figure S 2-5). Thus, the labeled AcC(sl)-X$_3$-gT can be used as a valid "tool" to probe its self-assembly and that of its analogues.

Furthermore, no significant difference was observed between C-K$_3$-gT and K$_3$-gT. Therefore, a transfer of the information concerning the self-assembly process of the AcC-X$_3$-gT/C-K$_3$-gT system to the Ac-X$_3$-gT/K$_3$-gT system appears justified.
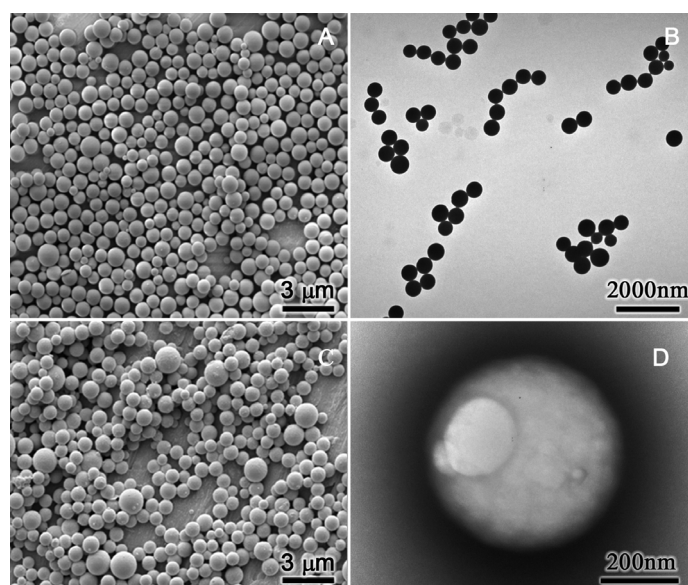
Figure 2-3: Representative SEM of (A) AcC-X$_3$-gT and (C) Ac-X$_3$-gT and TEM of (B) AcC-X$_3$-gT (D) AcC(sl)-X$_3$-gT after solvent exchange to dd water.

To obtain further insight into the self-assembly process upon solvent replacement, samples at different final ethanol concentrations (40 wt % − 0 wt % EtOH) were prepared and analyzed by EPR, DLS, and SLS.

The self-assembly process for AcC-X$_3$-gT (with 8.7% of AcC(sl)-X$_3$-gT and total initial peptide concentration of 1 mg/mL to ensure sufficient signal/noise ratio) was followed using EPR. The cw EPR spectra performed at different final ethanol concentrations showed two distinct species (Figure S 2-6), one characterized by narrow lines (so-called mobile species, with fast rotational correlation times) and one characterized by broad lines, large pseudo hyperfine splitting, which is typical of powder-like spectra (so-called immobile species, with slow rotational correlation times). The ratio of the two species varied with temperature and final ethanol concentration (Figure 2-4): Increasing the temperature together with the ethanol concentration led to an increase in the mobile species population. The mobile species was predominant at 40 wt % ethanol, with 65% of the total spectral area at 273 K. The immobile species, on the other hand, was the prevalent species at 4 wt % ethanol, with 100 to 98% of the spectral area in the 263 to 335 K range (Figure 2-4). The rotational correlation time ($\tau = 0.530$ ns at 293 K and 40 wt %) calculated for the micelle fraction at a size of 5.65 nm matched the rotational correlation time ($\tau = 0.531$ ns) obtained by simulating the spectrum with the fast motion regime EasySpin[33] "garlic" function using an isotropic model of motion. Thus, the mobile EPR species correlate with the micellar fraction. Similarly, the high correlation times of the immobile species (> 20 ns) correlate to the large dimensions observed for the peptide beads. The temperature and ethanol dependence of the EPR spectral fractions confirmed that both external factors can shift the equilibrium between the micelle and the peptide bead population.
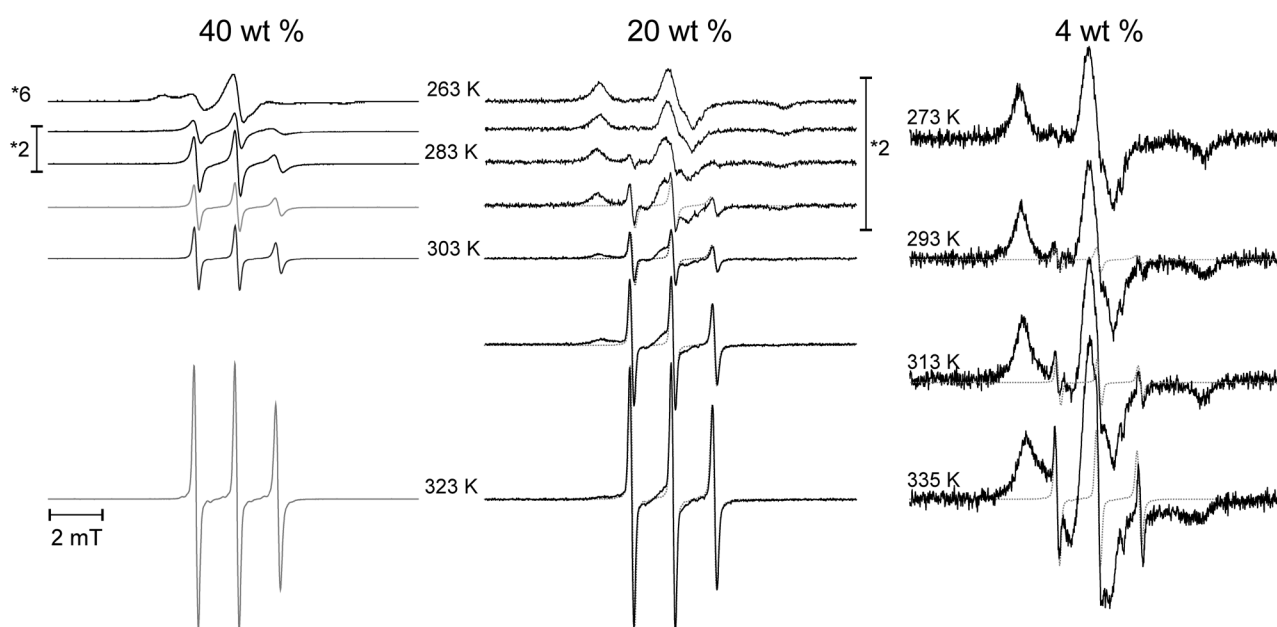
Figure 2-4: EPR spectra of AcC(sl)-X$_3$-gT / AcC-X$_3$-gT mixture as a function of final ethanol concentration and temperature. The spectra at 40 wt % EtOH were scaled and superimposed to the spectra obtained at the same temperature with different EtOH concentrations.

The self-assembly process for the same AcC-X$_3$-gT/ AcC(sl)-X$_3$-gT mixture (8.7%, c$_{tot}$ = 1 mg/mL) and final ethanol concentrations was monitored by DLS, which confirmed the observations from EPR. In the dissolved state in pure ethanol, no significantly higher scattering intensity was observed than for that of pure ethanol, indicating molecularly dissolved peptides. For water/ethanol mixtures, data were analyzed by the CONTIN algorithm and revealed up to three different species (correlation functions are given in Figure S 2-7). One species was found with a hydrodynamic radius in the range of 5 – 10 nm, which corresponds well with the size of micelles. With decreasing ethanol concentration an increasing fraction of larger particles at 100 – 150 nm was also present. At less than 20 wt % ethanol, a third species with a greater radius (*e.g.* R$_h$ ≈ 350 nm at 4 wt %) appeared and became the dominant species. It apparently emerged from the second species, since we found no structurally different morphologies in the final stage of the self-assembly. Nevertheless these particles have an increased radius and thus are considered a "matured" second species. It should be emphasized that the formation of the final particles was fully reversible; upon addition of ethanol the fraction of the second species increased to the diminishment of the third. Also, the self-assembly of the synthesized peptides into micelles and peptide beads was found to be a reversible process and the equilibrium between the different species was independent of the sample preparation (for example, see Figure S 2-8). The transition was also able to be induced by temperature variation: absorbance measurements allowed us to directly track the reversible formation of the final "matured" peptide particles (see Figure S 2-9 for temperature dependent absorbance measured at 20 wt % ethanol). Interestingly, the formation of the final "matured" peptide particles in dd water also depended on the initial concentration of the peptide in ethanol. The hydrodynamic radius remained constant at R$_h$ ≈ 130 nm up to an initial peptide concentration of approx. 0.5 mg/mL. For concentrations higher than 0.5 mg/mL the size of the peptide beads increased linearly with the initial peptide concentration (Figure 2-5 and SEM micrographs Figure S 2-10). Obviously, the onset of the second growth process requires a certain

"critical peptide concentration" similar to the critical micelle concentration of detergents. However, further experiments are needed to understand this process.
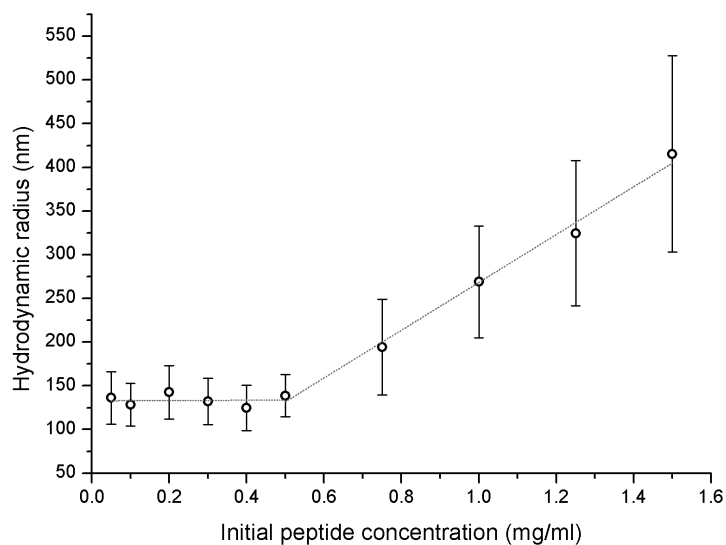

Figure 2-5: Size dependency of final peptide beads in dd H_2O upon initial peptide concentration. Error bars reflect the relative peak width from DLS (2nd cumulant analysis).

To derive further information on the structure and composition of the different peptide particles we performed static light scattering for dispersions at different final ethanol concentrations. For all samples the initial peptide concentration in pure ethanol was 1 mg/mL. The desired solvent composition was adjusted by solvent exchange and kept constant during the subsequent dilution steps. Figure 2-6A shows a representative Guinier-Plot for a peptide dispersion in a solvent mixture at 4 wt % ethanol. Under these conditions the radius of gyration of the particles was only slightly dependent on the final solvent composition. At the same time, the molar mass (M_w) of the particles drastically increased (*i.e.* by a factor of 500) with decreasing fraction of ethanol in the final dispersion. At the lowest final ethanol concentration of 4 wt % the particles had an M_w of $1.73 \cdot 10^{10}$ gmol^{-1}, corresponding to a particle composed of approximately 10^7 peptide molecules (Table 2-2).

Table 2-2: SLS summary for peptide beads in different EtOH concentrations.

EtOH wt %	R_g nm	M_w g mol^{-1}	A_2 mol dm³ g^{-2}	N_{AG}	δ_{app} g cm^{-3}
40	179	3.76×10^7	8.342×10^{-10}	2.14×10^4	0.006
30	189	1.61×10^8	-2.430×10^{-8}	9.16×10^4	0.02
20	201	2.44×10^9	-4.231×10^{-11}	1.39×10^6	0.26
12	210	1.01×10^{10}	2.857×10^{-10}	5.77×10^6	0.93
4	218	1.73×10^{10}	2.895×10^{-10}	9.87×10^6	1.44

Assuming the particles behave like homogenous hard spheres, an apparent density δ_{app} of the particles can be calculated accordingly[34]. Interestingly, the apparent density of the particles increased from 0.006 g cm^{-3} at 40 wt % ethanol to 1.44 g cm^{-3} at 4 wt % ethanol. Molar masses and

apparent densities at higher final ethanol concentrations (> 20%) can only be used as a rough estimate, since here a considerable fraction of small micelles, coexisting with the peptide beads, contributed negligibly to the scattering intensity. Nevertheless our data clearly indicate a transition from a loosely packed, highly solvent-swollen aggregate to more homogenous particles mainly consisting of densely packed peptides. Indeed, the observed value is in agreement with typical data for peptides [35] and consistent with the observed sedimentation of the particles.
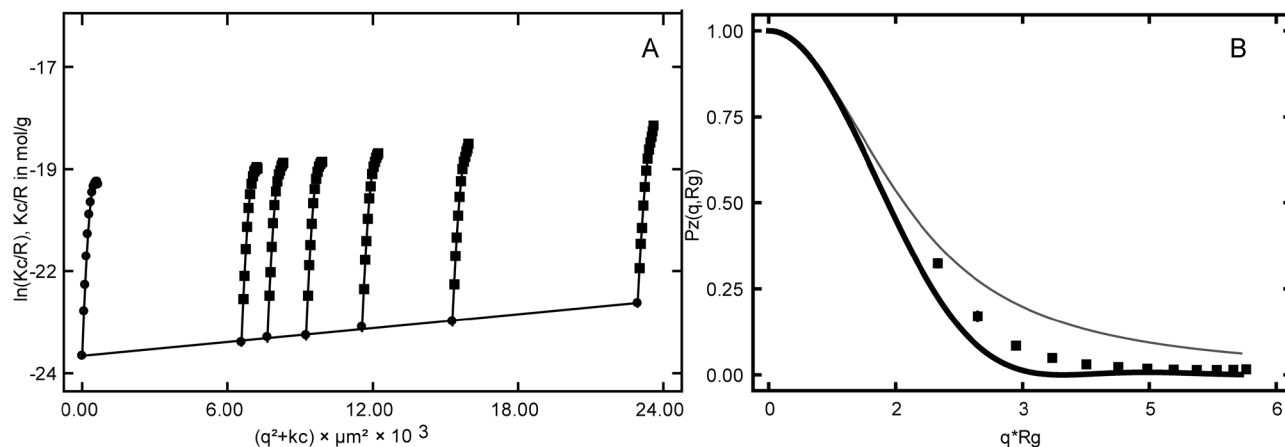

Figure 2-6: (A) Guinier plot of peptide beads in 4 wt % ethanol extrapolated to zero angle and concentration (B) Dependence of the particle scattering factor Pz on q for hard sphere (black line) and coil (grey line) compared with representative experimental data for 4 wt % Guinier plot (■).

Figure 2-6B shows the angular dependence of the particle scattering factor of the peptide beads. For comparison, the well-established theoretical functions for homogenous hard spheres (Figure 2-6B, black line, equation 3 in experimental part: *chapter 9.5*) and monodisperse polymer coils (Figure 2-6B, gray line, equation 4 in experimental part: *chapter 9.5*) have been included in the plot. Indeed, our data resemble the function for hard spheres, thus supporting the assumption of particles with a rather homogenous density distribution. It should be noted that the data for different final ethanol concentrations hardly differed, indicating that, during the "condensation" to more densely packed particles, their basic structure did not change significantly.

Thus, we hypothesize that the particles are formed by a hierarchical assembly process, starting with the formation of micelles that further aggregate into "multicompartment micelles" or peptide beads that increase their packing density and aggregation number with decreasing ethanol concentration. *Chapter 3* describes further experiments to clarify the inner structure of the particles.

In complementary experiments we used fluorescence quenching to analyze the accessibility of tryptophan within the aggregates. Here, the tryptophan fluorescence of the peptide $AcC-X_3-gT$ in 40 wt % ethanol was quenched with acrylamide. The comparison to lower ethanol concentrations was not possible due to scattering; therefore a pure tryptophan solution was used. The Stern-Volmer plots (Figure 2-7) deviate from a straight line, exhibiting a distinct upward curvature. Therefore, the data were fitted taking the contributions from static quenching and transient effects into account[36]. The Stern-Volmer constant K_{SV} for $AcC-K_3-gT$ (4.8 ± 0.3 M^{-1}) is in good agreement with literature values for gA in its molecularly dissolved state, indicating that the

tryptophans are freely accessible for the quencher[35b]. Obviously, there is no significant difference in accessibility between molecularly dissolved Trp-OH and the peptide self-assembly at 40 wt % ethanol (Figure 2-7). Hence, our results show that the micelles and peptide beads at 40 wt % ethanol do not possess barriers to penetration by acrylamide. This is in good agreement with the data from SLS, indicating a low packing density of the peptides inside the particles at rather high ethanol concentrations.
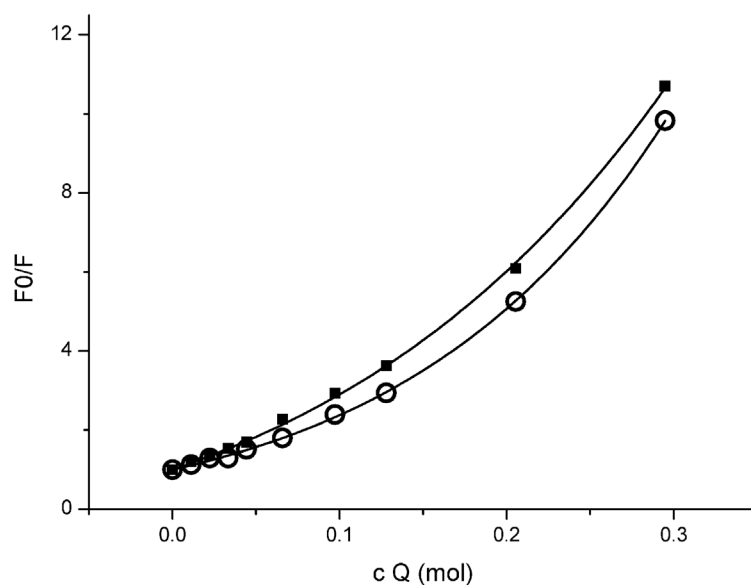
Figure 2-7: Stern-Volmer-Plot of AcC-X$_3$-gT in 40 wt % ethanol (○) and tryptophan (■) with increasing quencher concentration, indicating good accessibility of the tryptophans within the peptide self-assembly at 40 wt % ethanol.

2.4 Conclusion

This chapter describes an amphiphilic undecapeptide capable of forming micelles and peptide particles in aqueous-ethanol mixtures as a function of ethanol concentration and temperature. A repetitive [$_L$W-$_D$L] motif was introduced, which is the essential part of the peptide and which can be used as a general hydrophobic contributor in an amphiphilic molecule. The sequence was extended with a positively charged, hydrophilic lysine-, or an electrically neutral acetylated lysine group. The peptide with a charged oligolysine showed a well-defined cmc in aqueous solution and initially formed spherical micelles. An increasing fraction of larger aggregates, presumably multicompartment micelles, is formed as a result of increasing charge screening with appropriate counter ions. The acetylated lysine of the hydrophilic component of AcC-K$_3$-gT is less water soluble than the amphiphilic peptide based on the non-acetylated lysine. Generally, for the acetylated peptide, decreased solubility obviously favors a secondary aggregation of the individual micelles. The self-assembly process was initiated by solvent exchange. The experiments suggest that the hierarchical self-assembly of spherical aggregates from the investigated mini amphiphilic peptides starts in a dissolved monomeric state in pure ethanol. With increasing water concentration it evolves into a micellar solution. Once a threshold of solvent polarity is exceeded (*i.e.* decreasing ethanol concentration) the micelles themselves start aggregating into highly solvent-swollen particles or multicompartment micelles. The "open" and liquid structure of these primary

multicompartment micelles is also reflected by fluorescence quenching experiments with acrylamide, indicating free access of the quencher to the tryptophan residues within the aggregates. The peptide beads further condense and presumably fuse with residual small micelles below 20 wt % ethanol. This is reflected by a drastically increasing aggregation number and a considerably higher apparent density. It has to be emphasized, that a decreasing ethanol concentration ultimately led to rather rigid peptide particles that preserved their shape and dimensions even after isolation from the aqueous dispersion.
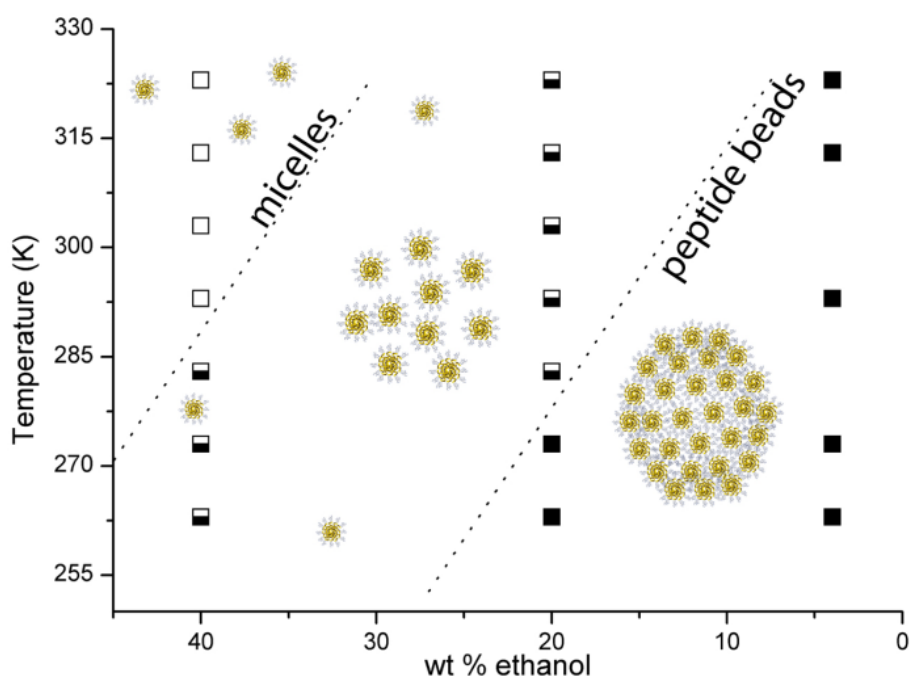
Figure 2-8: Phase diagram of the self-assembly of amphiphilic peptides in the multicompartment micelle model deduced from EPR measurement (■) >95% peptide beads, (◨) > 95% micelles, half-full squares refer to coexistence of micelles and peptide beads.

Macroscopically, the system can be described as an emulsion or suspension, depending on the concentration of ethanol. The organic solvent acts as the softener that keeps the separated peptide phase in a liquid state. As it is removed the droplets harden and form a suspension. Figure 2-8 shows a phase diagram summarizing the findings. Additional experiments are described in the next chapter of this thesis, to clarify the "inner" structure of the peptide beads. It should be emphasized that the transitions between the different species and/or their fractions in the mixtures were fully reversible. For the construction of the phase diagram data points from EPR measurements that allowed a convenient quantification of the respective species in the dispersions were used. Data from light scattering are in good agreement with these results. Furthermore, the structure of these multicompartment micelles or peptide beads at the same time offers hydrophilic and hydrophobic compartments that can be used to embed, for example, drugs (*cf. chapter 6*). Indeed, the system presented here was shown to encapsulate water soluble and –insoluble model drugs in high concentrations[25] and shows promise as a novel and bio-compatible drug delivery tool, as it is exclusively composed of amino acids.

2.5 Supporting information

Dimerization probed by GPC

Figure S 2-1 illustrates GPC elution profiles of Ac-X$_3$-gT and gramicidin in THF and EtOH, whereby a clear separation of monomer and dimer was visible as two peaks for gramicidin only. The amphiphilic peptide elution profile was characterized by a slightly broader peak and no indication of distinct dimerization.
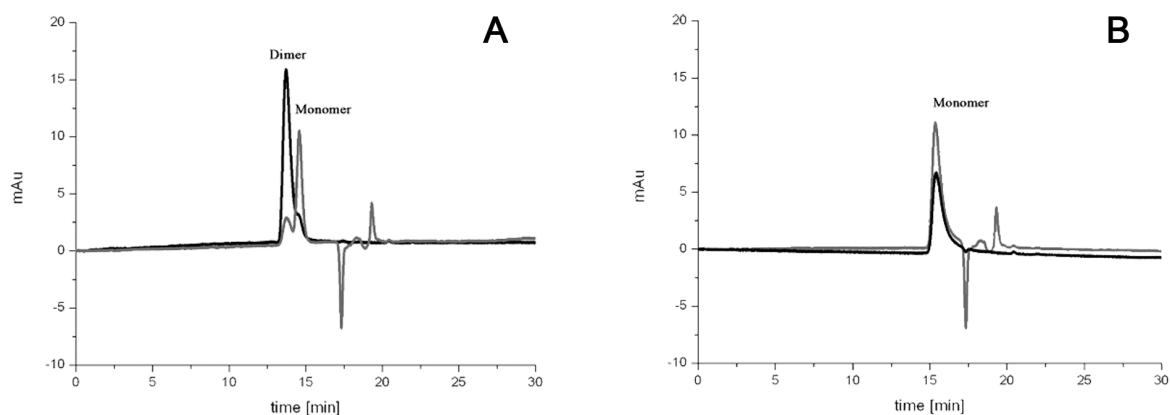
Figure S 2-1: A) GPC elution profiles of gramicidin monomer and dimer, and B) Ac-X$_3$-gT monomers in different solvents (THF black line, EtOH grey line).

Table S 2-1: Verification of mass and purity of the amphiphilic peptides used.

Code	Mass g/mol	Mass (MALDI-ToF-MS)	Purity (Area %, analytical HPLC)
K$_3$-gT	1485,9	1486.7	> 99 %
C-K$_3$-gT	1589,9	1588.6	97 %
Ac-X$_3$-gT	1653,9	1677.3 (M+Na$^+$)	98 %
AcC-X$_3$-gT	1757,9	1779.0 (M+Na$^+$)	96 %
AcC(sl)-X$_3$-gT	1947,0	1948.5	97 %

Behavior of C-K$_3$-gT as a surfactant

Amphiphilic peptides behave like surfactants. It therefore was possible to determine a critical micelle concentration (cmc), as illustrated in Figure S 2-2).
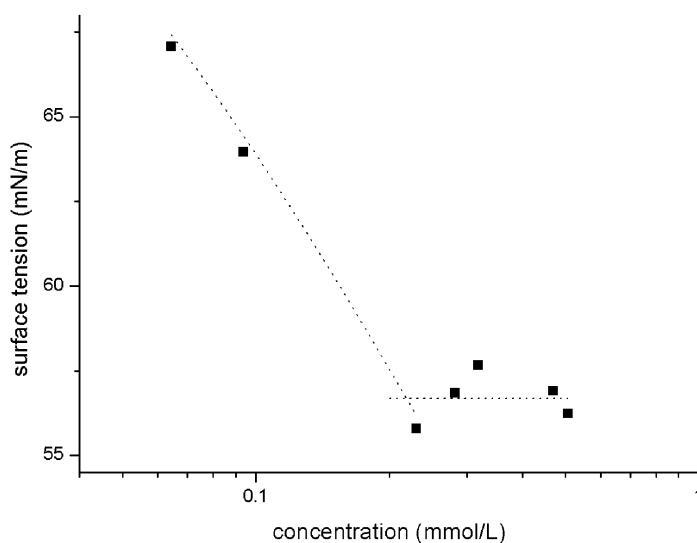
Figure S 2-2: Cmc determination of C-K$_3$-gT.

Self-assembly of C-K$_3$-gT into micelles
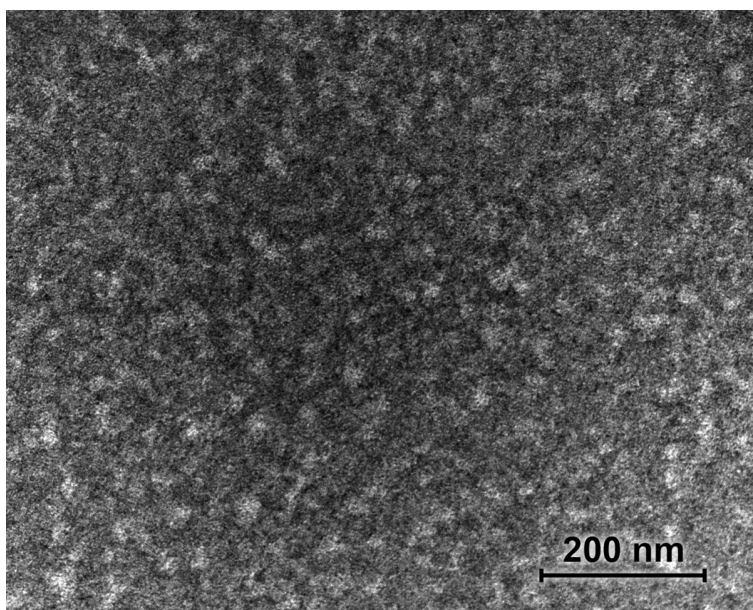
Figure S 2-3: Representative TEM image of C-K$_3$-gT micelles. The minor peptide bead fraction, which is not present in this micrograph, can be seen in the diagram shown in Figure 2-2 (blank) and Figure S 3-2.

Peptide bead formation due to charge shielding
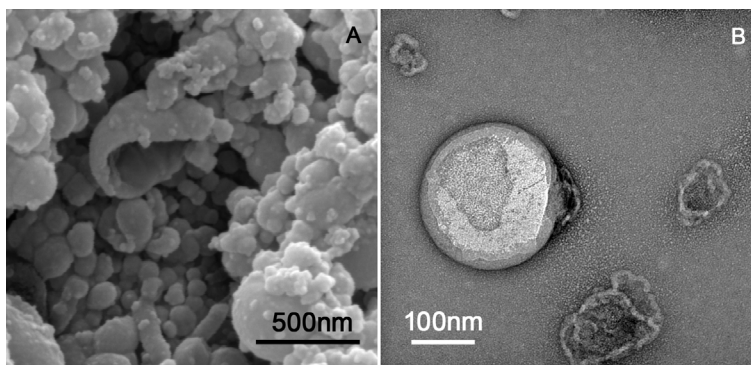
Figure S 2-4: A) SEM of C-K_3-gT with NaH$_2$PO4 (0,025mol/L) B) TEM of AcC-K_3-gT with NaSCN (0.1mol/L).

Self-assembly of Ac-X$_3$-gT

Self-assembled spherical structures – so-called peptide beads – from Ac-X$_3$-gT were imaged using SEM, TEM, and AFM (Figure S 2-5).
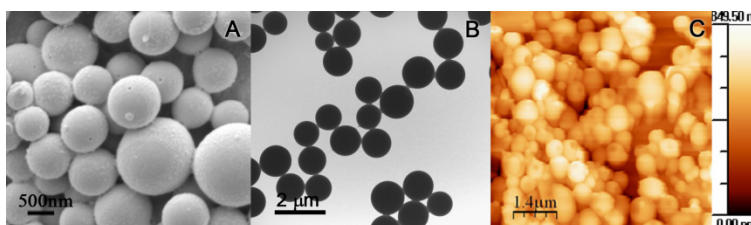
Figure S 2-5: A) SEM of Ac-X$_3$-gT peptide beads, B) TEM stained with uranyl acetate and C) AFM.

Cw EPR measurements in different ethanol/water mixtures
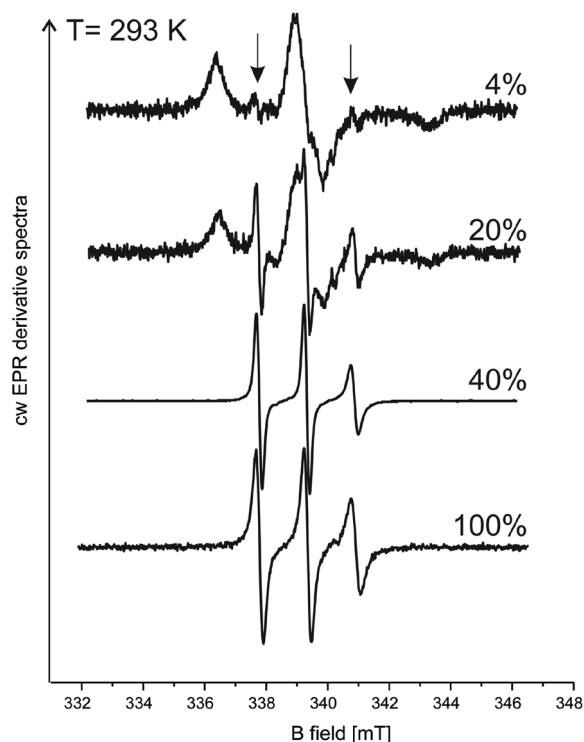
Figure S 2-6: cw EPR spectra of AcC-X_3-gT / AcC(sl)-X_3-gT mixtures depending of ethanol concentration. Arrows mark the characteristic features of the mobile species, which are getting dominant with increasing ethanol concentration.

Correlation functions
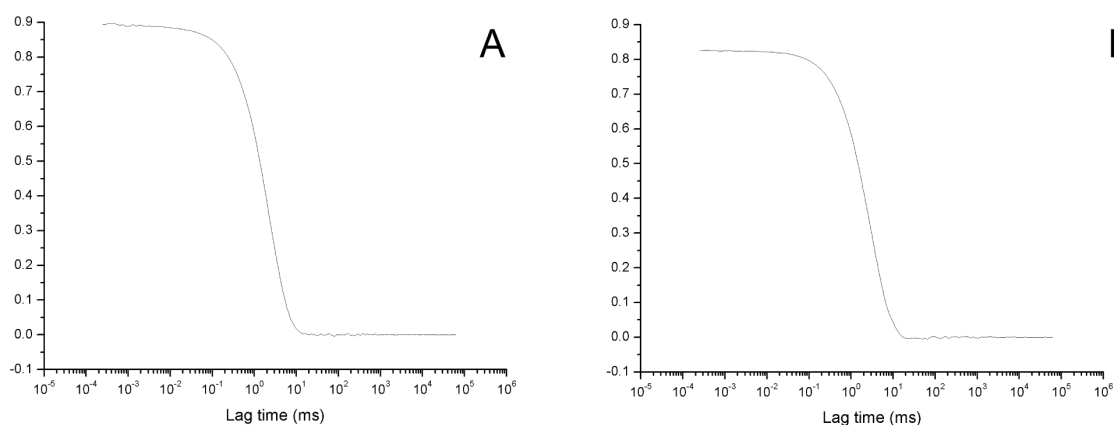
Figure S 2-7: Correlation functions of AcC-X_3-gT/AcC(sl)-X_3-gT mixture in A) 40 wt % ethanol and B) 4 wt % ethanol.

Equilibrium of Ac-X$_3$-gT in ethanol mixtures

Equilibrium between micelles and peptide beads arises in ethanol/water mixtures. Converting peptide solutions at 4 wt % ethanol to 40 wt % ethanol and vice versa (using dialysis) always produces the same characteristic DLS signals, proving the reversibility of the system. A diagram of the experiment and the corresponding results are presented in Figure S 2-8.
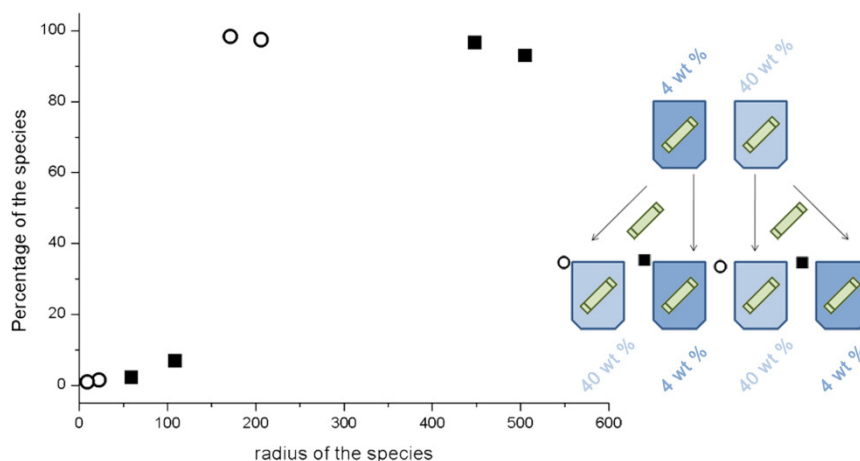
Figure S 2-8: Reversibility of the system: Two different starting points (4 wt % and 40 wt %) yield the same DLS features at 4 wt % (■) and at 40 wt % (○) final ethanol concentration.

Temperature-dependent self-assembly of Ac-X$_3$-gT

The self-assembly process was initiated by solvent exchange from 100 w % to 20 wt % ethanol. A reversible, temperature-dependent peptide bead formation was monitored at that ethanol concentration. Temperature-dependent UV absorption measurements tracked bead formation as absorption increased due to scattering. As Figure S 2-9 shows, peptide beads begin to assemble below 25 °C at 20 wt % ethanol. This process was reversible. The cooling (black line) - heating (red line) cycle exhibits a slight hysteresis due to the experimental setup.
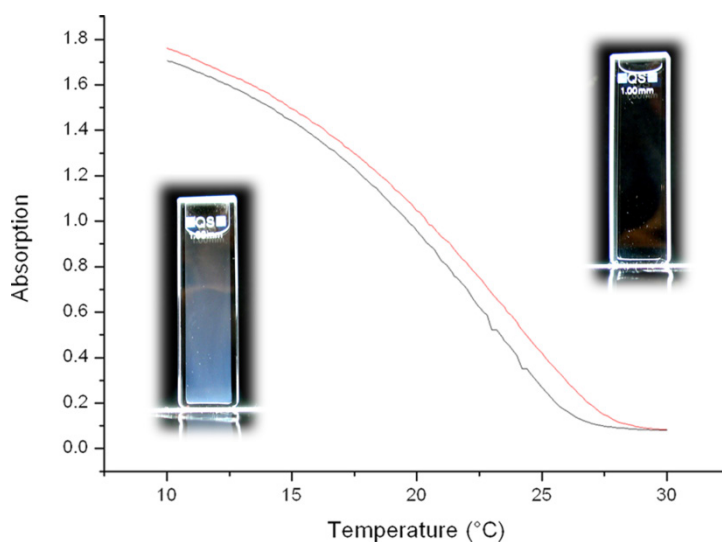
Figure S 2-9: UV measurement of temperature-dependent bead formation (heating (red line), cooling (black line)) using Ac-X$_3$-gT at 20 wt % EtOH. Photographs were taken at 4 °C (left) and RT (22 °C, right).

Size dependency of peptide beads in dd H$_2$O upon initial peptide concentration
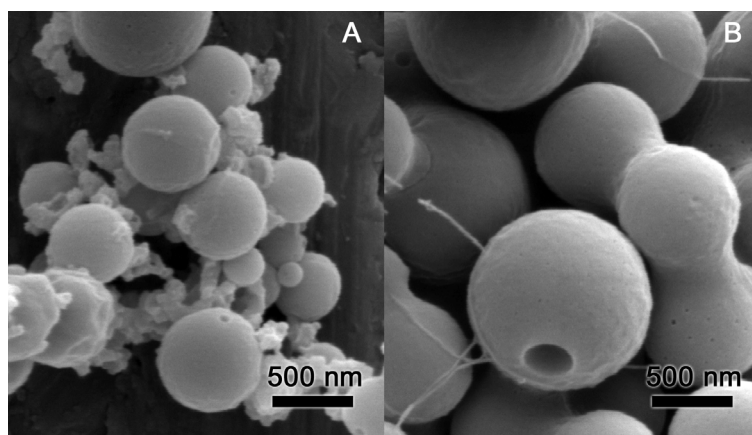
Figure S 2-10: SEM micrographs of Ac-X$_3$-gT at A) 1.0 mol/L B) 1.5 mol/L.

2.6 References

[1] C. Allen, D. Maysinger and A. Eisenberg, *Colloid Surface B* **1999**, *16*, 3-27.

[2] S. F. M. van Dongen, H.-P. M. de Hoog, R. J. R. W. Peters, M. Nallani, R. J. M. Nolte and J. C. M. van Hest, *Chemical Reviews (Washington, DC, United States)* **2009**, *109*, 6212-6274.

[3] a) F. Axthelm, O. Casse, W. H. Koppenol, T. Nauser, W. Meier and C. G. Palivan, *Journal of Physical Chemistry B* **2008**, *112*, 8211-8217; b) G. Delaittre, I. C. Reynhout, J. J. L. M. Cornelissen and R. J. M. Nolte, *Chem.-Eur. J.* **2009**, *15*, 12600-12603, S12600/12601-S12600/12615.

[4] M. Kumar, M. Grzelakowski, J. Zilles, M. Clark and W. Meier, *Proceedings of the National Academy of Sciences of the United States of America* **2007**, *104*, 20719-20724.

[5] R. Nehring, C. G. Palivan, O. Casse, P. Tanner, J. Tuxen and W. Meier, *Langmuir* **2009**, *25*, 1122-1130.

[6] a) D. Peer, J. M. Karp, S. Hong, O. C. Farokhzad, R. Margalit and R. Langer, *Nature Nanotechnology* **2007**, *2*, 751-760; b) V. Balasubramanian, O. Onaca, R. Enea, D. W. Hughes and C. G. Palivan, *Expert Opinion on Drug Delivery* **2010**, *7*, 63-78.

[7] F. Ahmed, R. I. Pakunlu, A. Brannan, F. Bates, T. Minko and D. E. Discher, *Journal of Controlled Release* **2006**, *116*, 150-158.

[8] a) J. Sun, Q. Shi, X. Chen, J. Guo and X. Jing, *Macromol. Chem. Phys.* **2008**, *209*, 1129-1136; b) Y. Yu and A. Eisenberg, *Journal of the American Chemical Society* **1997**, *119*, 8383-8384; c) L. Zhang and A. Eisenberg, *Science (Washington, D. C.)* **1995**, *268*, 1728-1731.

[9] J.-F. Lutz and A. Laschewsky, *Macromolecular Chemistry and Physics* **2005**, *206*, 813-817.

[10] A. Carlsen and S. Lecommandoux, *Curr. Opin. Colloid Interface Sci.* **2009**, *14*, 329-339.

[11] A. Mitra, J. Mulholland, A. Nan, E. McNeill, H. Ghandehari and B. R. Line, *J. of Controlled Release* **2005**, *102*, 191-201.

[12] E. P. Holowka, V. Z. Sun, D. T. Kamei and T. J. Deming, *Nat. Mater.* **2007**, *6*, 52-57.

[13] D. F. Evans, *The Colloidal Domain: Where Physics, Chemistry, Biology, and Technology Meet, 2nd*, **1998**, p. 640 pp.

[14] R. Fairman and K. S. Akerfeldt, *Current Opinion in Structural Biology* **2005**, *15*, 453-463.

[15] J. Rao, Z. Luo, Z. Ge, H. Liu and S. Liu, *Biomacromolecules* **2007**, *8*, 3871-3878.

[16] J. Lin, J. Zhu, T. Chen, S. Lin, C. Cai, L. Zhang, Y. Zhuang and X.-S. Wang, *Biomaterials* **2009**, *30*, 108-117.

[17] a) V. Malinova, S. Belegrinou, D. de Bruyn Ouboter and W. P. Meier, *Adv. Polym. Sci.* **2010**, *224*, 113-165; b) A. Koide, A. Kishimura, K. Osada, W.-D. Jang, Y. Yamasaki and K. Kataoka, *J. Am. Chem. Soc.* **2006**, *128*, 5988-5989.

[18] a) E. G. Bellomo, M. D. Wyrsta, L. Pakstis, D. J. Pochan and T. J. Deming, *Nature Materials* **2004**, *3*, 244-248; b) E. P. Holowka, D. J. Pochan and T. J. Deming, *J. Am. Chem. Soc.* **2005**, *127*, 12423-12428.

[19] J. Rodriguez-Hernandez and S. Lecommandoux, *J. Am. Chem. Soc.* **2005**, *127*, 2026-2027.

[20] a) M. R. Dreher, A. J. Simnick, K. Fischer, R. J. Smith, A. Patel, M. Schmidt and A. Chilkoti, *J. Am. Chem. Soc.* **2008**, *130*, 687-694; b) A. J. van Hell, C. I. C. A. Costa, F. M. Flesch, M. Sutter, W. Jiskoot, D. J. A. Crommelin, W. E. Hennink and E. Mastrobattista, *Biomacromolecules* **2007**, *8*, 2753-2761.

[21] a) M. Heim, L. Roemer and T. Scheibel, *Chemical Society Reviews* **2010**, *39*, 156-164; b) U. K. Slotta, S. Rammensee, S. Gorb and T. Scheibel, *Angewandte Chemie, International Edition* **2008**, *47*, 4592-4594.

[22] S. Santoso, W. Hwang, H. Hartman and S. G. Zhang, *Nano Letters* **2002**, *2*, 687-691.

[23] D. J. Adams, K. Holtzmann, C. Schneider and M. F. Butler, *Langmuir* **2007**, *23*, 12729-12736.

[24] a) M. Reches and E. Gazit, *Science (Washington, DC, U. S.)* **2003**, *300*, 625-627; b) M. Reches and E. Gazit, *Nature Nanotechnology* **2006**, *1*, 195-200.

[25] C. Dittrich and W. Meier, *Macromolecular Bioscience* **2010**, *10*, 1406-1415.

[26] W. R. Veatch, E. T. Fossel and E. R. Blout, *Biochemistry* **1974**, *13*, 5249-5256.

[27] L. Braco, M. C. Bano and C. Abad, *J. Chem. Educ.* **1992**, *69*, A113-A116.

[28] B. A. Wallace, *Journal of Structural Biology* **1998**, *121*, 123-141.

[29] B. G. Dzikovski, P. P. Borbat and J. H. Freed, *Biophys. J.* **2004**, *87*, 3504-3517.

[30] M. Pannier, S. Veit, A. Godt, G. Jeschke and H. W. Spiess, *Journal of Magnetic Resonance* **2000**, *142*, 331-340.

[31] W. Kunz, P. Lo Nostro and B. W. Ninham, *Curr. Opin. Colloid Interface Sci.* **2004**, *9*, 1-18.

[32] A. Aroti, E. Leontidis, M. Dubois, T. Zemb and G. Brezesinski, *Colloids and Surfaces, A: Physicochemical and Engineering Aspects* **2007**, *303*, 144-158.

[33] S. Stoll and A. Schweiger, *Journal of Magnetic Resonance* **2006**, *178*, 42-55.

[34] O. Stauch, R. Schubert, G. Savin and W. Burchard, *Biomacromolecules* **2002**, *3*, 565-578.

[35] a) W. S. Davidson and G. M. Hilliard, *J. Biol. Chem.* **2003**, *278*, 27199-27207; b) S. S. Rawat, D. A. Kelkar and A. Chattopadhyay, *Biophys. J.* **2004**, *87*, 831-843.

[36] M. R. Eftink and C. A. Ghiron, *Biochemistry* **1976**, *15*, 672-680.

3 Hierarchical organization of purely peptidic amphiphiles into peptide beads

Dirk de Bruyn Ouboter[a], Thomas B. Schuster[a], Alexandre Mantion[b], Wolfgang Meier[a]

[a]Department of Chemistry, University of Basel, Klingelbergstrasse 80, CH-4056 Basel, Switzerland.
[b]BAM Federal Institute for Materials Research and Testing, Richard-Willstätter-Str. 11, 12489 Berlin, Germany
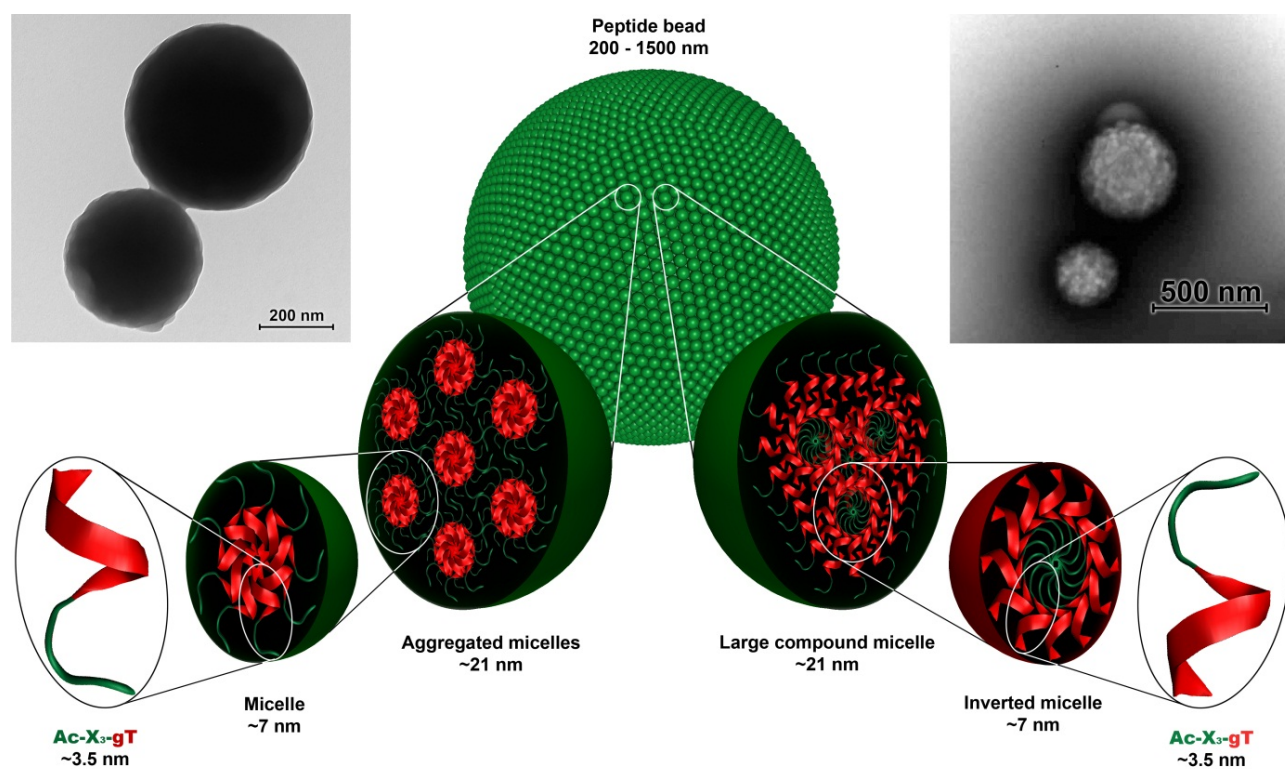
Two models of the hierarchical self-assembly of the peptide Ac-X$_3$-gT into peptide beads. TEM and SEM of the formed beads for comparison (left and right top corners).

Parts of this chapter were published in:

3.1 Abstract

This chapter focuses on the resolution of the inner structure of the spherical peptide particles, termed "peptide beads". The beads, with diameters between 200 to 1500 nm, result from hierarchical organization of micellar-like structures, a fact determined by a combination of investigations carried out by electron and atomic force microscopy (AFM), static and dynamic light-, and small angle X-ray scattering. These highly ordered structures agree with the concept of multicompartmentization and represent the first example of supramicellar assemblies based purely on peptides. New structural insights, as presented here, allow a better understanding of the peptide beads' capacity to embed hydrophobic and hydrophilic payloads and therefore provide new perspectives for drug delivery applications that may result from this new class of material.

3.2 Introduction

Future advanced materials will no longer rely merely on the chemical structure of a molecule *per se* but also on supramolecular chemistry, focusing on properties that emerge and are enabled by the assembly of a distinct number of molecular subunits. By exploiting non-covalent interactions, these systems come to possess new properties that reach beyond those of single molecules in bulk. The construction of advanced materials should exploit a bottom-up strategy that relies on self-assembly to allow large scale fabrication. Nature itself makes use of such systems, with enzymes and other proteins having well-defined secondary (α-helix, β-sheet) and quaternary structures (3D-assembly of individual subunits); each structure exhibiting distinct properties and thereby the potential for distinct functioning. Many of these possible functions may be lost without the well-controlled folding and assembly of a proteins' primary structure (sequence) into a precise secondary and quaternary structure. Small changes in the primary structure alone can perturb the assembly of the protein, along with its function. The precise folding of a protein or a small peptide from a linear sequence to a complex machine (e.g., an enzyme) may be considered self-assembly[1].

Based on virtually unlimited synthetic control over primary structure and ease of implementing point mutations, peptides represent fruitful molecules for the study of how self-assembly is controlled by the chemical structure of individual building blocks. Furthermore, peptidic materials are preferred for applications in the human body, due to a high level of biocompatibility and established degradation pathways that eliminate unwanted accumulation.[2]

Hybrid materials have been developed to combine the functionality of peptides with the versatility of hydrophobic/hydrophilic triggering of self-assembly[3]. Based on this concept, several groups have built peptide-based supramolecular assemblies by taking a non-peptidic hydrophobic contributor such as alkyl chains[4], poly(butadiene)[5] or modified amino acids (AAs)[6] and attaching a peptidic hydrophilic part. Other approaches use only AAs as building blocks[7], but are clearly inspired by macromolecular block-amphiphiles[8]. Although such systems form supramolecular functional materials, the polymeric character rules out the possibility of point mutations and therefore the ability for fine tuning. Short peptidic amphiphiles overcome this limitation. As Zhang

and Zhao[9] demonstrated, short peptides form various self-assembled structures, but in general it is difficult to build a purely hydrophobic block from peptides[10], due to the influence of the ubiquitous peptidic backbone and its hydrophilic amide bonds, which prevent a sequence from being hydrophobic throughout. The simple insertion of hydrophobic amino acids is therefore not enough. However, hiding the backbone within a helical secondary structure reduces influences by the surroundings. The influences of the backbone's hydrogen bonds in the hydrophobic part are therefore restricted to *intra*molecular interactions. This concept already emphasizes the need for a particular secondary structure to enable the formation of an amphiphilic diblock peptide.

We recently reported the synthesis, purification and characterization of *purely* peptidic amphiphiles[11] and provided insights into the process of self-assembly of the peptides into micelles and solid, spherical particles, termed "peptide beads" [12] (*cf. chapter 2*). The hydrophobic block, is inspired by the sequence and secondary structure of gramicidin A (gA), which is consistently constructed of hydrophobic amino acids that hide its backbone inside a β-helical secondary structure[13]. Moreover, due to its highly hydrophobic nature and its compatibility with the hydrophobic core of phospholipid membranes[14], gA is a suitable hydrophobic constituent. Governed by the affinity of gA-channels for one another, they are able to form rafts in lipid bilayers[15]. MacDonald et al.[15] as well as Brasseur et al.[16] suggested that this affinity originates as a result of the stacking of tryptophanes; they also calculated the spatial alignment by means of molecular dynamics simulations[16]. These considerations are additionally supported by the work of Kimura et al. who synthesized hybrid materials from gA and hydrophilic PEG and observed colloidal behavior in aqueous solution[17].

Although *chapter 2* suggested a hierarchical self-assembly process for the peptide beads, the used methods were not capable – due to lack of structural insight into the beads – to indisputably prove a persistence of previously formed micelles within the peptide beads formed subsequently. In this chapter we are interested to enter into structural details of the supramolecular assemblies generated by hierarchical self-assembly of purely peptidic amphiphiles. Understanding the underlying inner structure will allow a better understanding and prediction of the capacity of the peptide beads to embed hydrophobic as well as hydrophilic payloads[11]. This will support further applications in payload embedding and triggered release mechanisms. We performed microscopic and scattering experiments, established to characterize multicompartment micellar structures. The model of hierarchical self-assembly we propose, leads to a reasonable explanation of the embedding features of the peptide beads that support this new class of material during the development towards applications in drug delivery.

3.3 Results and discussion

The peptide K_3-gT is formed by N-terminal addition of three lysines to a truncated amino acid sequence of gA that corresponds to the last seven AAs of gA (Table 3-1). We already reported[12] that the peptide self-assembles into spherical micelles in aqueous solution, while the self-assembly of the fully acetylated analogue Ac-X_3-gT starts with the amphiphilic peptide in a dissolved monomeric state in pure ethanol (*cf. chapter 2*). Increasing water concentration induces

the formation process of small micelles ($R_h \approx 10$ nm). During further solvent exchange the threshold of solvent polarity is exceeded, leading to aggregation of the micelles into highly solvent-swollen particles ($R_h \approx 160$ nm). These particles then condense further and fuse with residual small micelles below ethanol concentrations of 20 wt%, ultimately leading to rigid solid peptide particles that preserve their shape and dimensions ($R_h \approx 350$ nm) even after isolation from the aqueous dispersion. The final size of the solid, spherical peptide particles, termed "peptide beads", can be controlled by the initial concentration of the peptide in ethanol[12].

Table 3-1: Code, sequence, and charge of amphiphilic peptides and the wildtype gA.

Code	Sequence [a]	Charges
wt-gA	*formyl*-LV-G-LA-DL-LA-DV-LV-DV-[LW-DL]$_3$-LW-*ethanolamine*	*0*
K$_3$-gT	*H*-LK$_3$-[LW-DL]$_3$-LW-*NH$_2$*	*4+*
Ac-X$_3$-gT	*Ac*-[LK*(Ac)*]$_3$-[LW-DL]$_3$-LW-*NH$_2$*	*0*

[a] one letter code, X = LK(Ac)

In this chapter we are interested to enter in more details of the hierarchical self-assembly of this amphiphilic peptide to understand in which respect the internal structure of the peptide beads will influence the embedding of payloads. The self-assembled peptide beads were investigated in pure water by SLS and DLS and showed a narrow size distribution. Guinier-Plot analysis (Figure 3-1A) revealed a size of $R_g = 236$ nm, which is consistent with dimensions reported earlier[12], during the process of bead formation. The ρ-parameter (Rg/Rh) of 0.79, calculated using the measured hydrodynamic radius (Rh) of 300 nm from DLS data analysis, is close to the theoretical value of $1/\sqrt{(5/3)} = 0.78$ for solid spheres[18]. When the angular dependence of the particle scattering factor (Figure 3-1B) is compared to the theoretical functions for homogenous, hard spheres (black line) and monodisperse polymer coils (gray line), respectively, a close fit to the hard sphere model is obtained. The spherical shape of the formed particles was visualized by scanning electron microscopy (SEM) of a dried sample as well (Figure 3-2A). The typical contrast gradient of solid particles in the transmission electron micrographs (TEM) and the SEM micrographs of a peptide bead broken-up by shock freezing proved the solid sphere character (Figure 3-2B & C).
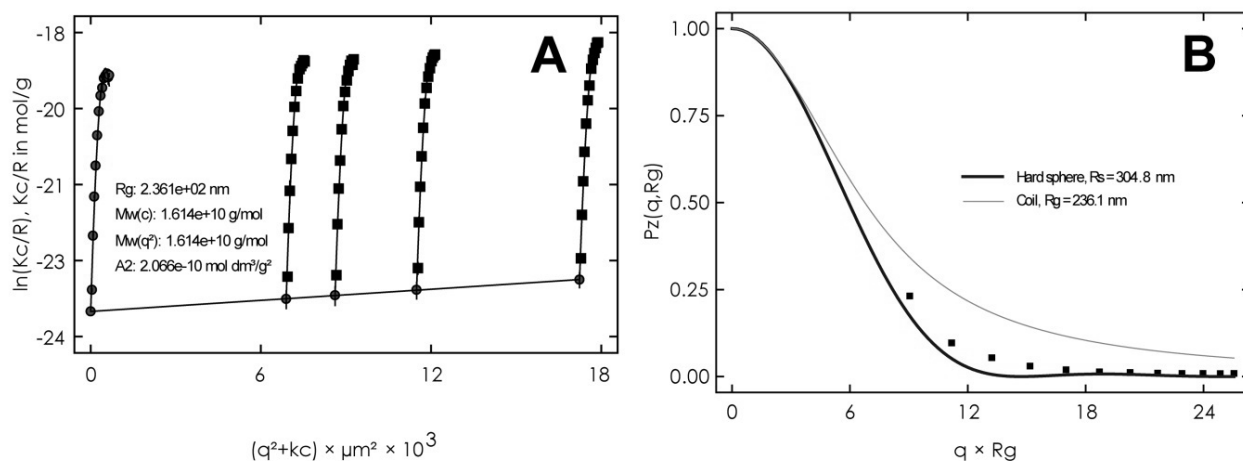
Figure 3-1: SLS analysis of Ac-X$_3$-gT peptide beads in water (0.25 mg/ml); A) Guinier Plot resulting an R$_g$ of 236 ± 7 nm, B) form factor analysis (-) hard sphere model, (-) coil model, (■) experimental data.

The earlier hypothesis, based on the investigated formation process, suggested an aggregation of previously formed micelles into the peptide beads. TEM of uranyl acetate stained peptide beads (Figure 3-2D) revealed smaller structures within the beads made visible by the contrast enhancement and thereby indicate an substructure, possibly composed of micelles within the final peptide beads. The measured radius of 10.7 ± 1.8 nm, gained from image analysis of the underlying smaller species within the stained peptide beads, is clearly in the range of micelle sizes (Figure S 3-1).
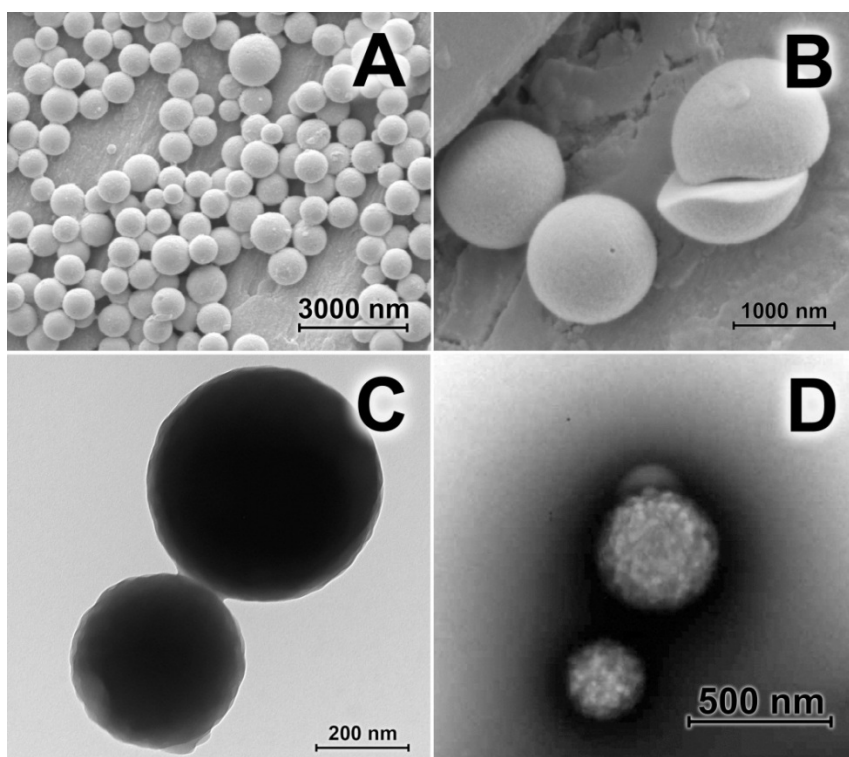
Figure 3-2: Ac-X$_3$-gT peptide beads: (A) SEM of dried sample 0.5 mg/ml; (B) SEM of shock-frozen and lyophilized sample 0.5 mg/ml; (C) TEM 0.25 mg/ml; (D) TEM with uranyl acetate staining 0.25 mg/ml.

The dimensions of the substructure were compared to micelles formed by the charged peptide analogue, K_3-gT. CONTIN-algorithm analysis of multi angular DLS measurements revealed a hydrodynamic radius of 11 nm for the micelles. As deduced from AFM and TEM images, a minor fraction of peptide beads is formed along with the micelles (Figure S 3-2). As the intensity of the scattered light is proportional to the radius to the power of six, this minor fraction of larger particles in the sample leads to a dramatic increase in the scattering intensity, making SLS evaluation of the small micelles impossible, even when only high q-values are considered. However, TEM image analysis of the micelles indicated a radius of 11.8 ± 2.2 nm (Figure S 3-1 & Figure S 3-3). Consequently, TEM as well as light scattering suggest that such micelles preserved their size within the Ac-X_3-gT peptide beads.

To obtain topography-based data, atomic force microscope (AFM) was used to compare K_3-gT micelles with the surface of Ac-X_3-gT peptide beads. Since the image quality in AFM relies on the flatness of the sample, we increased the size of the peptide beads by using an initial peptide concentration in ethanol of 1.5 mg/ml [12]. This led to beads with diameters larger than 1000 nm and therefore lower surface curvature. The scans performed on top of the beads revealed an astonishing similarity with the scans of the micelles (Figure 3-3).
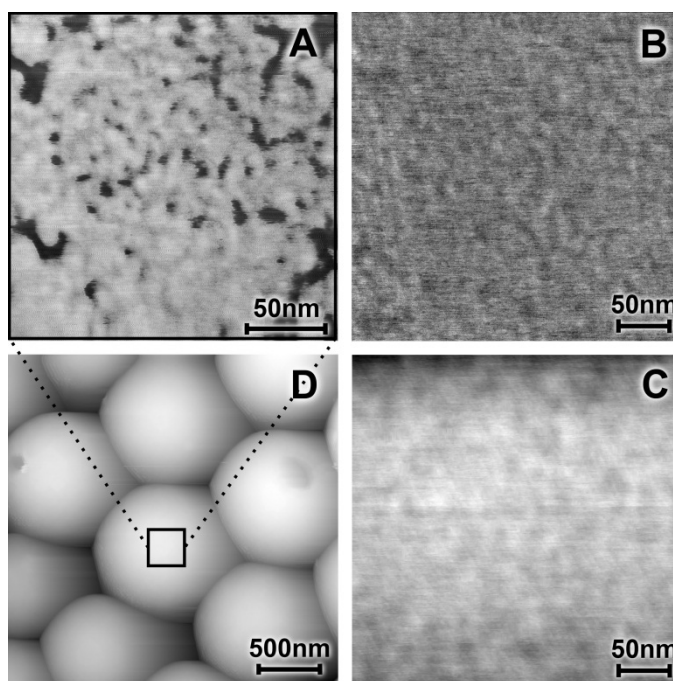
Figure 3-3: Surface of Ac-X_3-gT peptide beads in AFM phase contrast (A) showing structures with the same size as K_3-gT micelles on mica in phase contrast (B) and in topographic contrast (C). Peptide beads in AFM topographic contrast (D) shown for illustration.

Although the imaging techniques showed micelles within the peptide beads, they allowed only a limited view inside. To disturb the packing of micelles slightly, the initial peptide sequence was elongated with a cysteine, resulting in Ac-X_3-gT-C. This modification led to a rougher surface and a looser packing of the formed peptide beads (Figure 3-4). Lyophilisation of these loosely packed beads allowed a view into partially opened beads (Figure 3-4b) and also revealed a structure constructed of smaller, spherical subunits. In terms of a functional model, the packing of the

micelles into the peptide beads can be compared to a sintering process, commonly known as relating to metal particles or ceramics[19]. The diminished sintering effect in the case of Ac-X$_3$-gT-C can be explained by more form-stable micelles, presumably due to stronger *intra*micellar binding of newly formed disulfide bridges.
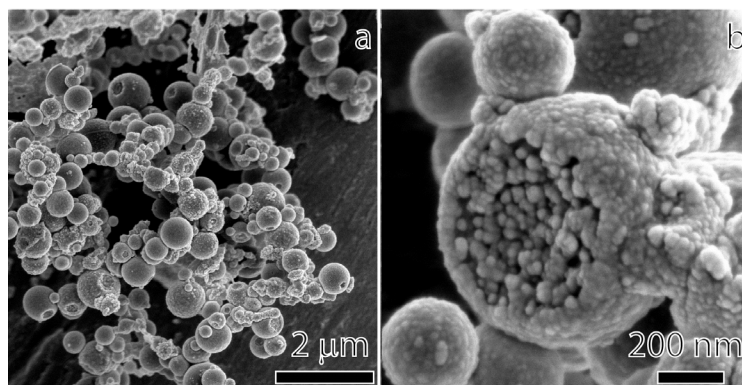
Figure 3-4: SEM of self-assembled peptide beads from Ac-X$_3$-gT-C (a); insights into a peptide bead revealing a structure constructed by smaller spherical subunits (b).

Although these images qualitatively demonstrate an assembly process that makes use of small, spherical structures that form the resulting peptide bead structures, *i.e.* multicompartment micelles, they are not associated with significant statistical data for the inside of the peptide beads. Therefore, we performed small angle x-ray scattering (SAXS) on a concentrated aqueous Ac-X$_3$-gT peptide bead sample, using a synchrotron source[20]. Even if the beads are larger than the experimentally available maximal size for SAXS – based on theory, but also indicated by a missing Guinier plateau and a missing Porod regime (that is, q does not scale with q^{-4} at higher q) – the collected data can be used to estimate the size of possible internal substructure.

The scaling of the experimental data with q^{-3} indicates a spherical structure. The absence of a Porod regime also supports the presence of a diffuse interface, since a clear electron density difference between the dispersant and the substructure's surface is missing. Moreover, this behavior is an agreement with a mass fractal behavior[21]. A classical data analysis using a single solid sphere distribution failed. We interpreted this as the consequence of the aggregated and polydisperse nature of the micelles as shown by microscopy. The use of a bimodal model is not possible without introducing broad errors. Therefore we turned to a two-level Beaucage fitting method, in which the size of the internal substructure was estimated to have a radius of gyration R$_g$ of 9.8 ± 0.2 nm that corresponds to the size of aggregated micelles with a spherical radius of 12.7 ± 0.3 nm on average (Figure 3-5). The radius corresponded well with the radii found in AFM, SEM, and TEM. Moreover, the pair distance distribution function (PDDF) showed the expected shape for solid particles[22] which, in this case, are micelles. To prove consistency, the averaged substructure using this model also had a diameter of approx. 12 nm. Based on the PDDF shape, the presence of inverted micelles with hollow core shell particles in this size can be ruled out.
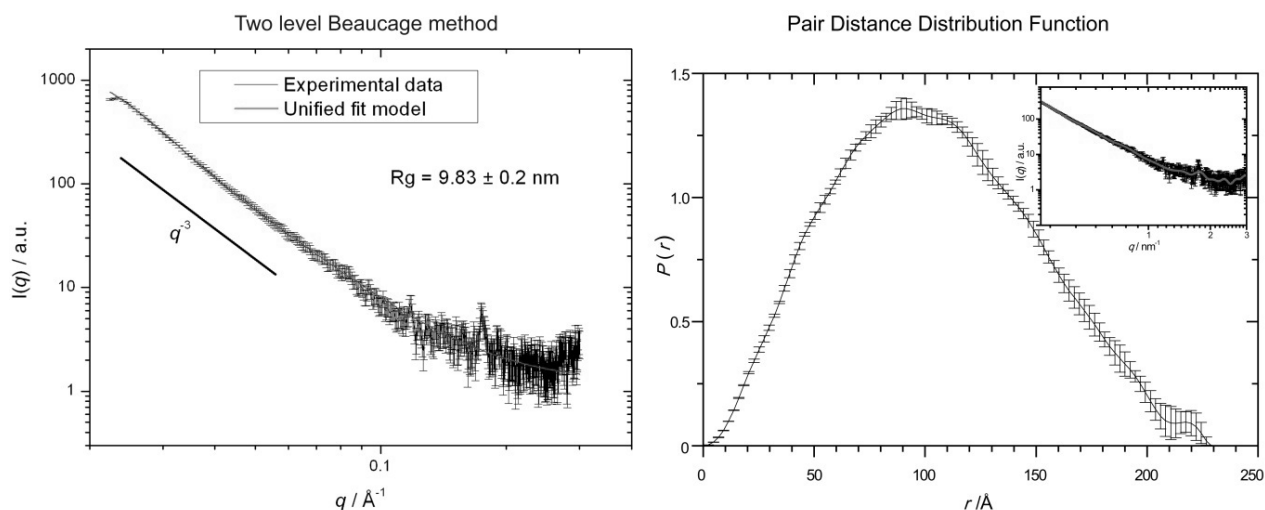
Figure 3-5: SAXS of peptide beads showing the sizes of substructures inside the beads. Two-level Beaucage method (left) and PDDF (right).

Deduced from the presented microscopic and scattering data, the peptide beads are formed by aggregation of smaller, spherical subunits of ~10 nm. The size is in the normal known range for micelles. Based on this fact, we built three-dimensional models of the peptide beads, where the well-known crystal structure of gramicidin-A[13b] was used for the gT part in combination with a simple, random coil for the three acetylated lysines. The model quickly revealed that a classical approach with one layer of molecules forming a micelle is not possible, since the radius of 10 nm cannot be spanned by one molecule. Ac-X$_3$-gT, with a preserved gramicidin-like secondary structure, has a length of approximately 2 nm. Even when assuming a structural change towards the most space demanding β-sheet alignment of 0.35 nm per AA, the peptide has a maximum length of 3.5 nm. Thus, another model than the classical one-layer-approach is necessary to understand the creation of micelles of the measured size. As mentioned above, static light scattering of pure K$_3$-gT micelles cannot be evaluated, due to the presence of a small fraction of peptide beads. SAXS measurements of a concentrated micelles sample were performed, but, due to the low contrast, gave no evaluable signal, even when using the high-flux synchrotron source. However, due to the similarity in size, the micelle assignment seems justified.

Defying the lack of further methods to resolve the micellar structure within the beads, we performed a Total Non-Negative Least Square analysis (TNNLS) of the X-ray scattering data for the peptide beads. Basically, the process consists of creating a computed-generation population of nano-objects, calculating the corresponding scattering curve and matching it iteratively with an experimental curve. Results are shown in Figure 3-6. Interestingly, the size distribution curve shows a polydisperse system. There are three diameters visible: one at 6.8 nm, one at 15.6 nm, and one at 21.2 nm. The 6.8 nm fits well with the dimension of two peptides self-assembled in a tail-to-tail or head-to-head mode, and is commensurate with the peptide size and the classical one layer approach to form a micelle or an aggregate of 7 nm in size. Both the 15.6 nm and the 21.2 nm can be interpreted as the diameter of the small species found with the other techniques, both being multiples of the 7 nm species. They are polydisperse, as shown by the absence of a clear minimum in the scattering curve. This is not surprising, as due to the aggregation, the

dispersant and the object lack a clearly defined border. This additional data supports a model, having three stages of self-assembly: first peptide with peptide in small aggregates, these then form larger micelles, which then aggregate up to the final peptide beads.
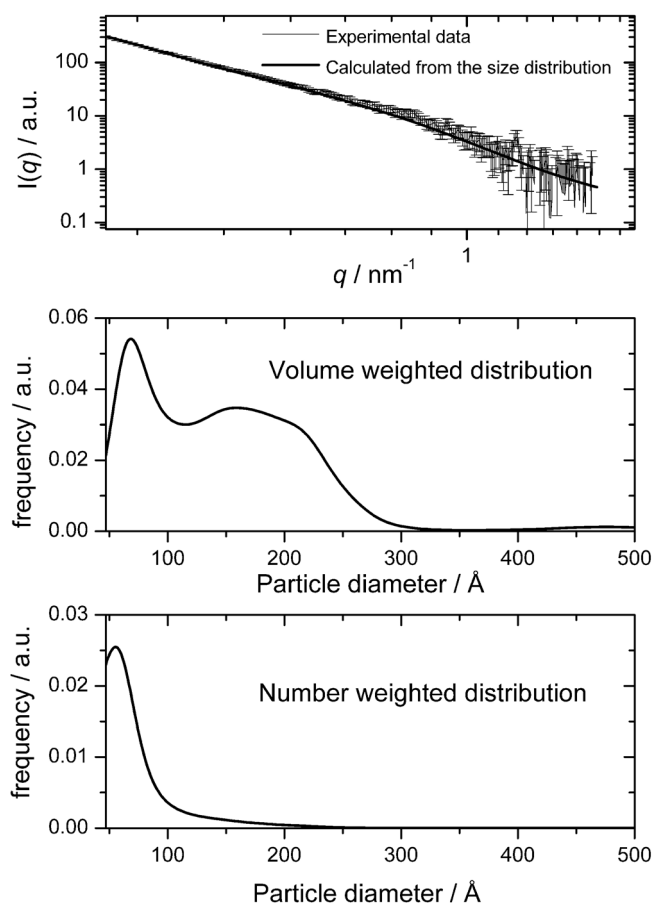
Figure 3-6: Fitted SAXS curves of Ac-X$_3$-gT using a TNNLS model, and the corresponding size distributions.

With the presented data we prove the persistence of spherical micelles of approximately 20 nm in diameter within the peptide beads. The evaluated data allows two possible models for the structure of the micelles (Figure 3-7): According to the *aggregated micelle model*, the peptides first form micelles of ~7 nm diameters, these then aggregate into 21 nm objects due to reduced solubility of the micelles with decreasing ethanol content, which also reduces the flexibility of the objects. Further decrease in ethanol content leads to the aggregation of the objects into the peptide beads until the aggregation process ends due to maturing of the particles into solid peptide beads, which occurs below 20 wt% ethanol as presented earlier[12] (*cf. chapter 2*). According to the *large compound micelle model*, the peptides first form inverted micelles (~7 nm) at very high ethanol concentrations, based on the good solubility of the gT sequence in ethanol. With decreasing ethanol content these inverted micelles, presumably stabilized due to H-bonding of the lysine part, start aggregating (~14 nm) and are then surrounded by a layer of remaining peptide to reveal the hydrophilic part to the now aqueous environment (~21 nm). The so formed structure, termed "large compound micelle", has been reported for block-co-polymers already[23]. Further decreasing ethanol content leads to aggregation of the 21 nm large compound micelles into peptide beads. Further experiments are needed to prove the structure of the micelles within

these hypothetical models. Nevertheless, they give two reasonable hierarchical self-assembly pathways.
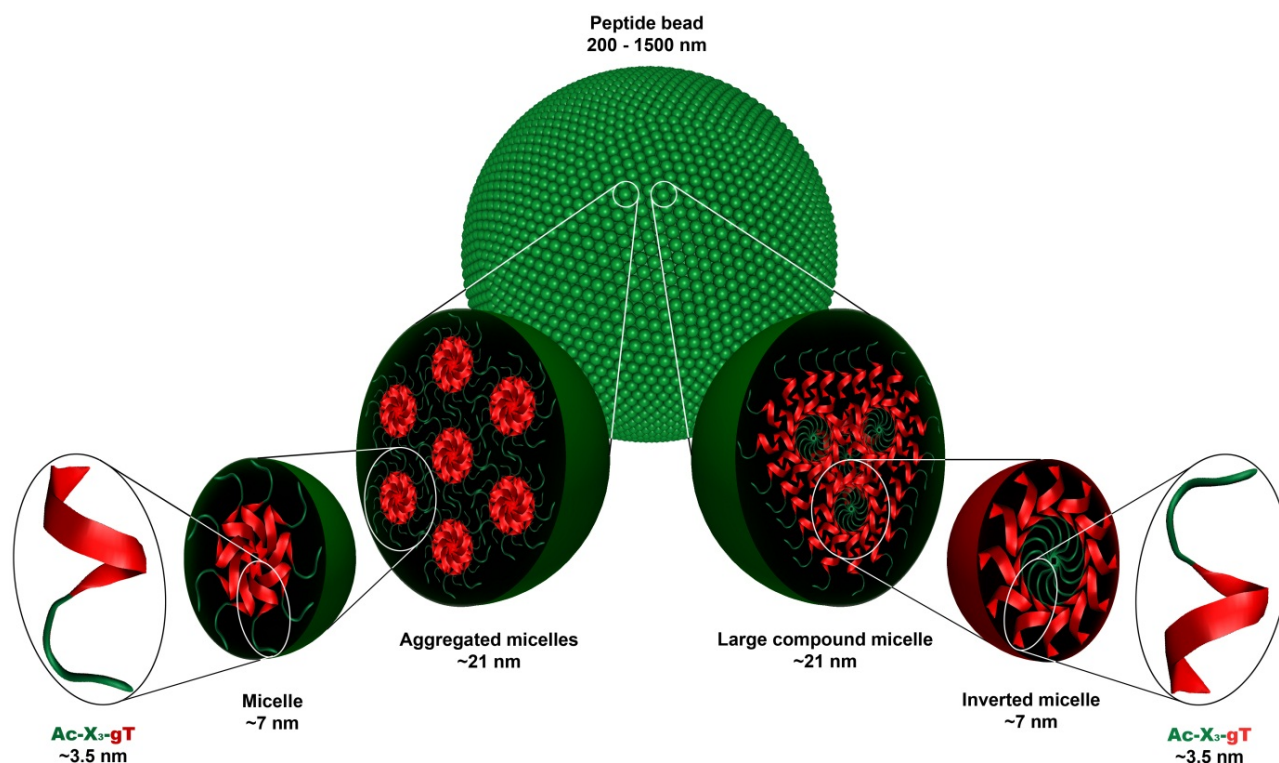
Figure 3-7: Hierarchical self-assembly into peptide beads: aggregated micelle model (left) and large compound micelle model (right)

In literature, two terminologies for models with similar behavior as the presented system can be found. For block-co-polymers, Eisenberg et al.[23] reported "large complex micelles" (LCM), later also called "large compound micelles"[24], that consist of aggregated, inverted micelles, surrounded by a final layer of the amphiphiles to form a hydrophilic shell, in the same fashion we described above. The other, more generalized and structural open terminology "multicompartment micelles" [25], first proposed by Ringsdorf[26], describes supramolecular aggregates with a hydrophilic shell and segregated hydrophobic cores. Therefore it is not limited to morphology, but rather describes properties. We consider the terminology "multicompartment micelles" the best to describe our system at the present time. Multicompartment micellar structures are promoted to entrap and release payloads with different hydrophilic and hydrophobic properties and have recently been produced by self-assembly, using triblock copolymer systems[25-26]. The embedding of hydrophilic and hydrophobic payload, was recently also shown for the present peptide beads[11]. As a logical consequence, the herein presented hierarchical self-assembled peptide beads potentially find application in drug delivery, due to the combination of the multicompartmentized structure, the high performance regarding encapsulation efficiency[11], and the biodegradable peptide-based origin.

3.4 Conclusion

This chapter reported in detail the inner structure of Ac-X$_3$-gT peptide beads to understand the hierarchical organization of the purely peptidic amphiphiles inside. The peptide Ac-X$_3$-gT is soluble in ethanol and forms peptide beads with controllable radii in the range of 100 to 800 nm when transferred to water. We showed with both, microscopic and scattering techniques, that the peptide beads are solid spheres, self-assembled in a hierarchical manner by aggregation of smaller spherical subunits of ~10 nm in radius. The size of these is comparable with micelles formed by the charged peptide analogue, K$_3$-gT. We therefore confirmed a previously made hierarchical formation process hypothesis[12] in structural detail by proving the persistence of spherical subunits in the size of micelles within the matured peptide particles. We introduced two hypothetical models – the *aggregated micelle model* and the *large compound micelle model* –for the inner structure of the subunits, based on SAXS experiments (Figure 3-7). In both of these models, the peptide beads hold segregated hydrophobic compartments in form of the micellar subunits and a continuous, rather hydrophilic micellar coronae compartment. Hence, the peptide beads offer compartments for payloads with different affinities, a property generally advertised for multicompartment micelles. In contrast to vesicular structures, which offer a very large volume/entity for hydrophilic payloads but relatively small volume/entity for hydrophobic payloads, multicompartment micelles are advantageous since they offer almost equal space for both species. Due to the small size, and the short distances between the hydrophobic regimes, our multicompartment micelles also possess optimal properties to embed macromolecules that have a hydrophilic backbone, sputtered with hydrophobic sections/residues, like for example DNA and RNA. Since the peptide beads are solid in their matured form, payloads are protected from the environment overall until their release by, e.g. degradation of the peptide or diffusion release mechanisms. Nevertheless, a representation of a small fraction of the payload that is embedded close to the outside is not excluded and might even be useful for functionalization or recognition applications (e.g., targeting, vaccine). Furthermore the solid character allows lyophilization and storage of the peptide beads, which can be a strong advantage in contrast to vesicle systems. For all these reasons, as well as for biodegradability, we see great potential in drug delivery applications for this new kind of peptidic material.

3.5 Supporting information
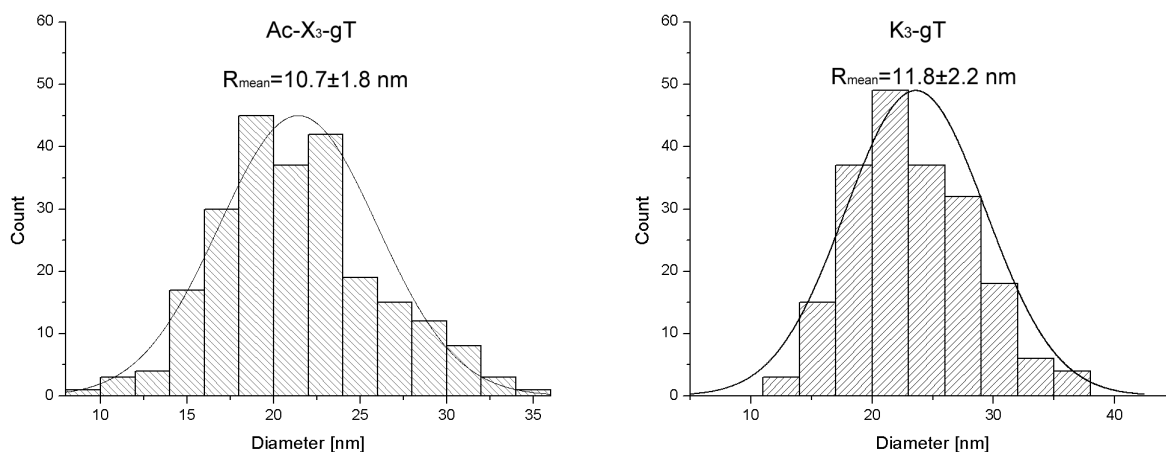
Figure S 3-1: TEM image analysis of the small species within the Ac-X$_3$-gT peptide beads (left) and K$_3$-gT micelles (right).
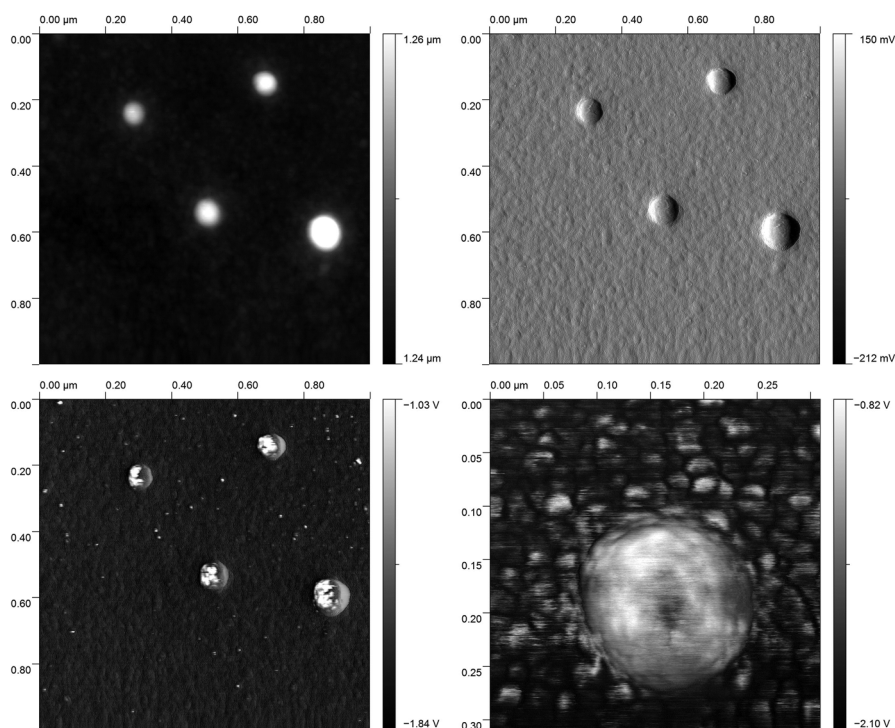
Figure S 3-2: AFM showing presence of peptide beads in main peptide micelle fraction. Topographic and amplitude contrast (top), phase contrast (bottom), zoom-in of bead (bottom right).
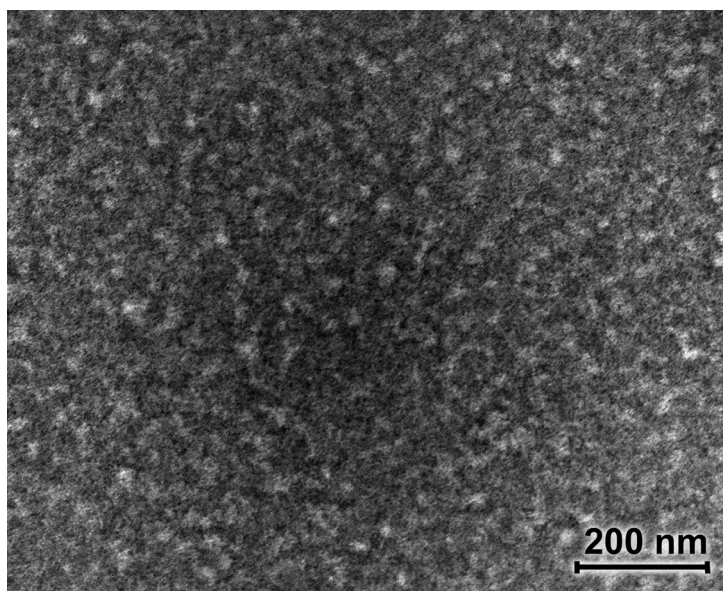
Figure S 3-3: TEM of K$_3$-gT micelles, stained with uranyl acetate.
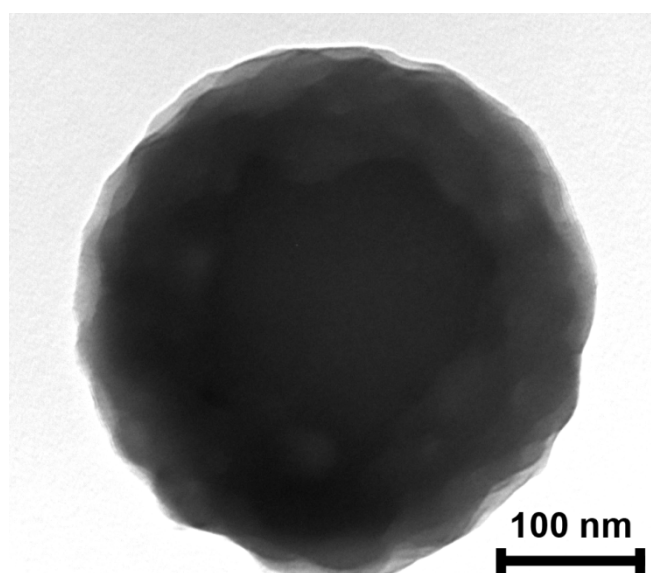
Figure S 3-4: TEM image of a small Ac-X$_3$-gT peptide bead with good transparency revealing an inner structure.

3.6 References

[1] A. D. Milov, Y. D. Tsvetkov, F. Formaggio, M. Crisma, C. Toniolo and J. Raap, *J. Am. Chem. Soc.* **2000**, *122*, 3843-3848.

[2] a) F. M. Veronese, *Biomaterials* **2001**, *22*, 405-417; b) C.-Y. Yang, B. Song, Y. Ao, A. P. Nowak, R. B. Abelowitz, R. A. Korsak, L. A. Havton, T. J. Deming and M. V. Sofroniew, *Biomaterials* **2009**, *30*, 2881-2898; c) D. F. Carmignac, *Cell Biochemistry and Function* **2003**, *21*, 298-298; d) J. F. Kennedy and M. M. He, *Carbohydrate Polymers* **2005**, *60*, 127.

[3] a) S. Yao, J. Babon Jeffrey and S. Norton Raymond, *Biophysical chemistry* **2008**, *136*, 145-151; b) J. Sun, C. Deng, X. Chen, H. Yu, H. Tian, J. Sun and X. Jing, *Biomacromolecules* **2007**, *8*, 1013-1017; c) J. Lin, J. Zhu, T. Chen, S. Lin, C. Cai, L. Zhang, Y. Zhuang and X.-S. Wang, *Biomaterials* **2009**, *30*, 108-117.

[4] H. A. Behanna, J. J. J. M. Donners, A. C. Gordon and S. I. Stupp, *Journal of the American Chemical Society* **2005**, *127*, 1193-1200.

[5] a) F. Checot, S. Lecommandoux, Y. Gnanou and H.-A. Klok, *Angewandte Chemie, International Edition* **2002**, *41*, 1339-1343; b) H. Kukula, H. Schlaad, M. Antonietti and S. Forster, *Journal Of The American Chemical Society* **2002**, *124*, 1658-1663.

[6] C. Schatz, S. Louguet, J.-F. Le Meins and S. Lecommandoux, *Angew. Chem., Int. Ed.* **2009**, *48*, 2572-2575.

[7] E. P. Holowka, D. J. Pochan and T. J. Deming, *J. Am. Chem. Soc.* **2005**, *127*, 12423-12428.

[8] V. Malinova, S. Belegrinou, D. de Bruyn Ouboter and W. P. Meier, *Adv. Polym. Sci.* **2010**, *224*, 113-165.

[9] S. G. Zhang and X. J. Zhao, *J. Mater. Chem.* **2004**, *14*, 2082-2086.

[10] D. J. Adams, K. Holtzmann, C. Schneider and M. F. Butler, *Langmuir* **2007**, *23*, 12729-12736.

[11] C. Dittrich and W. Meier, *Macromolecular Bioscience* **2010**, *10*, 1406-1415.

[12] T. B. Schuster, D. de Bruyn Ouboter, E. Bordignon, G. Jeschke and W. Meier, *Soft Matter* **2010**, *6*, 5596-5604.

[13] a) B. M. Burkhart, R. M. Gassman, D. A. Langs, W. A. Pangborn, W. L. Duax and V. Pletnev, *Biopolymers* **1999**, *51*, 129-144; b) B. M. Burkhart, R. M. Gassman, D. A. Langs, W. A. Pangborn and W. L. Duax, *Biophysical Journal* **1998**, *75*, 2135-2146.

[14] F. Qiu, Y. Chen and X. Zhao, *J. Colloid Interface Sci.* **2009**, *336*, 477-484.

[15] P. M. Macdonald and J. Seelig, *Biochemistry* **1988**, *27*, 2357-2364.

[16] R. Brasseur, J. A. Killian, B. De Kruijff and J. M. Ruysschaert, *Biochimica et Biophysica Acta, Biomembranes* **1987**, *903*, 11-17.

[17] S. Kimura, D.-H. Kim, J. Sugiyama and Y. Imanishi, *Langmuir* **1999**, *15*, 4461-4463.

[18] a) S. Hanessian, V. Vinci, K. Fettis, T. Maris and M. T. P. Viet, *J. Org. Chem.* **2008**, *73*, 1181-1191; b) O. Stauch, R. Schubert, G. Savin and W. Burchard, *Biomacromolecules* **2002**, *3*, 565-578.

[19] a) C. S. Wright, *Powder Metallurgy* **1996**, *39*, 268-269; b) O. Lame, D. Bellet, M. D. Michiel and D. Bouvard, *Nuclear Instruments and Methods in Physics Research Section B: Beam Interactions with Materials and Atoms* **2003**, *200*, 287-294.

[20] O. Paris, C. Li, S. Siegel, G. Weseloh, F. Emmerling, H. Riesemeier, A. Erko and P. Fratzl, *J. Appl. Crystallogr.* **2007**, *40*, s466-s470.

[21] P. Schmidt, *Journal of Applied Crystallography* **1991**, *24*, 414-435.

[22] H. Schnablegger and Y. Singh, *A Practical Guide to SAXS*, Anton Paar, Graz, Austria, **2006**, p.

[23] L. Zhang and A. Eisenberg, *Science (Washington, D. C.)* **1995**, *268*, 1728-1731.

[24] a) J.-F. Gohy in *Block Copolymer Micelles*, *Vol. 190* (Ed. V. Abetz), Springer Berlin / Heidelberg, **2005**, pp. 65-136; b) C. Giacomelli and R. Borsali in *Disordered Phase and Self-Organization of*

Block Copolymer Systems, *Vol.* Eds.: R. Borsali and R. Pecora), Springer Netherlands, **2008**, pp. 133-189.

[25] a) S. Kubowicz, J.-F. Baussard, J.-F. Lutz, A. F. Thuenemann, H. von Berlepsch and A. Laschewsky, *Angewandte Chemie, International Edition* **2005**, *44*, 5262-5265; b) J.-F. Lutz and A. Laschewsky, *Macromolecular Chemistry and Physics* **2005**, *206*, 813-817; c) H. von Berlepsch, C. Boettcher, K. Skrabania and A. Laschewsky, *Chemical Communications (Cambridge, United Kingdom)* **2009**, 2290-2292; d) C. Zhong and D. Liu, *Macromolecular Theory and Simulations* **2007**, *16*, 141-157; e) K. Skrabania, H. von Berlepsch, C. Boettcher and A. Laschewsky, *Macromolecules (Washington, DC, United States)* **2010**, *43*, 271-281.

[26] H. Ringsdorf, P. Lehmann and R. Weberskirch, **1999**, pp. BTEC-001.

4 From fibers to micelles using point mutated amphiphilic peptides

Thomas B. Schuster, Dirk de Bruyn Ouboter, Cornelia G. Palivan, Wolfgang Meier

Department of Chemistry, University of Basel, Klingelbergstrasse 80, CH-4056 Basel, Switzerland.
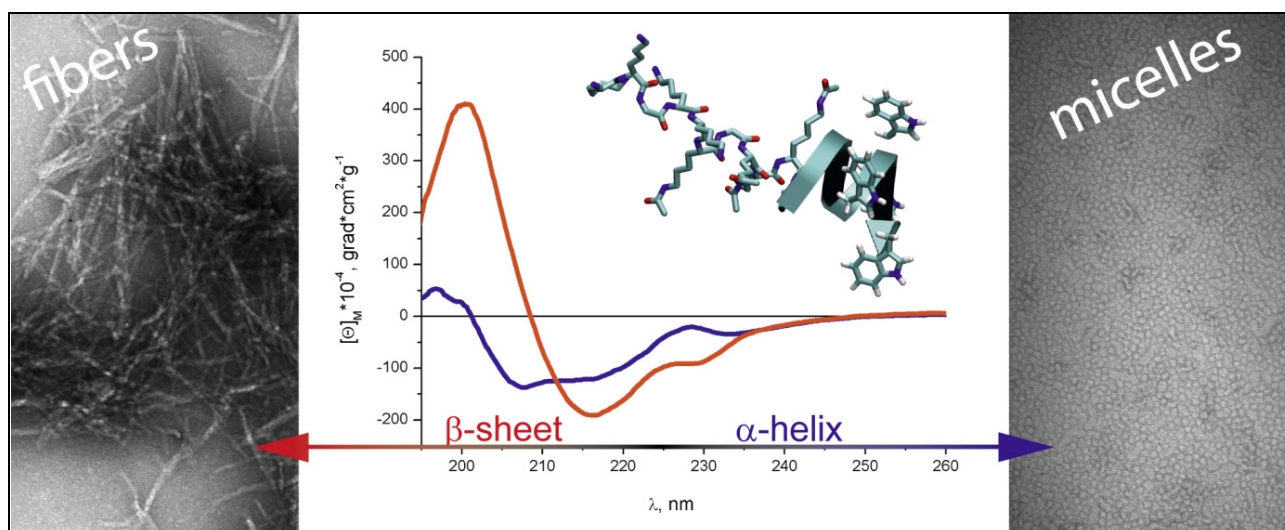
A change in secondary structure from β-sheet to α-helix – enabled by controlled point mutation – allowed the control of the self-assembled supramolecular structure from fibers to micelles.

4.1 Abstract

In chapter 4, a library of purely peptidic amphiphiles is presented, leading to different self-assembled structures as they were received from the peptide in the earlier chapters. Besides the successful solid-phase peptide synthesis (SPPS), the characterization of the short amino acid sequences with amphiphilic character are presented with the aim of gaining insight into their self-assembled supramolecular structures. The peptide design includes three parts: (a) a charged lysine part, (b) an acetylated lysine part and (c) a constant hydrophobic rod-like helix, based on gramicidin A. By stepwise replacement of free lysine (K) with acetylated lysine (X) a library of a total of ten peptides Ac-X_8-gA and K_mX_{8-m}-gA (m ranging from 0 to 8) was generated. By using point mutations, the degree of acetylation (DA) and thus the overall amphiphilicity of the peptides was adjusted, which led to a change in the secondary structure in the aqueous environment from a β-sheet to an α-helix. This transition generated a significant change in the morphology of the self-assembled structures from fibers to micelles. Two different regions where observed with the conformation of the hydrophilic part of the peptide: one region, a β-sheet-like secondary structure, inducing fiber formation (high DA), the other an α-helical-like secondary structure generating micelle formation (moderate and low DA). The micellar structures depended on the degree of acetylation, which influenced their critical micelle concentration (cmc). These morphology regions were determined by a combination of circular dichroism, dynamic light scattering, surface tension, and transmission electron microscopy that allowed correlation of the generated supramolecular architectures with the fine changes obtained by means of the point mutation strategy.

4.2 Introduction

Self-assembled nanostructures are attracting ever more attention, in particular in aqueous solution, due to fundamental aspects that concern the nature of the folding processes as well as the wide range of applications as carriers in drug delivery, templates for surface oriented applications, or nanodevices in combination with active molecules.[1] At the focus of this interest is the fabrication of nanostructures such as micelles, nanotubes or vesicles that can be combined with active molecules, such as biological entities, to generate complex hybrid systems.[2] Ranging from systems that are completely synthetic (polymers, inorganic compounds) to biological (phospholipids, polypeptides), interest in medically-oriented applications stems from the possibility of producing superstructures that are able to both accommodate the active entity and preserve its structure/function in biological conditions. Even if the diversity of the polymeric systems that are able to generate supramolecular structures is very extensive, biocompatibility plays a crucial role for any biomedical application [1-3]. This requirement limits significantly the types of polymers or copolymers to only those that are biocompatible, such as, for example, poly(ethylene oxide), poly(dimethylsiloxane) or poly(glutamic acid).[4] But this limitation does not apply to poly(amino acids) i.e. polypeptides, which appear ideal for the development of supramolecular structures, since it is anticipated that they will be both biocompatible and biodegradable. Furthermore, they offer broad chemical functionality due to the diversity of AA side chains combined with specific AA sequences that define specific recognition sites[5] (e.g. RGD

sequence for cell adhesion) or act similar to cell penetrating peptides (arginine rich sequences)[6]. Another important feature of peptides is their secondary structure, e.g. β-sheet or α-helix, reflecting a three dimensional conformation that supports specific interactions and properties. The complete folding and assembly of a protein into its quaternary structure is an outcome that depends on the interaction between the solvent and the protein structure, leading to often advantageous electrostatic interactions and hydrogen-bonding combined with the hydrophobic effect. Thus, in the self-assembly of natural systems the secondary, the tertiary, and the quaternary structures are interconnected and serve to create the final supramolecular conformation that favors a specific functionality. The secondary structure and the overall 3D conformation are encoded in the primary sequence, and these structures are then modulated via effects on the secondary structure arising from environmental conditions such as pH, ionic strength, temperature, and type of solvent. A pH-induced, so-called helix – coil transition of poly(L-lysine) and poly(L-glutamic acid) was used to create micelles that are able to invert their corona and core regions in so-called "schizophrenic" behavior.[7] The same approach was used when polypeptides were combined with biocompatible polymers, in a co-micellated system of poly(glutamic acid) -b- poly(propylene oxide) -b- poly(glutamic acid)/ poly(ethylene oxide) -b- poly(propylene oxide) for controlled drug release [7-8]. These examples illustrate in excellent fashion how the self-assembly of polypeptides derived from polymerization techniques can be controlled by changes in a molecule's secondary structure. However, polypeptides obtained by polymerization techniques bear the inherent drawbacks of polymerization that produce a molecular weight distribution that can differ slightly from batch to batch, and that fails to provide a controlled, defined sequence of differing amino acids.

It is possible to overcome these limitations by using solid-phase peptide synthesis (SPPS), which is limited to peptides up to 50 AAs.[9] Zhang and co-workers produced ionic, self-complementary peptides by solid-phase peptide synthesis, and investigated their supramolecular architectures after the self-assembly process.[10] When very short amphiphilic peptides, e.g. V_6K_2 self-assembled into net-like structures of tubes and vesicles,[11] the 3D structures have been found to be highly sensitive to the purity of the peptides.[12] Qui et al. showed the successful assembly of catanionic $A_6K^{\pm}$ into fibers.[13] A series of six 32-mers with a constant hydrophilic part and a variable hydrophobic part based on phenylalanine/alanine ratio was used to fine-tune drug and gene co-delivery.[14] Hashimoto et al. showed that micelles using the 28-mer Pep-L12 are biodegradable and are a potential gene carrier system[15]. However, the mentioned studies do not include investigations on secondary structure. This was examined on a 24-meric peptide, designed from a 20 kDa barnacle cement protein, and was found to be constant while self-assembling into a filament structure. This peptide, however, does not exhibit an amphiphilic character and self-assembly was induced by salt addition[16]. Shera et al. compared a 15-mer designed amphiphilic peptide to its alternating analogue – with identical AAs but of a different sequence – and related its self-assembled morphologies to the observed primary β-sheet conformation, not present in the analogue[17]. General studies in solution that include the influence of secondary structure do exist – especially for polypeptides – but, to our best knowledge, a systematic study using a series of amphiphilic small (≤ 25 AA) defined and controlled sequences – i.e. not synthesized by

polymerization – for the purpose of understanding superstructures that are generated by self-assembly have not yet been reported.

As a key to understanding protein/peptide folding and self-assembly of the primary sequence, point mutation represents the best choice to induce, in a controlled way, a precise change of one specific AA in the primary sequence. In the present study we investigate the impact of point mutations on a short peptide series, on the control of amphiphilicity, on secondary structure and on the self-assembled morphologies. The amphiphilic peptides successfully synthesized by SPPS via Fmoc strategy[18] allowed us to create a library of ten peptides with progressively changing properties. Their constant hydrophobic part was inspired by the pentadecamer gramicidin A (gA), consisting of only hydrophobic AAs in an alternating D, L configuration, which generates β-helical membrane channels[19]. The C-terminal ethanolamine group of gA was replaced by an amide group and its N-terminus was used to start a hydrophilic sequence of lysine (K, pK_a of 10.2) and acetylated lysine (X). Acetylated lysine corresponds to the removal of a charge and thus elimination of electrostatic repulsion, with expected impact on the secondary structure and morphology of the resulting assemblies. Glycine was introduced after every 3rd lysine or acetylated lysine to prevent a decrease in yield by creation of a homooligomer.

The degree of acetylation (DA) directly affects the number of charges and the corresponding hydrophilicity. The peptides of our library can be divided into three parts in terms of increasing hydrophilicity: (a) a highly hydrophilic-, charged lysine part with a space-demanding hydration shell, (b) a moderate hydrophilic, acetylated lysine part without electrostatic repulsion of the amine groups, and (c) a hydrophobic rod-like helix based on gA. Depending on the hydrophilic character of the peptides, the self-assembly process leads to different supramolecular structures that have been analyzed in relation to the primary structure.

4.3 Results and discussion

4.3.1 Design of amphiphilic peptides

The synthesized peptide library is based on SPPS via the Fmoc strategy, with the schematic structure K_mX_{8-m}-gA with: K_m (K – lysine, m – number of lysines), X_{8-m} (X – acetylated lysine), and a gA sequence of 14 highly hydrophobic amino acids, which remains constant and represents 56% of the total sequence (Table 4-1). Only one peptide, Ac-X_8-gA, has an acetylated N-terminus, so that the peptide is completely neutral, while only one peptide, K_8-gA is completely non-acetylated. As an example, the peptide K_4X_4-gA has the following sequence: *H*-LLys$_2$-Gly-LLys$_2$-(LLys-Ac)-Gly-(LLys-Ac)$_3$-LVal-Gly-LAla-DLeu-LAla-DVal-LVal-DVal-LTry-DLeu-LTry-DLeu-LTry-DLeu-LTrp-*NH$_2$* (Figure 4-1).

Table 4-1: Properties of the peptide K_mX_{8-m}-gA library with its schematic representation (DA – degree of acetylation).

Label	Hydrophobicity	DA	No. of charges	Scheme
Ac-X$_8$-gA	0.62	9/9	0	
X$_8$-gA	0.57	8/9	1	
K$_1$X$_7$-gA	0.55	7/9	2	
K$_2$X$_6$-gA	0.53	6/9	3	
K$_3$X$_5$-gA	0.52	5/9	4	
K$_4$X$_4$-gA	0.50	4/9	5	
K$_5$X$_3$-gA	0.49	3/9	6	
K$_6$X$_2$-gA	0.47	2/9	7	
K$_7$X$_1$-gA	0.45	1/9	8	
K$_8$-gA	0.44	0/9	9	
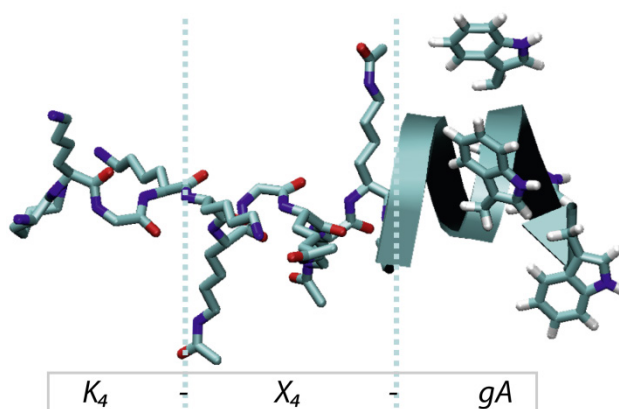
$$K_4 \quad - \quad X_4 \quad - \quad gA$$

Figure 4-1: Schematic representation of K_4X_4-gA, including oligolysine (K_4), acetylated oligolysine (X_4), and β-helical gA[20].

The design of the peptide library provides a linear increase in charge starting at neutral (Ac-X$_8$-gA), until reaching a total number of nine charges/molecule, for K$_8$-gA. This is associated with the changes in the degree of acetylation (DA), which thus gradually tunes the hydrophobicity. The library of short peptides – each consisting of only 25 AA with a precise primary sequence – was used to detect morphological transformations upon self-assembly in solution, based on the slightest changes in the amphiphilic design. Our interest concerned the study of whether and in what respect a very fine change to only one residue in the primary structure would affect the 3D conformation of the peptides.

4.3.2 Amphiphilic character of the peptide library

As expected from the design of the molecules, the properties of the peptides changed continuously within the library. For example, stepwise acetylation leads to a progressively increasing mass, and corresponds to a progressive increase in hydrophilicity of the peptide series. The variation in hydrophobicity was evidenced by the increased retention time on a RP-HPLC column (Figure 4-2). While hydrophobic sequences such as gA are usually very difficult to produce[21], the used synthesis and purification provides peptides with very high purity.
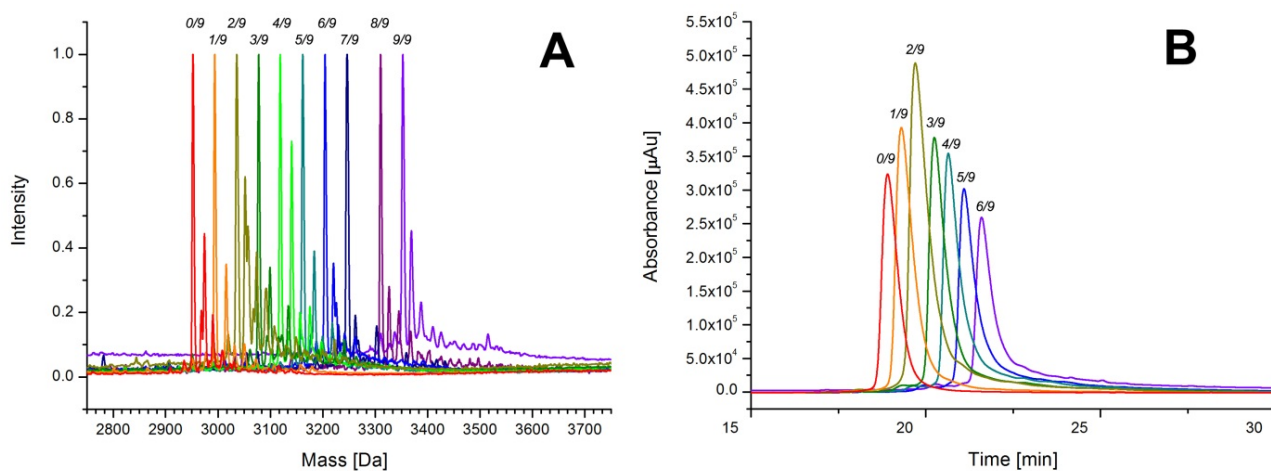
Figure 4-2: A) MALDI-TOF-MS and B) HPLC overlay of the peptide library. The curves are assigned with the degree of acetylation (*cf.* Figure 4-1).

As the self-assembly process takes place by solvent exchange from molecular dissolved amphiphiles in solution, the solubility of the peptide library was analyzed in different solvents at concentration of $1\,mg\,mL^{-1}$. In DMF all of the peptides were soluble (Figure 4-3A). We observed two types of behaviors with respect to solubility, in both the ACN/water mixture and in ethanol: peptides partially soluble (Ac-X_8-gA to K_2X_6-gA) and peptides completely soluble for smaller DA (K_3X_5-gA to K_8-gA). Thus, we observed a breakpoint in solubility between K_2X_6-gA and K_3X_5-gA (DA 6/9 and 5/9), which was not expected due to the continuously increasing hydrophilicity of the amphiphiles and continuous increase in retention time. Consequently, we assume that conformational changes along the peptide backbone are responsible for inducing intermolecular interactions, thereby explaining the observed solubility behavior. Therefore, we analyzed the secondary structure and evaluated the folding themes in ethanol by circular dichroism (CD). Even though Ac-X_8-gA to K_3X_5-gA showed low solubility in ethanol, CD spectra were measured for diluted solutions. All CD spectra (Figure 4-4 left) corresponding to peptides ranging from Ac-X_8-gA (DA 8/9) to K_2X_6-gA (DA 6/9) exhibited a negative cotton effect around 218 nm and a positive cotton effect around 200 nm (Figure 4-4 right, red line) and were assigned to a β-sheet configuration (217 nm and 198 nm,).[22] Starting from K_3X_5-gA, different CD spectra were observed with a negative cotton effect around 208 nm and 219 nm, as well as a positive cotton effect around 197 nm (Figure 4-4 right, blue line). These values correspond to an α-helical character (208 nm, 222 nm and 192 nm).[22] K_3X_5-gA contains only one acetylated lysine less as compared to K_2X_6-gA, but exhibits a completely different CD-spectrum and therefore marks the breakpoint in the behavior of the peptide series (Figure 4-4). Thus, the abrupt change in solubility behavior of peptides corresponds to a different secondary structure of the peptides, namely a β-sheet for K_2X_6-gA as compared to an α-helix for K_3X_5-gA. The low solubility found in different solvents for peptides Ac-X_8-gA to K_2X_6-gA can be explained by intermolecular interactions that are known for β-sheet-like structures that form higher-order assemblies of ribbons, fibers, and amyloids[23].

It is interesting to note that the α-helical and β-sheet-like secondary structures for our charged and uncharged peptides differ from that usually assigned to lysine homopolymer 2.5$_1$-helical and α-helical conformations, respectively[24]. However this difference is not surprising and is caused by

the introduction of a residue other than lysine (glycine) after each third AA. The deviation from a homooligomeric hydrophilic part is actually 20% and thus contributes significantly to the secondary structure.

Figure 4-3: Solubility of the amphiphiles in A) DMF B) ACN/water (1:1) C) ethanol.
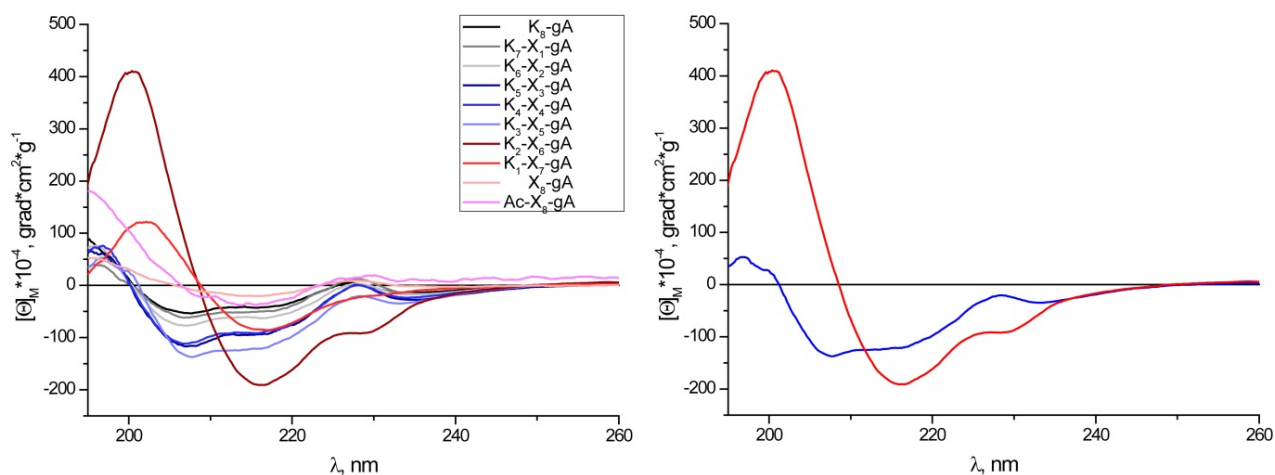
Figure 4-4: CD spectra of the full peptide library (left). Extracted CD spectra of K_2X_6-gA (red line, β-sheet) and K_3X_5-gA (blue line, α-helix) in ethanol representing the two different secondary structures (right).

The area in CD spectra between 210 and 260 nm is strongly affected by the structure adopted by the gA-sequence of peptide amphiphiles, and includes a characteristic maximum at 223 nm[25]. This is preserved throughout the whole library, even if the signal intensity is decreased by the superimposed spectra of the hydrophilic part. Therefore, we found the structure of the hydrophobic sequence little affected by the presence of the hydrophilic part of peptides and equally so by the variation of their DA. This agrees with the stable structures known for gA and gA-analogues found in different conditions of solvents or matrices[26]. Analysis of overall shape of CD spectra therefore indicates that the variation in the primary sequence caused a transition in the secondary structure of the hydrophilic part from a β-sheet to an α−helix.

The hydrophobic contributor gA is based on the alternating D, L configuration and its secondary structure and self-assembly changes completely if only L-configured amino acids are used for its synthesis (LgA). This became evident by comparing the water soluble amphiphile K_6-gA with its

analogue, the all L-configured K_6-LgA. While K_6-gA forms mainly micelles such as K_3X_6-gA to K_8-gA (Figure 4-5), K_6-LgA exhibits a great tendency to form gels in ethanol and water, and was only soluble in trifluoroethanol (TFE). The CD spectra no longer exhibit the maximum at 223 nm, as was observed for K_6-gA, and its secondary structure, as derived from CD in TFE (Figure 4-5), was assigned to a β-sheet structure. Thus, the intramolecular hydrogen-bonds that stabilize the D,L configured gA helix are most likely intermolecular hydrogen-bonds between the β-sheet structures of the gA entirely L-configured. Therefore, the folding of the hydrophobic gA-helix is crucial to the amphiphilicity of the entire peptide and only occurs in the case of the D, L − alternating configuration.

To observe the superstructures formed by the self-assembly of the peptide series in solution TEM was used. Self-assembly was induced by changing the surrounding polarity during the exchange of the organic solvent to dd water. TEM images show fibers as the main superstructure generated by peptides ranging from X_8-gA to K_2X_6-gA (Figure 4-6 A to C). Fibers have a length ranging from less than 30 nm up to 800 nm and can even self-assemble further into a "helical superstructure," although in a rather disorderly manner (Figure 4-6 B/C).
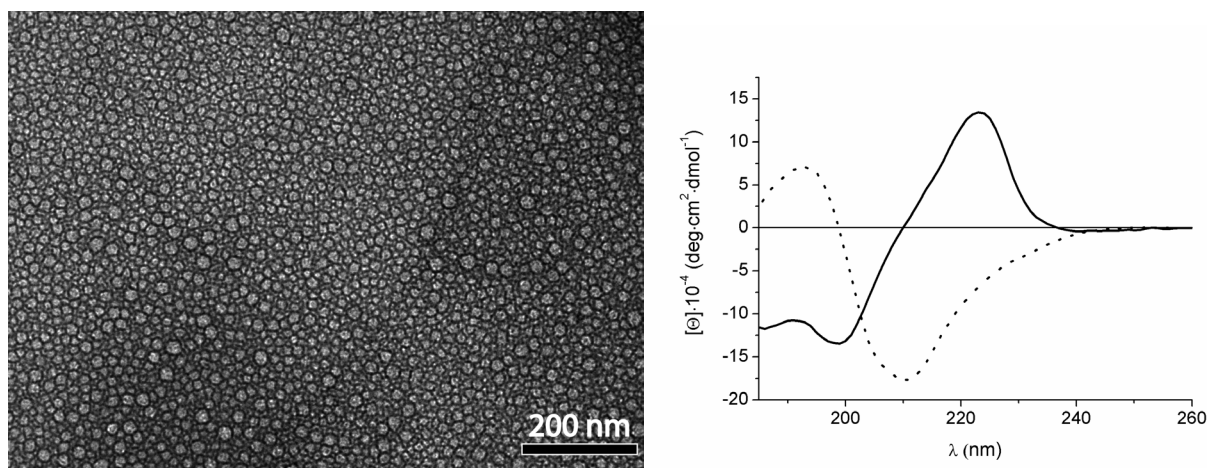
Figure 4-5: TEM of K_6-gA (left) with the CD spectra of K_6-gA (solid line) and K_6-LgA (dashed line) in TFE.

Additionally, two other superstructures have been found for Ac-X_8-gA: triangles and nanospheres with a diameter of about 100 nm. Nanospheres resemble peptide beads of related amphiphilic peptides[18] *(cf. chapter 2 and 3)*, while triangles (Figure 4-6 E) represent an unexpected structure and experiments that should explain their formation are ongoing. The triangular superstructures have also been demonstrated for peptides ranging from Ac-X_8-gA to K_1X_7-gA.

The analysis of TEM images for peptides with an α-helical character indicates the formation of superstructures containing worm-like micelles and regular micelles (Figure 4-6 D). Micelles with a radius of 6 ± 1 nm were the major component observed for peptides ranging from K_4X_4-gA to K_8-gA. The excellent solubility of peptides K_3X_5-gA to X_8-gA in aqueous solution is therefore associated with the α-helical secondary structure, which prevents the creation of intermolecular hydrogen-

bonds and therefore favors the formation of micelles. Peptide nanoparticles have also been observed for these peptides, but at a significantly lower fraction than that of the micellar.
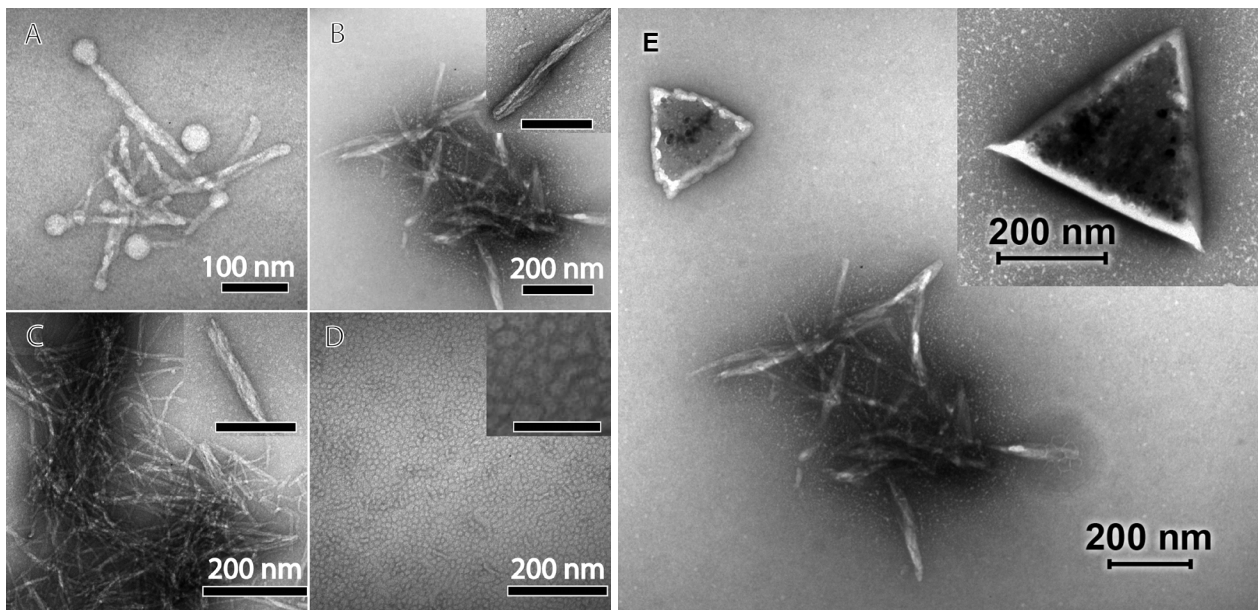
Figure 4-6: TEM of various peptide assemblies in dd H_2O: A) X_8-gA, B) K_1X_7-gA, C) K_2X_6-gA, D) K_3X_5-gA (inset scale bar 50 nm), E) X_8-gA triangles.

4.3.3 Degree of acetylation influences micellization behavior

In order to gain greater insight into the behavior of micelles DLS was used in combination with ζ-potential, which provides information on the superstructures and their surface charges. DLS of K_3X_5-gA to K_8-gA revealed, in addition to micelles, another superstructure population. In combination with TEM images, we determined that micelles at a size of 7 ± 3 nm represent the major component, while the second population – assigned to peptide nanoparticles at a radius of 50 nm – represents only a minor component.
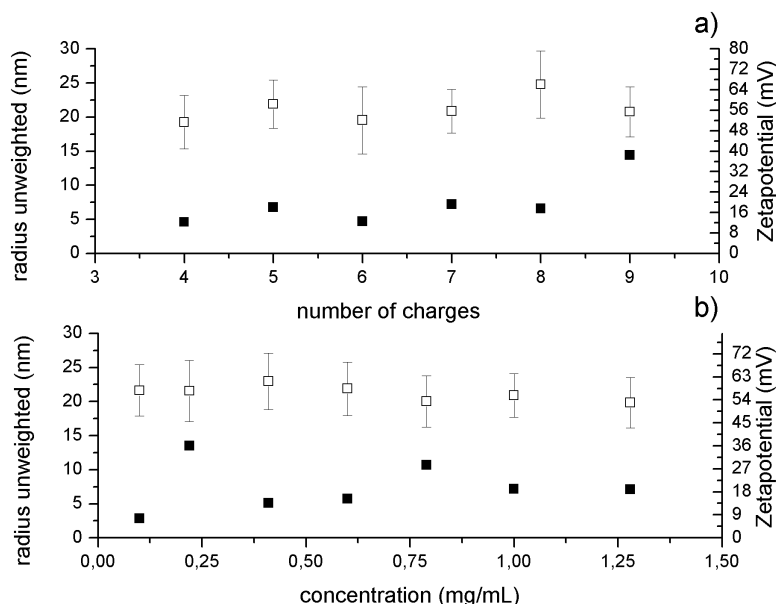
Figure 4-7: Hydrodynamic radius obtained from DLS (■) and ζ-potential values (□) for micellar species of a) K_3X_5-gA to K_8-gA and of b) K_6X_2-gA at different concentrations.

Peptide particles and micelles exhibit a hydrodynamic radius that does not depend on either the degree of acetylation (DA 3/9 to 9/9) or on the peptide concentration (0.1 – 1.28 mg mL^{-1}). Similarly, the ζ-potential did not change upon varying the DA and concentration. Because the peptide nanoparticle population is a minor component, we neglected its influence on the ζ-potential, and only the micelle population has been taken into account. As illustrated in Figure 4-7, ζ-potential values lie between 52 and 64 mV and are comparable to values obtained for a saturated polylysine surface (60 to 80 mV).[27] Aggregation of the amphiphiles into micelles governs the surface charge, and likely limits the aggregation number and dissociation of the lysine-counter ions. Therefore, the surface charge and consequently the ζ-potential values were basically independent of the number of amine-groups and peptide concentration. However, it is known that micelle formation depends on the amphiphile concentration and environmental conditions that include pH, T, buffer and ionic strength[28]. In this respect we noted with interest that the impact of DA on micelle formation could hardly be detected by DLS and the ζ-potential and therefore tensiometric mesurements were performed for peptides ranging from K_3X_5-gA to K_8-gA. Amphiphiles decrease the surface tension of water with increasing concentration until a critical micelle concentration (cmc) is reached and excess molecules are assembled mainly into micelles.
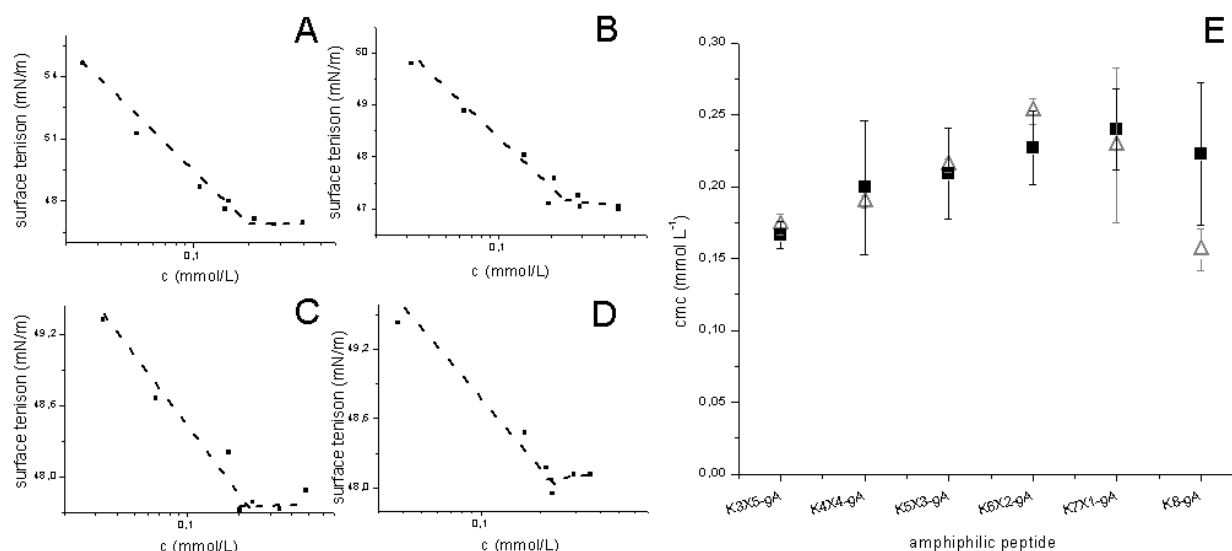
Figure 4-8: Surface tension of aq. peptide solutions of A) K_3X_5-gA B) K_4X_4-gA C) K_5X_3-gA D) K_6X_2-gA. E) cmc of peptides in H_2O (■) and in buffer, pH = 7.4 (△).

The process of micelles formation for K_3X_5-gA to K_6X_2-gA can be followed in Figure 4-8 A-D. Cmc values calculated for these peptides both in H_2O and in buffer (pH = 7.4) indicated no difference related to the solvent for peptides ranging from K_3X_5-gA to K_5X_3-gA, while starting with K_6X_2-gA a different behavior was observed (Figure 6D). In water, the cmc increased slightly with the number of charges/molecule for the whole series of peptides, and a plateau was obtained starting with K_6X_2-gA. In buffer, K_6X_2-gA represents a maximum, which is followed by a decrease in cmc values upon increasing the number of charges/molecule. From K_3X_5-gA (DA 5/9) to K_6X_2-gA (DA 3/9) – with all peptides exhibiting the same hydrophobic gA part – the self-assembly was driven by the hydrophilic part, indicated by an equal rise in cmc per charge for both solvent media. The reason for the plateauing of the cmc for dd H_2O with decreasing DA might be due to incomplete dissociation of the amine functionalities and the counter ions – defining the surface charge of the micelles. It is known that increasing the salt concentration of the media induces a decrease in the cmc, as reported for sodium alkyl sulphates[29] or 1-oleoyl-lysophosphatidic acid.[30] The presence of ions serves to shield the negative charges of neighboring headgroups, and thus favors micelle formation, i.e. leads to decreasing cmcs. However, comparing the dd H_2O solution and the buffer solution, decrease in cmcs in buffer were only observed for K_7X_1-gA and K_8-gA and were simultaneous with the cmc values on the plateau in dd H_2O. Therefore counter ion exchange, from hydroxide to multivalent ions and organic buffer ions (EDTA, TRIS) is likely to account for this decrease in cmc. Similar to other systems,[31] the presented responsiveness towards ionic strength may find usage in biomedical applications.

4.4 Conclusion

In chapter 4, a library of amphiphilic peptides (Ac-X_8-gA to K_8-gA) is presented, that contain three parts: (a) a charged lysine part (b) an acetylated lysine part, and (c) a hydrophobic gA, whereby the overall amphiphilicity is reflected in and controlled by the degree of acetylation or number of charges, respectively.

A basic structural change was located between DA of 6/9 (K_2X_6-gA) and 5/9 (K_3X_5-gA). Variation of the primary sequence caused a transition in the secondary structure of the hydrophilic part from β-sheet to α–helix. This switch-over was found to be responsible for the change in morphology from fibers to micelles i.e. the secondary structure was a function of the degree of acetylation. These morphological changes suggested based on solubility testing, and were confirmed by CD and TEM measurements.

The second change in properties was observed with a DA of less than 2/9, beyond which a reduction in cmc in buffer took place. A lower DA of 2/9 obviously has a negligible impact on self-assembly but provides means to regulate the system, e.g. adjustment of the cmc by adding salt.

The peptide library can be divided into two main regions at high DA (9/9 to 6/9) β-sheet-like secondary structures were found and correlated with fiber formation on the macroscopic scale and, at moderate and low DA (5/9 to 0/9), the peptides possessed an α-helical-like secondary structure and assembled into micelles. A second, minor population was found in both regions, and was assigned to peptide nanoparticles. Point mutation allowed tuning of the hydrophilic part of an amphiphilic peptide and thereby enabled to localize the origin of differences in morphologies and behavior on a molecular level. The importance of the secondary structure for the hydrophilic part (α-helix β-sheet) as a crucial parameter for the self-assembly was highlighted. Similarly, the alternating D, L configured gA-sequence is essential to its function as a hydrophobic contributor.

This study represents a first step towards the creation of molecular switches such as we find in nature, where proteins are converted into the active or inactive state by structural changes upon phosphorylation. Here – a proof of concept – acetylation of K_3X_5-gA to K_2X_6-gA converted water soluble micelles into water insoluble fibers. Creation of an *in situ* reversible acetylation should be the next logical step and could open the door to new biomimetic smart materials and biomedical applications.

4.5 References

[1] A. Carlsen and S. Lecommandoux, *Curr. Opin. Colloid Interface Sci.* **2009**, *14*, 329-339.

[2] A. Taubert, A. Napoli and W. Meier, *Curr. Opin. Chem. Biol.* **2004**, *8*, 598-603.

[3] S. Belegrinou, J. Dorn, M. Kreiter, K. Kita-Tokarczyk, E.-K. Sinner and W. Meier, *Soft Matter* **2009**, *6*, 179-186.

[4] a) A. Koide, A. Kishimura, K. Osada, W.-D. Jang, Y. Yamasaki and K. Kataoka, *J. Am. Chem. Soc.* **2006**, *128*, 5988-5989; b) V. Balasubramanian, O. Onaca, R. Enea, D. W. Hughes and C. G. Palivan, *Expert Opinion on Drug Delivery* **2010**, *7*, 63-78; c) K. Kita-Tokarczyk, J. Grumelard, T. Haefele and W. Meier, *Polymer* **2005**, *46*, 3540-3563.

[5] W. R. Veatch and E. R. Blout, *Biochemistry* **1974**, *13*, 5257-5264.

[6] E. P. Holowka, V. Z. Sun, D. T. Kamei and T. J. Deming, *Nat. Mater.* **2007**, *6*, 52-57.

[7] J. Rao, Z. Luo, Z. Ge, H. Liu and S. Liu, *Biomacromolecules* **2007**, *8*, 3871-3878.

[8] a) S. Ghosh, S. K. Singh and S. Verma, *Chemical Communications (Cambridge, United Kingdom)* **2007**, 2296-2298; b) J. Lin, J. Zhu, T. Chen, S. Lin, C. Cai, L. Zhang, Y. Zhuang and X.-S. Wang, *Biomaterials* **2009**, *30*, 108-117.

[9] W. C. Chan, P. D. White and Editors, *Fmoc Solid Phase Peptide Synthesis: A Practical Approach*, **2000**, p. 346 pp.

[10] a) S. G. Zhang and X. J. Zhao, *J. Mater. Chem.* **2004**, *14*, 2082-2086; b) S. G. Zhang, *Nat. Biotechnol.* **2003**, *21*, 1171-1178.

[11] G. von Maltzahn, S. Vauthey, S. Santoso and S. Zhang, *Langmuir* **2003**, *19*, 4332-4337.

[12] D. J. Adams, K. Holtzmann, C. Schneider and M. F. Butler, *Langmuir* **2007**, *23*, 12729-12736.

[13] F. Qiu, Y. Chen and X. Zhao, *J. Colloid Interface Sci.* **2009**, *336*, 477-484.

[14] N. Wiradharma, Y. W. Tong and Y.-Y. Yang, *Macromolecular Rapid Communications* **2010**, *31*, 1212-1217.

[15] T. Hashimoto, R. Iwase, A. Murakami and T. Yamaoka, *Polymer Degradation and Stability* **2009**, *94*, 1349-1353.

[16] M. Nakano, J.-R. Shen and K. Kamino, *Biomacromolecules* **2007**, *8*, 1830-1835.

[17] J. N. Shera and X. S. Sun, *Biomacromolecules* **2009**, *10*, 2446-2450.

[18] T. B. Schuster, D. de Bruyn Ouboter, E. Bordignon, G. Jeschke and W. Meier, *Soft Matter* **2010**, *6*, 5596-5604.

[19] B. A. Wallace, *Biophys. J* **1986**, *49*, 295-306.

[20] L. E. Townsley, W. A. Tucker, S. Sham and J. F. Hinton, *Biochemistry* **2001**, *40*, 11676-11686.

[21] a) A. K. Khandpur, S. Foerster, F. S. Bates, I. W. Hamley, A. J. Ryan, W. Bras, K. Almdal and K. Mortensen, *Macromolecules* **1995**, *28*, 8796-8806; b) A. Laschewsky, *Current Opinion in Colloid & Interface Science* **2003**, *8*, 274-281; c) N. S. Cameron, A. Eisenberg and G. R. Brown, *Biomacromolecules* **2002**, *3*, 124-132.

[22] a) N. Greenfield and G. D. Fasman, *Biochemistry* **1969**, *8*, 4108-4116; b) C. Toniolo, A. Polese, F. Formaggio, M. Crisma and J. Kamphuis, *Journal of the American Chemical Society* **1996**, *118*, 2744-2745.

[23] a) J. D. Tovar, R. C. Claussen and S. I. Stupp, *J. Am. Chem. Soc.* **2005**, *127*, 7337-7345; b) A. M. Ruschak and A. D. Miranker, *J. Mol. Biol.* **2009**, *393*, 214-226; c) S. Gilead and E. Gazit, *Angew. Chem., Int. Ed.* **2004**, *43*, 4041-4044.

[24] A. V. Mikhonin, N. S. Myshakina, S. V. Bykov and S. A. Asher, *Journal of the American Chemical Society* **2005**, *127*, 7712-7720.

[25] C. Dittrich and W. Meier, *Macromolecular Bioscience* **2010**, *10*, 1406-1415.

[26] B. A. Wallace, *Journal of Structural Biology* **1998**, *121*, 123-141.

[27] S. Tanimoto, T. Iwata, H. Yamaoka, M. Yamada and K. Kobori, *Research Letters in Materials Science* **2009**, No pp. given.

[28] a) A. Ponta and Y. Bae, *Pharmaceutical Research* **2010**, *27*, 2330-2342; b) Y. Jin, X.-D. Xu, C.-S. Chen, S.-X. Cheng, X.-Z. Zhang and R.-X. Zhuo, *Macromolecular Rapid Communications* **2008**, *29*, 1726-1731; c) G. Gunnarsson, B. Joensson and H. Wennerstroem, *J. Phys. Chem.* **1980**, *84*, 3114-3121; d) M. R. Dreher, A. J. Simnick, K. Fischer, R. J. Smith, A. Patel, M. Schmidt and A. Chilkoti, *J. Am. Chem. Soc.* **2008**, *130*, 687-694.

[29] M. Venanzi, G. Pace, A. Palleschi, L. Stella, P. Castrucci, M. Scarselli, M. De Crescenzi, F. Formaggio, C. Toniolo and G. Marletta, *Surface Science* **2006**, *600*, 409-416.

[30] Z. Li, E. Mintzer and R. Bittman, *Chemistry and Physics of Lipids* **2004**, *130*, 197-201.

[31] F. Checot, A. Brulet, J. Oberdisse, Y. Gnanou, O. Mondain-Monval and S. Lecommandoux, *Langmuir* **2005**, *21*, 4308-4315.

5 Exploiting dimerization of amphiphilic peptides to form vesicles

Thomas B. Schuster, Dirk de Bruyn Ouboter, Nico Bruns, Wolfgang Meier

Department of Chemistry, University of Basel, Klingelbergstrasse 80, CH-4056 Basel, Switzerland
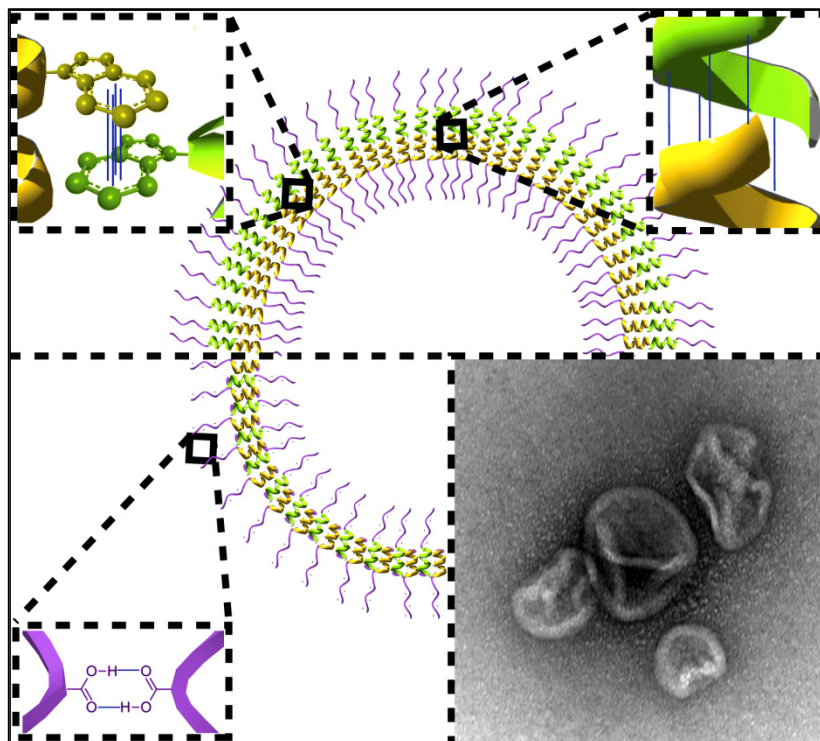
Short, purely peptidic amphiphiles self-assembled into vesicles due to dimerization; these additional interactions led to the formation of stable peptide membranes. The vesicles demonstrated pH responsiveness and the ability to encapsulate hydrophobic and hydrophilic moieties within their structure and therefore may be used as an advanced biodegradable drug delivery system.

5.1 Introduction

Medicine in the future will make use of drug delivery systems (DDSs) that transport drugs directly to a targeted tissue. To maximize drug efficacy and minimize side effects, the active substance should be segregated from physiological fluids during circulation, for example by cargo encapsulation. One morphology in focus for such an application is vesicles that self-assemble from amphiphilic building blocks, such as lipids[1], block copolymers[2], and block copolypeptides[3] – amino acid (AA) analogues of block copolymers. These vesicles can entrap a drug payload in their aqueous cavities or in the hydrophobic leaflet of their membranes and thus transport the payload through the blood stream.

Materials based on AAs are preferred for applications in the human body due to their biocompatibility. Peptide degradation pathways that are intrinsic to the body eliminate the problem of accumulation, especially for patients undergoing long-term therapy. Moreover, peptides can be designed to fold into well-ordered secondary structures, and AAs offer a diversity of functional groups that can be used as chemical handles to create selectively-labelled nanostructures.

Deming et al.[4] and Lecommandoux et al.[5] reported vesicles formation using peptide-based amphiphilic block copolymers synthesized by ring-opening polymerization of N-carboxy anhydrides (NCAs). This technique was also used to synthesize a variety of peptide-based polymers [6] and combine them with synthetic polymers to obtain block copolymer hybrids. A diversity of self-assembling bioconjugates exist which have been shown to be useful in the field of material science, e.g. bio-medical applications.[7] A drawback of such polymers is their synthesis via polymerization, which does not allow the creation of block copolypeptides with a defined sequence of amino acids.

On the other hand, peptides can be precisely synthesized by bioengineering techniques or solid-supported peptide synthesis (SPPS). Short peptides are well-suited to control and direct the self-assembly of amphiphiles into higher order structures such as micelles and vesicles, e.g. by exchanging a single AA. The use of peptide hybrids can lead to the formation of superstructures such as vesicles[8], also in coexistence with large compound micelles[9] and nanofibers.[10] Creating the necessary hydrophobic block using peptides, however, proved a difficult task, due to the hydrophilic character of the peptide backbone. Thus, not many suitable hydrophobic blocks exist.

Examples of amphiphilic short peptides that were successfully designed to assemble into membranes and vesicles have therefore rarely been reported: Zhang et al.[11] reported self-assembled superstructures which, however, proved to be highly sensitive to the purity of the peptide[11c].

The driving force for membrane formation, the segregation in solvophobic blocks, is not strong enough due to insufficient, non-homogeneous hydrophilic and hydrophobic surfaces. Mastrobattista et al.[12] reported recombinantly produced amphiphilic peptides with an additional conical geometry of the hydrophobic part that directs the self-assembly towards nano-sized

vesicles. However the polyproline II (PP II) secondary structure displays the hydrophilic backbone and therefore lacks a completely hydrophobic part.

5.2   Results and discussion

Here, we present an approach to limit the influence of the hydrophilic backbone. Additionally we used localized specific points of non-covalent binding, between the short peptides in order to stabilize a formed membrane. Besides $\pi-\pi$ stacking another key parameter is intermolecular hydrogen bonding, involved in supramolecular assemblies [10, 13] that include β-sheet[7a, 14] or cyclic peptides[15]. We investigate the requirements posed in the formation of peptide vesicles. By providing different potential dimerization sites in addition to the intrinsic inter- and intramolecular $\pi-\pi$ stacking of tryptophan-rich domains (Figure 5-1a), we expected that additional interactions by such sites would induce and stabilize bilayer formation. The amphiphilic peptides in this work were designed to allow for dimerization perpendicular to the membrane via tail-to-tail dimerization (Figure 5-1b), or by lateral association of two peptides, via carboxyl dimerization (Figure 5-1c), or by charge compensation of oppositely charged hydrophilic components (Figure 5-1d).
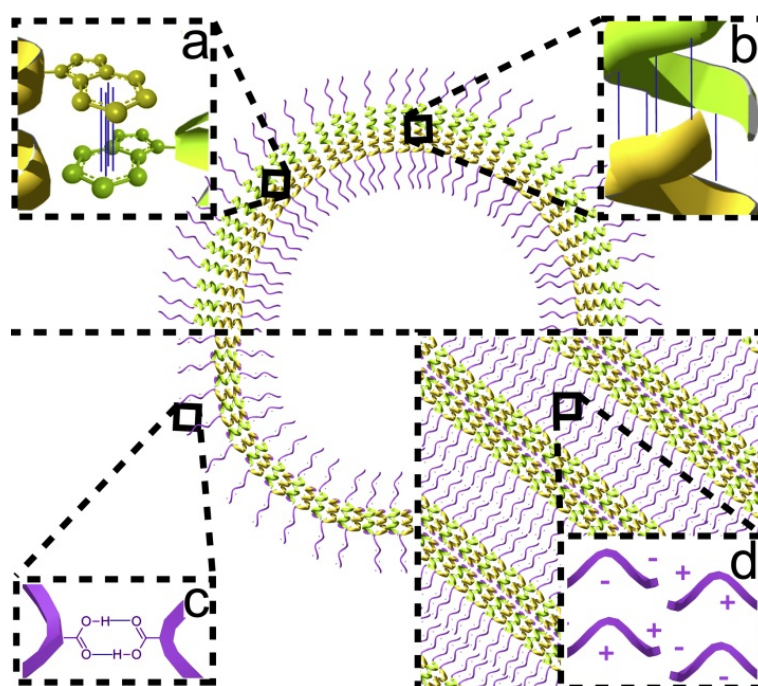
Figure 5-1: Vesicle stabilization through a) Trp-Trp interactions (π-π - stacking) b) gA-OEt-dimerization c) carboxyl dimerization and d) charge compensation.

Amphiphilic design is fundamental to every supramolecular aggregation, whether in the form of micelles, tubes or vesicles. A hydrophilic to hydrophobic AA ratio of about 1:3 is comparable to lipids and appears to be favourable for membrane formation.[16]

Thus, we chose the hydrophilic to hydrophobic ratio in our amphiphilic peptides accordingly. The hydrophobic part was inspired by gramicidin A (gA). This pentadecapeptide, known as antibiotic for gram positive bacteria, features an alternating D, L configuration, leading to a β-helix from which all of the hydrophobic side chains project outwardly.[17] The surface of the helix, i.e. the rod,

is therefore hydrophobic and the hydrophilic backbone is hidden within. Gramicidin A is a membrane peptide that can assemble and form patterns that are thought to stabilize both inter- and intra-molecularly by $\pi-\pi$ stacking of the tryptophan-rich domains.[18] Gramicidin A is insoluble in aqueous solution and forms dimers in lipid bilayers. A truncated version (gT) of gA was recently shown by our group to be effective as a hydrophobic contributor in an amphiphilic peptide, and led to self-assembled structures such as micelles and solid peptide particles.[19] However, these peptides did not form vesicles, presumably because they lacked the opportunity to form dimers.

For this work we synthesized new, short, amphiphilic peptides 22 and 25 AAs in length with a predefined sequence by means of SPPS. The produced amphiphilic peptides are shown in Table 5-1. They were examined in terms of whether they formed vesicles by using TEM, CryoTEM, and static- and dynamic light scattering techniques (SLS/DLS).

Table 5-1: Code and sequence of the amphiphilic peptides.

Code[a]	Sequence[a]
Ac-X$_8$-gA	*Ac*-[LK(Ac)]$_2$-G -[LK(Ac)]$_3$-G-[LK(Ac)]$_3$-LV-G-LA-DL-LA-DV-LV-DV-[LW-DL]$_3$-LW-*NH$_2$*
Ac-X$_8$-gA-OEt	*Ac*-[LK(Ac)]$_2$-G -[LK(Ac)]$_3$-G-[LK(Ac)]$_3$-LV-G-LA-DL-LA-DV-LV-DV-[LW-DL]$_3$-LW-*OEt*
Ac-E$_6$-gA	*Ac*-LE$_3$-G-LE$_3$-LV-G-LA-DL-LA-DV-LV-DV-[LW-DL]$_3$-LW-*NH$_2$*
Ac-K$_6$-gA	*Ac*-LK$_3$-G-LK$_3$-LV-G-LA-DL-LA-DV-LV-DV-[LW-DL]$_3$-LW-*NH$_2$*

[a] one letter code, X = LK(Ac)

Tail-to-tail dimerization that results from the formation of hydrogen-bonds between corresponding amino acids in the final turn of the helix is known from wild-type gA in hydrophobic environments (Figure 5-1b).[17] GPC led to a separation into a monomer and dimer peak. The conditions thereby simulate a hydrophobic membrane core and illustrated the potential dimerization of the modified gA structure. Ac-X$_8$-gA exhibits a C-terminal amide function on the hydrophobic end, which decreases the probability of tail-to-tail dimerization,[19] most probably due to non-matching hydrogen bond partners, accompanied by reduced hydrophobic interactions. Gramicidin is known to dimerize in apolar solvents. A reduction in retention time in GPC traces indicated the presence of gA-dimers. Consequently, GPC showed only a single peak (Figure 5-2). Similar Ac-X$_8$-gA-OEt dimers are eluted earlier compared to Ac-X$_8$-gA. The mass difference of only 29 g mol^{-1} is negligible.

To increase hydrophobic interactions, an ethoxyl group (OEt) was used to mask the terminal amide function of the amphiphilic peptide. In this way, we eliminated the last remaining hydrophilic moiety on the hydrophobic end of Ac-X$_8$-gA-OEt, and thus expected the facilitation of tail-to-tail dimerization, which would be perpendicular to the membrane (Figure 5-1b). Indeed, a decrease in retention time caused by dimerization was found in GPC for the esterified Ac-X$_8$-gA-OEt (Figure 5-2). As a result of this modification, vesicle formation was observed for Ac-X$_8$-gA-OEt, which was not the case for Ac-X$_8$-gA.[20] Figure 5-3a shows collapsed vesicles. These resulted from the drying effect on the TEM grid and thereby verified that the objects had a hollow structure. Perpendicular (relative to the membrane) dimerization of membrane subunits, is thought to support and lead to membrane association, most likely in a bilayer-type conformation.
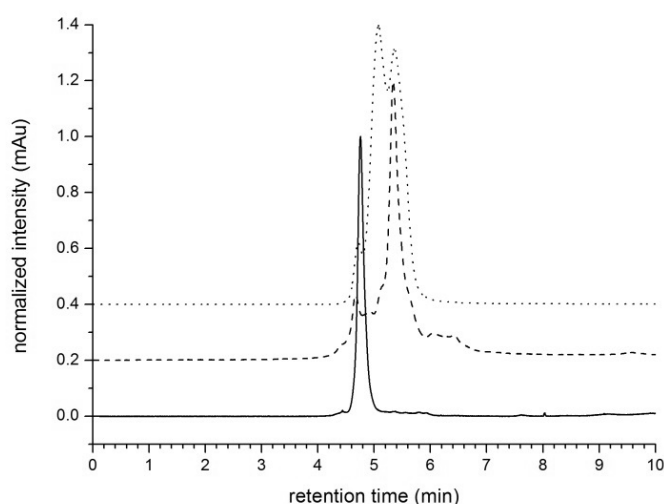
Figure 5-2: GPC of monomeric Ac-X_8-gA (dashed line) and dimerized Ac-X_8-gA-OEt (solid line) compared with the dimer and monomer peaks of wild-type gramicidin A (dotted line).

Another type of dimerization between amino acid residues can be caused by the formation of hydrogen bonds between two carboxylic acids (Figure 5-1c). Glutamic acid, more precisely the carboxyl functionality thereof, forms dimers and polyglutamic acids consequently associate.[21] They can even form a β-structure in a condensed Langmuir-Blodgett film.[22] At neutral pH, oligo- and polyglutamic acids are charged and adopt an extended 2.5_1 helix, or PP II, conformation.[23] We aimed to exploit this type of dimerization of the hydrophilic block by using negatively charged oligoglutamic acid (E, pKa of 4.7) as the hydrophilic component in an amphiphilic peptide Ac-E_6-gA. Indeed, collapsed vesicles were observed when this peptide was allowed to self-assemble, as shown in the TEM micrograph in Figure 5-3b. That implies that actually a peptide membrane was formed. In CryoTEM thin sheet fragments were observed also illustrating the formation of thin peptide membranes. Its thickness deduced from the CryoTEM images is 5 ± 1 nm. The membrane of the vesicles formed by Ac-E_6-gA cannot be stabilized by dimerization through the hydrophobic chain ends, as it was the case for Ac-X_8-gA-OEt. Thus, the association and dimerization of the hydrophilic block are the essential factors that allow the formation of stable Ac-E_6-gA membranes in a vesicle. Considering the length of an amphiphilic peptide of about 3.7 nm, the measured membrane thickness suggests that the hydrophobic parts of the amphiphiles share one layer instead of forming a bilayer, the expected morphology of membranes formed by Ac-X_8-gA-OEt (Figure 5-3c).

Light scattering provided further evidence of vesicle formation (Figure 5-4). Ac-E_6-gA exhibited a radius of gyration (R_g) of 194 nm and a molecular weight (M_w) of $3.3 \cdot 10^8$ g mol^{-1}. A Guinier plot is shown for Ac-E_6-gA in Figure 5-4a. The measured M_w of the vesicle corresponds to 130,000 aggregated peptide molecules. Assuming the gA helix represents the group that requires the most space (r=1.5 nm[17c], A=$(2r)^2$sin60°), these values would either fit a peptide bilayer, or a single peptide layer where two gA form a double helix, a structure also known from wild-type gA[17]. The

latter arrangement would also allow two oligoglutamic parts to approach each other to a favourable distance for H-bonding.
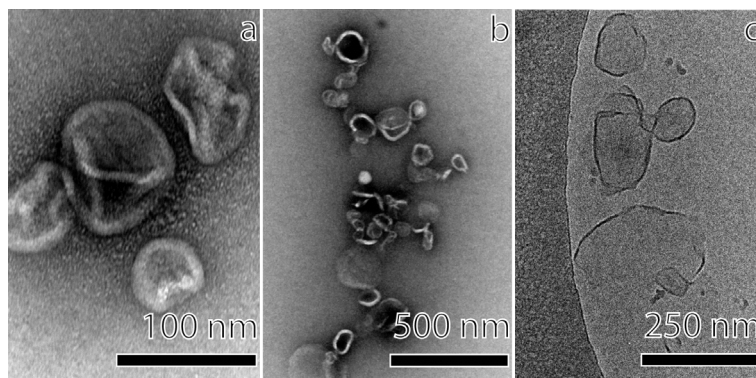
Figure 5-3: TEM of self-assembled structures of a) Ac-X_8-gA-OEt b) Ac-E_6-gA and c) CryoTEM of Ac-E_6-gA.

R_g, together with the hydrodynamic radius (R_h) of 205 nm from DLS data analysis, permits the calculation of the φ-parameter (R_g/R_h) – an indicator of the underlying structure – of 0.95. This value is close to the typical value for hollow spheres (1.0),[24] while differences from this might arise due to the presence of micelles in the system, which would lower the φ-parameter towards that of micelles (0.75). We found that the dimensions of the vesicles did not depend on the concentration of amphiphilic peptides, as shown by DLS (2nd cumulant fit, 90°) up to a concentration of 0.7 mg mL^{-1}. Above approx. 1 mg mL^{-1} aggregates are formed which were also observed by TEM and CryoTEM.
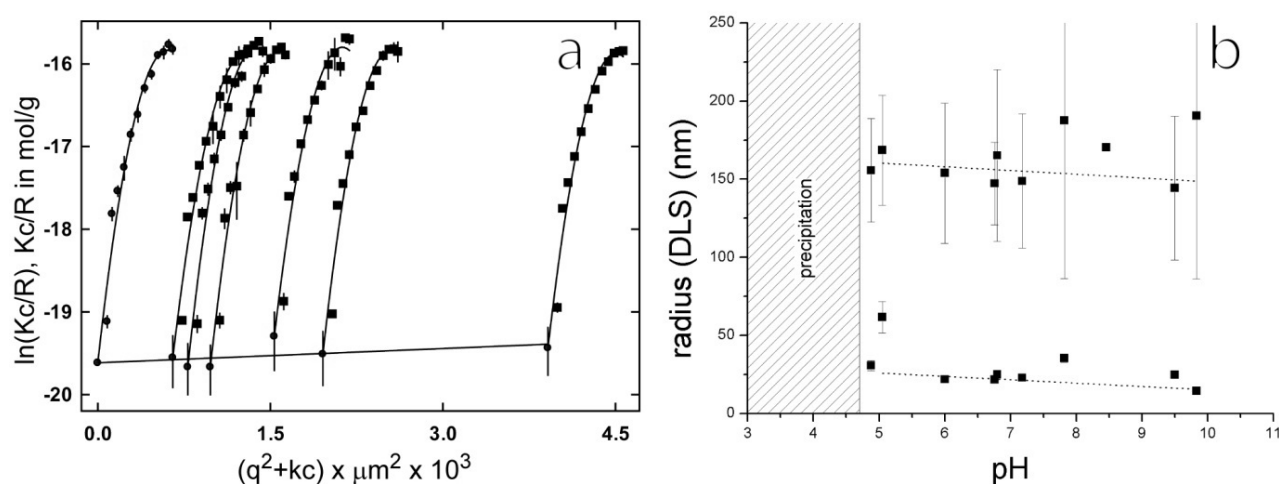
Figure 5-4: a) Static light scattering analysis (Guinier plot) and b) pH response of Ac-E_6-gA (DLS).

We expected that charge compensation would also drive the association of oppositely charged moieties. Mixtures of poly(L-lysine) (PLL) and poly(glutamic acid) (PGA) are known to form a β-sheet-like structure[23a, 25] and to interact electrostatically (Figure 5-1d). The amphiphilic peptide Ac-K_6-gA (K = lysine, pKa 10.2), the positively charged analogue of Ac-E_6-gA, exhibits the same amphiphilic design and hydrophilic-to-hydrophobic ratio as Ac-E_6-gA but lacks carboxyl dimerization. Not surprisingly, we found that it assembles into micelles and solid spherical objects,

but not into vesicles (data not shown). However, when mixed with Ac-E$_6$-gA, it did generate multi-lamellar structures at molar ratios of Ac-K$_6$-gA between 0.3 and 0.8 (Figure 5-5). Electron micrographs showed a lamellar thickness of 8.3 ± 1.3 nm, which is double the length of the amphiphiles. Thus, lateral association of neighbouring, oppositely charged hydrophilic peptide blocks induced membrane formation. Moreover, perpendicular dimerization took place despite the hydrophilic chain end of the gA block. The interaction of both types of dimerization resulted in lamellar structures and not in vesicles.
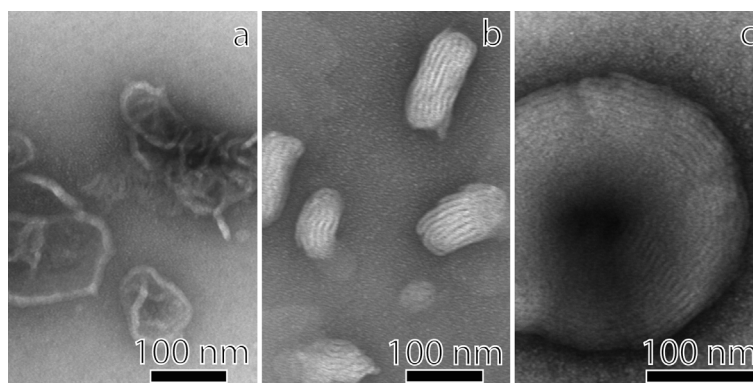
Figure 5-5: TEM of Ac-E$_6$-gA and Ac-K$_6$-gA mixtures with molar ratios of a) 0.2 b) 0.4 and c) 0.6.

Once having obtained vesicles from short amphiphilic peptides, these peptosomes were explored in initial experiments to investigate their use as functional, nano-sized containers, e.g. for drug delivery.

The introduction of pH-sensitive glutamic acid was expected to lead to a pH-responsive "smart" material. Therefore, the response to a change in acidity was monitored by DLS. The self-assembled structures were stable over a wide range of pH, but they precipitated when the pK$_a$ was exceeded (Figure 5-4b).

Vesicles possess the potential to encapsulate hydrophilic moieties within aqueous cores and to integrate hydrophilic compounds within the hydrophobic membrane layer. In an initial trial, we successfully accomplished this, respectively, with hydrophilic Alexa Fluor 488 and hydrophobic BODIPY 650/665 within Ac-E$_6$-gA assemblies (Figure 5-6). The co-localization of both fluorophores indicates the presence of vesicles. Not all fluorescent spots that showed fluorescence of the hydrophobic fluorophore showed fluoresce in the green channel. Therefore, micelles were also present next to vesicles, because the micelles are only able to accommodate the hydrophobic fluorophore in their cores.
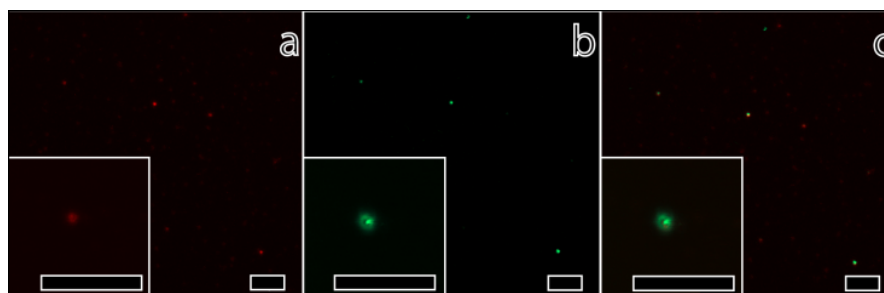
Figure 5-6: Laser scanning microscopy images of Ac-E_6-gA-based vesicles and micelles loaded with BODIPY 650/665 and Alexa Fluor 488; a) red fluorescence of the hydrophobic BODIPY, b) green fluorescence of the hydrophilic Alexa Fluor, and c) overlay, co-localized fluorophores, which indicate vesicles. Scale bars = 10 µm.

5.3 Conclusion

In conclusion, we found that additional intermolecular non-covalent bonds and interactions are necessary to stabilize vesicles formed from small amphiphilic peptides. A crucial requirement for the formation of stable peptide membranes appears to be the dimerization of peptides, which were specifically designed into the amphiphiles (Figure 5-1). Dimerization in the lateral or perpendicular directions, and thus the formation of a stabilized membrane subunit, produced stable, purely peptidic vesicles and may well apply to other systems.

The novel systems presented here offer hydrophilic and hydrophobic compartments to encapsulated different drugs and could be used e.g. for gene delivery, since the design includes charged moieties. Furthermore, the peptidic vesicles are expected to be biodegradable and thus have great potential as a DDS.

5.4 References

[1] J. A. Opsteen, J. J. L. M. Cornelissen and J. C. M. van Hest, *Pure and Applied Chemistry* **2004**, *76*, 1309-1319.

[2] a) O. Onaca, R. Enea, D. W. Hughes and W. Meier, *Macromolecular Bioscience* **2009**, *9*, 129-139; b) K. Kita-Tokarczyk and W. Meier, *Chimia* **2008**, *62*, 820-825; c) C. G. Palivan, C. Vebert, F. Axthelm and W. Meier, **2007**, pp. 32/31-32/26.

[3] A. Carlsen and S. Lecommandoux, *Curr. Opin. Colloid Interface Sci.* **2009**, *14*, 329-339.

[4] a) E. G. Bellomo, M. D. Wyrsta, L. Pakstis, D. J. Pochan and T. J. Deming, *Nature Materials* **2004**, *3*, 244-248; b) E. P. Holowka, V. Z. Sun, D. T. Kamei and T. J. Deming, *Nat. Mater.* **2007**, *6*, 52-57.

[5] J. Rodriguez-Hernandez and S. Lecommandoux, *J. Am. Chem. Soc.* **2005**, *127*, 2026-2027.

[6] a) K. T. Kim, M. A. Winnik and I. Manners, *Soft Matter* **2006**, *2*, 957-965; b) C. Schatz, S. Louguet, J.-F. Le Meins and S. Lecommandoux, *Angew. Chem., Int. Ed.* **2009**, *48*, 2572-2575.

[7] a) J.-F. Lutz and H. G. Boerner, *Progress in Polymer Science* **2008**, *33*, 1-39; b) J. Sun, C. Deng, X. Chen, H. Yu, H. Tian, J. Sun and X. Jing, *Biomacromolecules* **2007**, *8*, 1013-1017; c) J. Lin, J. Zhu, T. Chen, S. Lin, C. Cai, L. Zhang, Y. Zhuang and X.-S. Wang, *Biomaterials* **2009**, *30*, 108-117; d) F. Checot, S. Lecommandoux, Y. Gnanou and H.-A. Klok, *Angewandte Chemie, International Edition* **2002**, *41*, 1339-1343; e) H. Kukula, H. Schlaad, M. Antonietti and S. Forster, *Journal Of The American Chemical Society* **2002**, *124*, 1658-1663.

[8] S. Kimura, D.-H. Kim, J. Sugiyama and Y. Imanishi, *Langmuir* **1999**, *15*, 4461-4463.

[9] L. Ayres, P. Hans, J. Adams, D. W. P. M. Loewik and J. C. M. van Hest, *J. Polym. Sci., Part A Polym. Chem.* **2005**, *43*, 6355-6366.

[10] H. A. Behanna, J. J. J. M. Donners, A. C. Gordon and S. I. Stupp, *Journal of the American Chemical Society* **2005**, *127*, 1193-1200.

[11] a) S. Santoso, W. Hwang, H. Hartman and S. G. Zhang, *Nano Letters* **2002**, *2*, 687-691; b) Y.-R. Yoon, Y.-b. Lim, E. Lee and M. Lee, *Chem. Commun.* **2008**, 1892-1894; c) D. J. Adams, K. Holtzmann, C. Schneider and M. F. Butler, *Langmuir* **2007**, *23*, 12729-12736; d) S. Vauthey, S. Santoso, H. Gong, N. Watson and S. Zhang, *Proceedings of the National Academy of Sciences of the United States of America* **2002**, *99*, 5355-5360.

[12] a) A. J. van Hell, A. Klymchenko, P. P. Burgers, E. E. Moret, W. Jiskoot, W. E. Hennink, D. J. A. Crommelin and E. Mastrobattista, *Journal of Physical Chemistry B* **2010**, *114*, 11046-11052; b) A. J. van Hell, C. I. C. A. Costa, F. M. Flesch, M. Sutter, W. Jiskoot, D. J. A. Crommelin, W. E. Hennink and E. Mastrobattista, *Biomacromolecules* **2007**, *8*, 2753-2761.

[13] E. Jahnke, I. Lieberwirth, N. Severin, J. P. Rabe and H. Frauenrath, *Angewandte Chemie, International Edition* **2006**, *45*, 5383-5386.

[14] V. Castelletto, G. E. Newby, Z. Zhu, I. W. Hamley and L. Noirez, *Langmuir* **2010**, *26*, 9986-9996.

[15] a) S. Loschonsky, J. Couet and M. Biesalski, *Macromolecular Rapid Communications* **2008**, *29*, 309-315; b) R. Gokhale, J. Couet and M. Biesalski, *physica status solidi (a)* **2010**, *207*, 878-883.

[16] J. Yoon, M. Ree, Y. Hwang, S. W. Lee, B. Lee, J.-S. Kim, H. Kim and S. N. Magonov, *Langmuir* **2004**, *20*, 544-549.

[17] a) R. Sarges and B. Witkop, *Journal of the American Chemical Society* **1965**, 2027-2030; b) D. W. Urry, *Proceedings of the National Academy of Sciences of the United States of America* **1971**, *68*, 672-676; c) B. A. Wallace, *Biophys. J* **1986**, *49*, 295-306.

[18] a) R. Brasseur, J. A. Killian, B. De Kruijff and J. M. Ruysschaert, *Biochimica et Biophysica Acta, Biomembranes* **1987**, *903*, 11-17; b) M. Diociaiuti, F. Bordi, A. Motta, A. Carosi, A. Molinari, G. Arancia and C. Coluzza, *Biophysical Journal* **2002**, *82*, 3198-3206.

[19] T. B. Schuster, D. de Bruyn Ouboter, E. Bordignon, G. Jeschke and W. Meier, *Soft Matter* **2010**, *6*, 5596-5604.

[20] T. Schuster, D. de Bruyn Ouboter, C. Palivan and W. Meier, *manuscript preparation* **2010**.

[21] a) T. Makovec, *Biochemistry and Molecular Biology Education* **2000**, *28*, 244-247; b) E. J. Spek, Y. Gong and N. R. Kallenbach, *Journal of the American Chemical Society* **1995**, *117*, 10773-10774.

[22] N. Higashi, M. Shimoguchi and M. Niwa, *Langmuir* **1992**, *8*, 1509-1510.

[23] a) A. V. Mikhonin, N. S. Myshakina, S. V. Bykov and S. A. Asher, *Journal of the American Chemical Society* **2005**, *127*, 7712-7720; b) A. L. Rucker and T. P. Creamer, *Protein Science* **2002**, *11*, 980-985.

[24] O. Stauch, R. Schubert, G. Savin and W. Burchard, *Biomacromolecules* **2002**, *3*, 565-578.

[25] F. Boulmedais, M. Bozonnet, P. Schwinte, J. C. Voegel and P. Schaaf, *Langmuir* **2003**, *19*, 9873-9882.

6 Peptide beads: applications and biocompatibility

Dirk de Bruyn Ouboter [a], Thomas B. Schuster [a], Vijay Shanker [b], Wolfgang Meier [a]

[a] Department of Chemistry, University of Basel, Klingelbergstrasse 80, CH-4056 Basel, Switzerland.
[b] Department of Biomedicine, University Hospital Basel, Hebelstrasse 20, CH-4031 Basel, Switzerland.
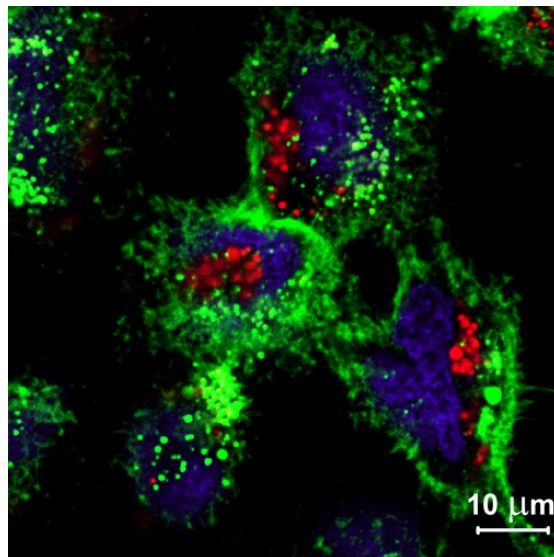
Fluorescently stained human liver cancer cells with internalized siRNA-loaded peptide beads in confocal laser scanning microscopy.

Red: siRNA in peptide beads, green: membrane, blue: nucleus.

6.1 Abstract

Chapter 6 presents the drug delivery applications potential of self-assembled peptide beads. Internalization of hydrophobic and hydrophilic payload-filled peptide beads by THP-1 macrophages, THP-1 monocytes, and hepatocellular carcinoma cells (HuH-7) was demonstrated. In addition to the bead-forming peptide Ac-X$_3$-gT, a positively charged lysine peptide analogue was used and, as a result of charge compensation, increased the embedding efficiency of RNA/DNA material to 99%. Internalization of the resulting gene delivery vehicles by HuH-7 cells led to specific gene silencing, for the case of siRNA, and antibiotic resistance and shRNA production, followed by gene silencing for the case of a delivered plasmid (DNA). Furthermore, the co-embedded drugs, paclitaxel and doxorubicin, inside the peptide beads were delivered to THP-1 monocytes, causing the intended cell death, due to the activity of the anti-cancer drugs. The new class of peptidic drug delivery material did not cause any measurable toxicity during the experiments and therefore suggests a biocompatible drug delivery vehicle for multi-drug delivery and gene therapy.

6.2 Introduction

Novel medications will require advanced, functional delivery systems to allow efficient drug delivery, protect sensitive ingredients, reduce side-effects, and increased time in circulation (*cf. chapter 1.3*). Hydrophilic drugs often possess good solubility, but are quickly degraded or eliminated from the body. Hydrophobic drugs, on the other hand, lack solubility and accumulate in hydrophobic organelles[1]. Several diseases are known to require multi-drug treatment[2], leading to the necessity of delivering and releasing the hydrophobic as well as the hydrophilic drugs simultaneously to a specific target. One example of such a need is cancer treatment in a combination therapy using hydrophilic doxorubicin and hydrophobic paclitaxel[3]. Doxil and Abraxane represent nano-carrier based drug delivery formulations of these drugs[4]; however, they remain separated as individual formulations, while they potentially could be even more efficient in combination. Multicompartmentized delivery systems – capable of embedding both drugs – would enable a deposition of only one formulation containing two drugs into a tumor and therefore allowing the simultaneous release of the two active ingredients[5].

Another important task of nano-sized delivery systems is protecting drug molecules from the environment, where they are exposed to degradation processes. Gene therapy has been promoted as having outstanding potential to cure diseases on a genetic level[6]. The use of siRNA – small interfering RNAs composed of only 15 to 25 base pairs – can temporarily stop, i.e. silence the transcription of specific genes into their peptides/proteins[7]. The technology virtually enables the treatment of almost every disease that has a basis established in gene hyperactivity, whereby the full decryption of the human genome becomes of great advantage. The use of plasmids – carrying the sequences for small hairpin RNA (shRNA) that is cleaved by the cellular machinery into siRNA – can permanently silence a gene[2]. In contrast to siRNA, a plasmid reproduces during mitosis and therefore represents a very powerful method for gene therapy. Both siRNA and the DNA plasmids are prone to degradation before reaching their destination in such an application, which seems

logical, because the body naturally protects itself from foreign genetic information. This fact, however, corroborates the need for a surrounding, protective layer to enable successful delivery into cells[2]. In nature, viruses perform this task. Synthesis of empty viruses and filling them with selected genetic information is possible[7-8], but this is a formidable task associated with high costs and, unfortunately, cannot be considered for large-scale production of pharmaceuticals. Classical transfection reagents allow gene delivery in cell models, but they tend to be toxic and cause – depending on the dose and time – partial or full cell death, which is incompatible with human gene therapy.

In recent years, great efforts have been made in research to develop smart material drug delivery vehicles capable of delivering RNA/DNA. An example is the covalent binding of a photolytic chromophore to siRNA [9]. In such a construct, the photocaged compound is inactive and protected from biochemical or biological degradation until released by light treatment. Another example is the encapsulation of RNA/DNA material in poly(D,L-lactide-co-glycolide)(PLGA) microspheres[10]. When internalized, the payload is released by degradation of the polymer and diffusion through the polymer matrix. Gary et al.[11] provide a good overview of polymer-based siRNA delivery in a recent review.

Besides their main task of encapsulation and delivery of active components, the material used ideally exhibits biocompatibility and biodegradability. These are very important properties and their absence has caused several potentially applicable systems to fail (*cf. chapter 1.3*). Amino acid based materials are generally considered biocompatible and biodegradable, due to the fact that they are an intrinsic component of the human body and they have established degradation pathways. This chapter presents the development of the peptide beads as referred to in *chapters 2 and 3* for drug delivery applications. The nano-sized peptide beads used herein are formed by aqueous self-assembly of purely peptidic amphiphiles dissolved in ethanol[12]. Their structure was investigated and described earlier and was referred to as a multicompartment micelle *(chapter 3)* capable of embedding hydrophilic and hydrophobic payloads[13].

6.3 Results and discussion

6.3.1 Peptide bead formation and payload embedding

The results presented herein were produced with two short, purely peptidic amphiphiles. Both peptides consist of an hydrophobic part, representing a seven amino acid long, alternating D-leucine / L-tryptophan sequence (gT) and a hydrophilic part of either three lysines or acetylated lysines (see Table 6-1). The charged peptide K_3-gT forms micelles with a radius of ~10 nm in aqueous solutions. The acetylated and uncharged analogue Ac-X_3-gT is soluble in ethanol and forms spherical peptide particles, termed "peptide beads", having adjustable diameters between 200 and 1500 nm when solvent is displaced by water. The beads exhibit solid character at ethanol concentrations below ~20 % wt. Above this concentration, the peptide is a loose aggregate of micelles or individual micelles. The exact behavior as a function of ethanol concentration and temperature was described earlier [12] (*cf. chapter* 2).

Table 6-1: Code, sequence, and charge of charged (K) and uncharged (X = LK(Ac)) amphiphilic peptides.

Code	Sequence	Charge (at pH 7)
K$_3$-gT	H-$_L$K$_3$-[$_L$W-$_D$L]$_3$-$_L$W-NH_2	$4+$
Ac-X$_3$-gT	Ac-[$_L$K(Ac)]$_3$-[$_L$W-$_D$L]$_3$-$_L$W-NH_2	0

With the embedding method as used – a straight forward co-encapsulation – the payload was dissolved in ethanol or water, followed by mixing with the ethanol solution of the peptide to obtain solutions of at least 50 % ethanol. Subsequent dialysis against water yielded peptide beads with embedded payloads. As reported earlier for the hydrophobic and hydrophilic dyes, rose bengal and carboxy fluorescein[13], respectively, the payloads are not only embedded but considerably enriched inside the peptide beads. We observed identical embedding behavior for other payloads also, namely BODIPY630 (hydrophobic), Alexa488 (hydrophilic), doxorubicin, paclitaxel, siRNA, and plasmids (DNA), examples shown in Figure 6-1.

We observed no measurable influence on the self-assembled structure of the peptide within the range of the concentrations used for hydrophobic or for RNA/DNA payloads. For hydrophilic doxorubicin, however, we noted an impairment in self-assembly when more than 50 % of payload mass was used relative to peptide. Above such concentrations, the size of the resulting peptide beads was drastically reduced, presumably due to shielding of the stabilizing peptide-peptide π-π-interactions by the payload (*cf. chapter 5*). However, such high payload-to-carrier ratios are usually not necessary.
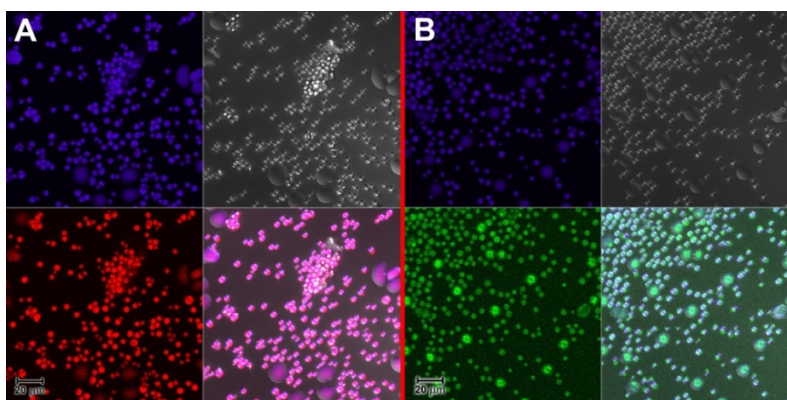
Figure 6-1: Confocal laser scanning micrographs of peptide beads with embedded payload, scale bars 20 μm. A) BODIPY 633 (red), peptide (blue), differential interfering contrast (DIC) (grey), overlay. B) Alexa 488 (green), peptide (blue), DIC (grey), overlay.

The enrichment of payloads in the peptide beads reduces the need for a method to separate non-embedded payloads from the aqueous dispersion. However, the fact that the peptide beads have a higher density than the surrounding water (1.4 g/cm^3) [12] allows easy separation of non-embedded molecules by multiple centrifugation and decantation.

Embedding efficiency (%ee) is defined as %ee = [c]$_{embedded}$/[c]$_{total}$*100. In case of RNA/DNA payloads embedded in Ac-X$_3$-gT peptide beads, the measured embedding efficiency was only

2 – 4 %ee, which speaks for a passive embedding effect (embedding the available payload with the same concentration as on the surrounding solution in the volume of the carrier)[14]. Premixing RNA with the positively charged peptide analog K_3-gT followed by peptide bead formation with Ac-X_3-gT enabled active embedding and raised the embedding efficiency to as high as 99.8 %ee (enrichment of the available payload within the carrier). Within the precision of the experiment, this represents a complete embedding of all available RNA, making any further step for separation of payload-filled beads and free payload dispensable. The low embedding efficiency when using Ac-X_3-gT only was obviously caused by the repulsive negative charges of the base pairs. However, the use of both the charged and the uncharged peptide (K_3-gT and Ac-X_3-gT) was found to influence peptide bead self-assembly: An excess of positive charges (from the K_3-gT) also led to the formation of peptide beads of the usual dimensions, but within 24 hours the beads aggregated and developed a strong affinity for glass. A balanced, overall charge, and therefore an equilibrated, mutual compensation of the positive charges from the peptide and the negative charges of the RNA, was found to be necessary to yield finely dispersed but heavily loaded peptide beads (Figure 6-2).
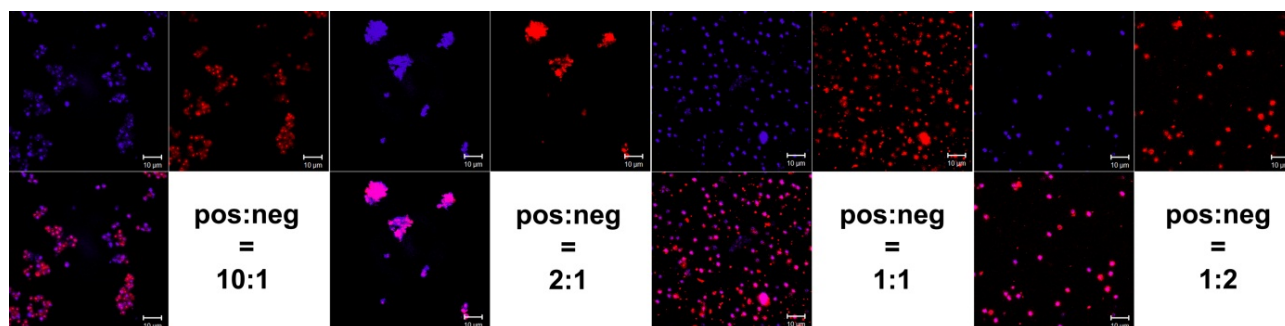
Figure 6-2: CLSM of siRNA-cy3 (red) loaded peptide beads (blue) and overlay (purple) at different ratios of positively charged peptide to negatively charged siRNA, revealing aggregation of the beads at ratios with an excess of positive charges. Embedding efficiencies >99.5%. Scale bars 10 µm.

Payloads such as the siRNA have a length of approximately 6 nm, whereas plasmids are larger and have a spherical diameter of ~500 nm. However, neither was seen in TEM of the payload-embedded peptide beads. In contrast, the loaded peptide beads looked similar to the unloaded beads (Figure 6-3). Thus, the large plasmids obviously curled-up during embedding, fitting into one bead, a phenomenon that was induced by the charge compensation and the peptide amphiphilicity.
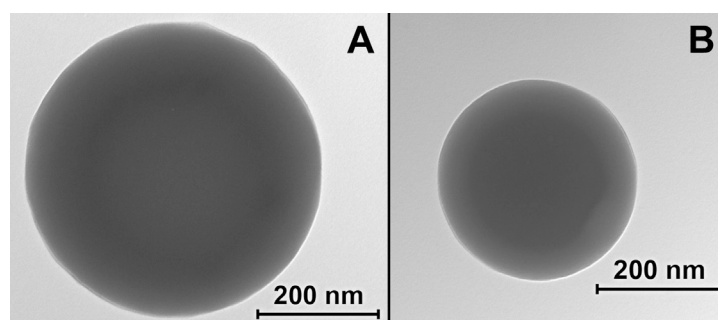
Figure 6-3: Representative TEM showing the similarity of unloaded (A) and siRNA loaded (B) peptide beads. The difference in size is within the common size distribution of the beads.

6.3.2 Cell internalization

Three different cell lines were used in order to test cellular uptake of the K_3-gT/Ac-X_3-gT peptide beads: THP-1 (human acute monocytic leukemia cell line) monocytes, THP-1 macrophages, and HuH-7 hepatocytes (hepato cellular carcinoma cells). To visualize the internalization of the potential drug delivery vehicles, cy3-labeled siRNA (250 nM, 99%ee) as well as BODIPY633 (75 nM) were used as payloads for 0.25 mg/ml and 0.5 mg/ml peptide beads, respectively. The cells were incubated with the peptide beads in a 1:5 dilution in cell growth media for 48 h. As revealed by confocal laser scanning microscopy (CLSM), shown by way of example in Figure 6-4, both kinds of beads were internalized by the cells. Internalization of the carrier is a necessary step in the development of a drug delivery system. However, after internalization, the functional payload preserved in this way has to be released at its site of action. In the case of siRNA, this is the cytosol. Diffuse fluorescence in cells indicated a release of the payload from the peptide beads to the cytosol. However, in the case of the siRNA, whether this diffuse fluorescence in the cytosol is from intact siRNA or from the remaining cy3 molecules after the decomposition of the siRNA cannot be determined. Therefore, it could not be determined whether functional siRNA was released. In order to clarify this, specific gene silencing using siRNA or a plasmid, as well as the toxic effect of doxorubicin and paclitaxel were tested.
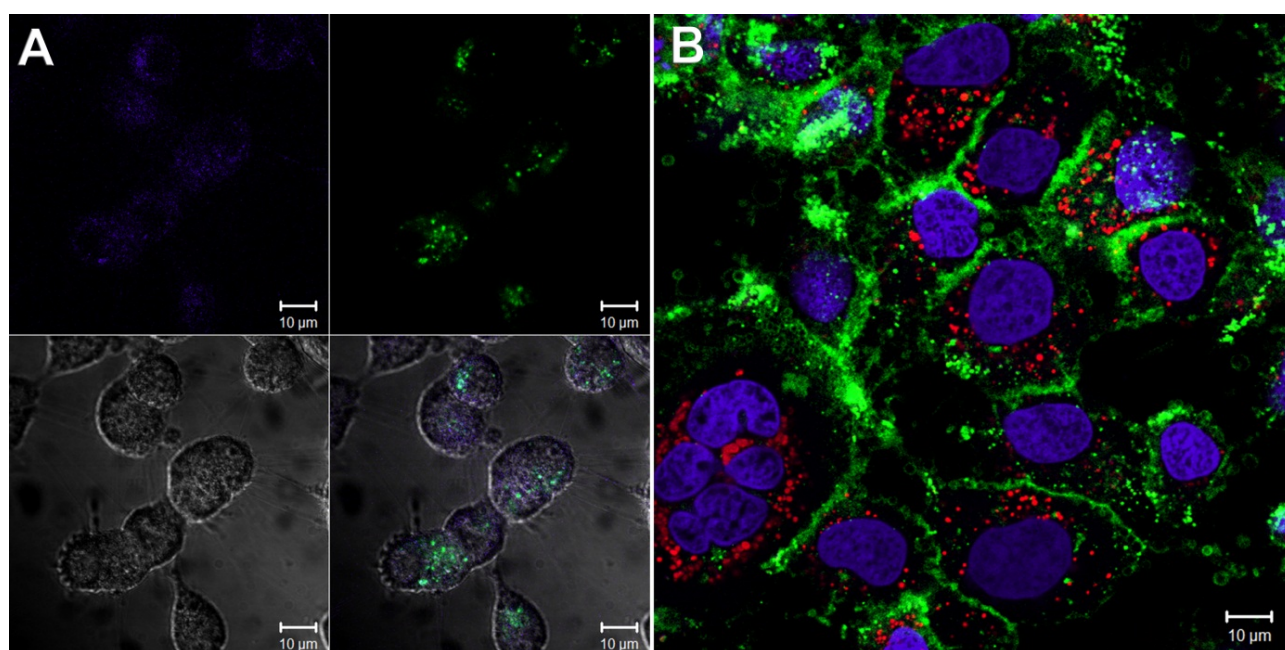
Figure 6-4: CLSM of hepatocytes. A) Internalization of BODIPY633 (green) loaded peptide beads (blue) into hepatocytes visualized in transmission channel (grey). B) Internalization of cy3-siRNA (red) loaded peptide beads into hepatocytes; nucleus (blue) and plasma membrane (green) fluorescently stained for visualisation.

6.3.3 Toxicity and therapeutic effect

We compared pure (unloaded) peptide beads with control samples (no beads added) during all experiments and always obtained similar results within the limits of experimental error. The resulting absence of any toxic effect by the peptide beads (see Figure 6-5 & Figure 6-6) is an indication of the biocompatibility of the purely peptidic amphiphiles used.
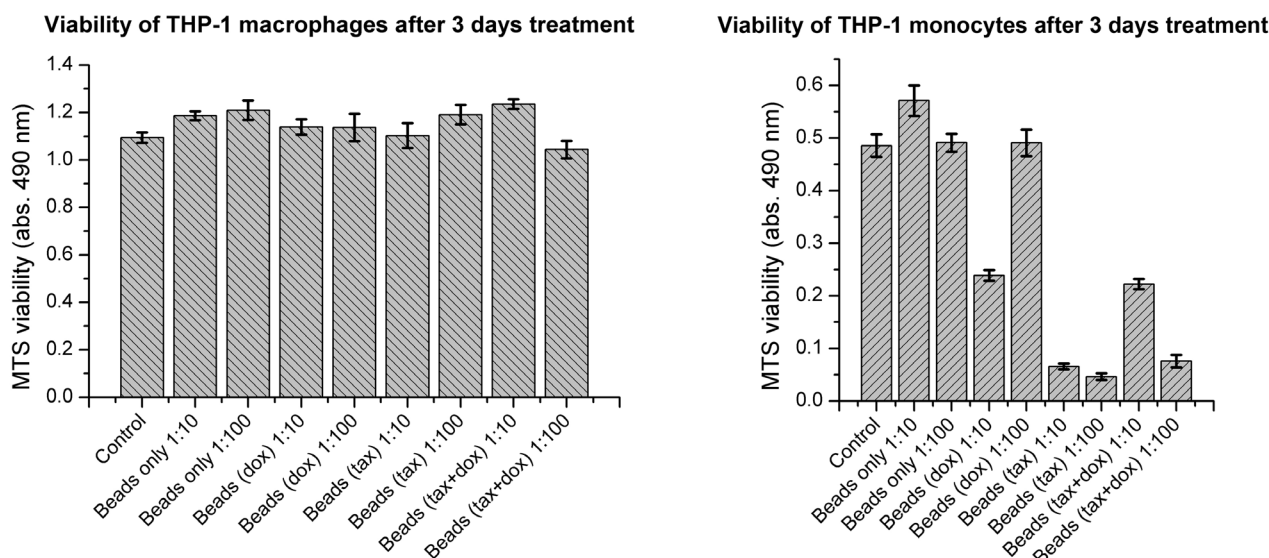
Figure 6-5: Comparison of cell viability (by MTS assay) between THP-1 macrophages and THP-1 monocytes after 3-day treatment with peptide beads loaded with the anti-cancer drugs paclitaxel and doxorubicin. Different dilutions shown. Plots visualize the lack of toxic effect by the pure peptide beads as seen form the "beads only" samples (left and right), and the desired effect of the drugs in monocytes (right).

The therapeutic effect of potentially delivered drugs was tested in order to determine not only the internalization of the peptide beads but also a functional drug delivery system at a cellular level. Therefore, cell viability tests were performed with doxorubicin, paclitaxel, and doxorubicin/paclitaxel-loaded peptide beads using THP-1 macrophages and THP-1 monocytes. To minimize non-specific delivery of the drugs, the prepared peptide beads were separated from non-embedded drugs by triple centrifugation/decantation and offered to the cells for 24 h and 72 h in two different concentrations. As Figure 6-5 reveals, all drug-loaded samples significantly reduced cell viability, as expected from doxorubicin and paclitaxel residing in monocytes. However, for the mixture of doxorubicin and paclitaxel, a reduced effect with higher bead concentrations was observed. This is puzzling and might be related to concentration dependent embedding properties. In any case, further experiments are needed to understand and fully clarify this behavior. Since the mechanisms of action of both drugs take place during cell multiplication, no effect was monitored in the non-multiplying macrophages, also indicating no toxic effect of the material used.

In principle, paclitaxel and doxorubicin can enter a cell without a drug vehicle. Although such behavior was minimized by separating free drug from the beads, it cannot be ruled out completely. Therefore the specific silencing of a target gene with siRNA as well as the delivery of a vector in the form of a plasmid was tested in hepatocytes. Neither of these payloads can enter a

cell without the help of a vehicle, because the material would be degraded. Gene silencing by the siRNA as well as effects of the delivered plasmid sequence (siRNA production and antibiotic resistance) are capable of demonstrating successful delivery and therefore show the potential of the peptide beads as a drug delivery system.

We used GAPDH siRNA (silencing the transcription of the housekeeping gene glyceraldehyde 3-phosphate dehydrogenase (GAPDH)), negative control siRNA (a scrambled sequence, causing no silencing), a psiSTRIKE-Neomycin vector (containing a hairpin target sequence of PP2Acα that allows expression of siRNA against PP2Acα, and a sequence coding for antibiotic resistance), and as control, the same vector with a scrambled sequence for the siRNA (causing no silencing)[15]. Overexpression of PP2Acα in hepatocytes has recently been shown to play an important role in liver cancer development. Although we used the silencing of this gene only as proof of principle, it raises the possibility of finding application in hepatitis C-induced liver cancer treatment[15-16].

As Figure 6-6 A&B show, the siRNA as well as the plasmid caused gene silencing compared to the negative control siRNA, negative control plasmid, and the control, measured by quantitative real time polymerase chain reaction (qRT-PCR). The monitored silencing was at the limit of significance. However, it appeared that there was always more silencing in the samples than in the controls. To prove the statistical significance of the silencing – which, at 15%, was highest for the plasmid – the cells were cultivated for three weeks after being kept in the presence of plasmid-loaded peptide beads for 96 h (Figure 6-6C). Plasmid transfected cells also replicated the plasmid itself during multiplication. To prove the successful delivery, cells transfected with plasmid were selected by addition of antibiotic in culture medium, which caused the non-transfected cells to die. The survival of the selected cells, resulting from the delivered antibiotic resistance, alone indicates the capacity of the peptide bead system to deliver a payload into the cells. The performed qRT-PCR of the stability-selected cells showed a significant silencing of 33%, caused by the siRNA produced by the delivered plasmids. The effective gene delivery capacity of the peptide beads was therefore demonstrated.
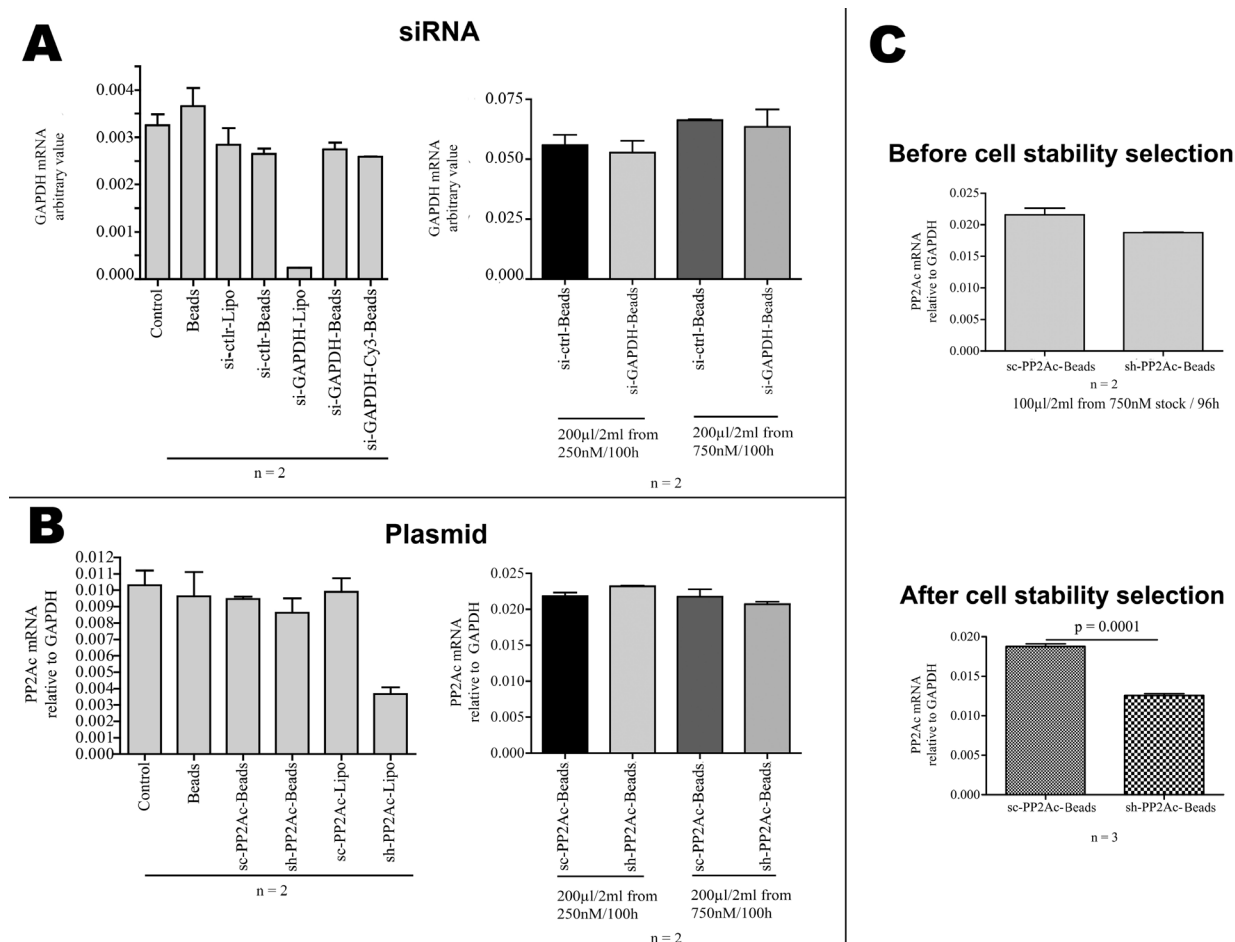
Figure 6-6: Real-Time-PCR results of gene silencing in HuH-7 hepatocytes. The comparison between control experiments, peptide beads, conventional transfection agent Lipofectamine 2000 (Lipo), siRNA (A) and plasmid (B) loaded peptide beads shows the lack of toxicity by the delivery system as well as gene silencing. The effect was significantly increased by cell stability selection of plasmid transfected cells (C), proving gene delivery effective.

In order to understand the uptake pathway, and to explain the low silencing with siRNA and with the plasmid after 96 h incubation, preliminary trafficking experiments were performed to locate the peptide beads within the cell. CLSM with cy3-siRNA and a Lysotracker assay (a fluorescent dye, labeling the acidic conditions of the lysosome) was performed.

A large fraction of the beads – especially the bigger beads – was found in the lysosome after 48 h of treatment with the peptide particles. However, small beads or released payload were also found outside the lysosome, obviously the cause for the silencing (Figure 6-7). Current findings allow two explanations that can be approached to increase the silencing. Firstly, bigger beads are being trapped and, together with payload, decompose in the lysosome, while smaller beads undergo different uptake-pathways and release the payload in the cytoplasm. The low fraction of the small beads would explain the low amount of siRNA delivered and the low silencing. The second possibility is that the solid peptide beads are trapped in the lysosome and, due to their solid character, protect the payload from decomposition. However, this intense protection might also hinder the payload from being released. Nevertheless, the monitored silencing and transfection with the plasmid proves the delivery to be functional. To understand the process,

further experiments are necessary, *e.g.* trafficking, quantifying the internalization efficiency, and analyzing the release mechanism. Although such experiments are very interesting, they are out of the scope of this thesis, which started with the synthesis of the peptides from scratch.
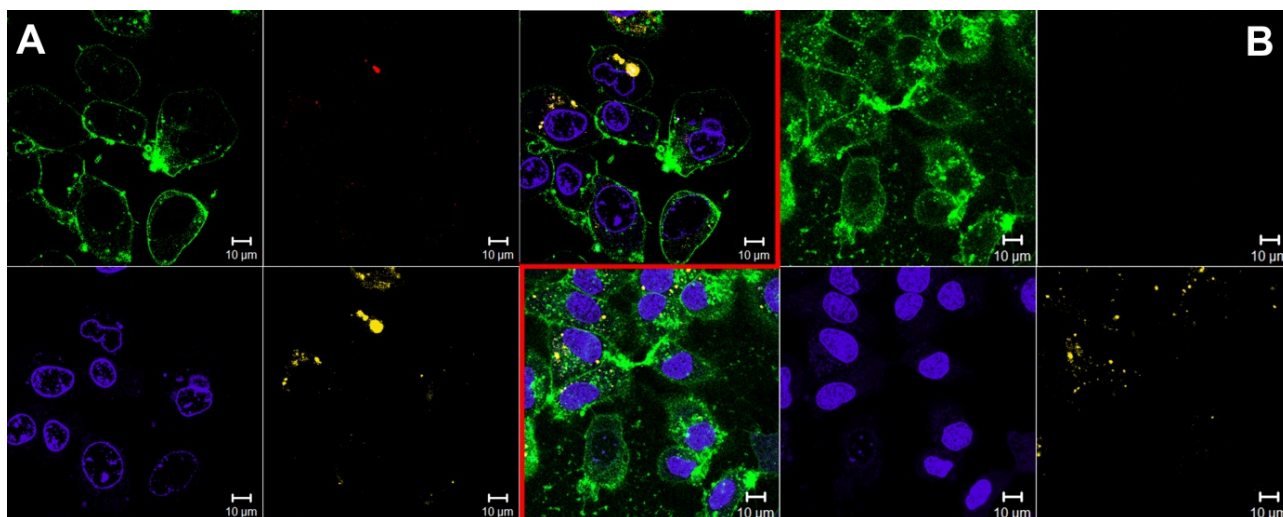
Figure 6-7: CLSM of stained hepatocytes, plasma membrane (green), nucleus (blue), lysotracker (yellow), delivered siRNA(red). A) Cell culture with internalized cy3-siRNA filled peptide beads. B) Control without peptide beads/siRNA.

6.4 Conclusion

The presented uncharged, short, and purely peptidic amphiphile is capable of embedding various payloads with different hydrophilic and hydrophobic properties in peptide beads of 100 – 1500 nm in size. Such a capacity is useful to simultaneous deliver drugs of variable solubilities, as shown with doxorubicin and paclitaxel. The drugs were embedded separately as well as in combination in the peptide beads. The delivery of the drugs to THP-1 monocytes caused the death of the cells due to the toxic intervention of the guest molecules within the cancer cell amplification. In THP-1 macrophages, no effect was monitored, since the non-dividing cells are not prone to the mechanism of action of the two anti-cancer drugs. For the embedding of RNA/DNA related materials, the embedding efficiency was increased from 3% to 99.5% by compensating the payloads' charges with counter-charged peptide amphiphiles. Thus, the embedding of all available payload molecules made post-embedding purifications unnecessary. It further allows for a very high payload concentration to be delivered. Therefore, the peptide beads fulfill the highly aspired requirements for drug delivery vehicles regarding encapsulation efficiency[14].

The capacity of the presented peptide bead system to deliver and release RNA/DNA payloads, causing delivery of a gene and silencing with siRNA, respectively, reflects a first indication of the peptide amphiphiles' capacity as a carrier in gene therapy/delivery. The currently achieved 33% of specific gene silencing reflects proof of principle and does not diminish the value of the system, because the material caused no measurable toxic effect during the experiments. Therefore, and due to its amino acid based nature, it can currently be viewed as a biocompatible system. The mechanism of uptake of the peptide beads as well as the release of the payloads are both not yet understood. Combinations of peptide degradation, diffusion, counter ion exchange, or

deprotonation due to a changing pH are possible to release the RNA/DNA material. A better understanding of these mechanisms in regard to the used system might lead to modifications to enhance the delivery/release efficiency. From the current results, we assume that good protection of the payloads, due to the solid character of the beads, helps the payload resist the harsh lysosomal conditions until escape from the lysosome. However, this also leads to a slow release of the payloads. It would therefore be favorable to include a trigger in the beads, allowing controlled and accelerated release. As an example, the co-encapsulation of gold-nanoparticles within the beads could introduce an IR-excitable heat source that would allow triggering of payload release.

In final summation, we have presented a biocompatible, non-toxic, purely peptidic drug-delivery system that is capable of hosting hydrophilic and hydrophobic molecules, RNA, and DNA, delivering the host into cells without the need of additional uptake-stimulating substances. Therefore, we showed the potential of purely peptidic amphiphiles for drug delivery applications.

6.5   References

[1] S. Svenson in *Carrier-Based Drug Delivery*, *Vol. 879* American Chemical Society, **2004**, pp. 2-23.

[2] F. Xie, M. Woodle and P. Lu, *Drug Discovery Today* **2006**, *11*, 67-73.

[3] S. M. Temkin, *Clin. Ovarian Cancer Other Gynecol. Malig.* **2008**, *1*, 30-32.

[4] Y. Malam, M. Loizidou and A. M. Seifalian, *Trends in Pharmacological Sciences* **2009**, *30*, 592-599.

[5] a) M. Delcea, A. Yashchenok, K. Videnova, O. Kreft, H. Mohwald and A. G. Skirtach, *Macromolecular Bioscience* **2010**, *10*, 465-474; b) H. Ringsdorf, P. Lehmann and R. Weberskirch, **1999**, pp. BTEC-001; c) J.-F. Lutz and A. Laschewsky, *Macromolecular Chemistry and Physics* **2005**, *206*, 813-817.

[6] a) N. Toub, J. R. Bertrand, A. Tamaddon, H. Elhamess, H. Hillaireau, A. Maksimenko, J. Maccario, C. Malvy, E. Fattal and P. Couvreur, *Pharmaceutical Research* **2006**, *23*, 892-900; b) R. Koukiekolo, S. M. Sagan and J. P. Pezacki, *FEBS Letters* **2007**, *581*, 3051-3056.

[7] D. M. Dykxhoorn, C. D. Novina and P. A. Sharp, *Nature reviews. Molecular cell biology* **2003**, *4*, 457-467.

[8] K. Matsuura, K. Watanabe, T. Matsuzaki, K. Sakurai and N. Kimizuka, *Angewandte Chemie* **2010**, *122*, 9856-9859.

[9] J. P. Casey, R. A. Blidner and W. T. Monroe, *Molecular Pharmaceutics* **2009**, *6*, 669-685.

[10] a) A. Khan, M. Benboubetra, P. Z. Sayyed, K. Wooi Ng, S. Fox, G. Beck, I. F. Benter and S. Akhtar, *Journal of Drug Targeting* **2004**, *12*, 393-404; b) M. Husmann, S. Schenderlein, M. Lück, H. Lindner and P. Kleinebudde, *International Journal of Pharmaceutics* **2002**, *242*, 277-280.

[11] D. J. Gary, N. Puri and Y. Y. Won, *Journal of controlled release : official journal of the Controlled Release Society* **2007**, *121*, 64-73.

[12] T. B. Schuster, D. de Bruyn Ouboter, E. Bordignon, G. Jeschke and W. Meier, *Soft Matter* **2010**, *6*, 5596-5604.

[13] C. Dittrich and W. Meier, *Macromolecular Bioscience* **2010**, *10*, 1406-1415.

[14] K. Kita and C. Dittrich, *Expert Opinion on Drug Delivery* **2011**, *8*, 329-342.

[15] F. H. T. Duong, V. Christen, S. Lin and M. H. Heim, *Hepatology* **2010**, *51*, 741-751.

[16] a) G. Randall, A. Grakoui and C. M. Rice, *Proceedings of the National Academy of Sciences of the United States of America* **2003**, *100*, 235-240; b) F. H. T. Duong, V. Christen, M. Filipowicz and M. H. Heim, *Hepatology* **2006**, *43*, 796-806.

7 Densely packed composite peptide-gold nanoparticles

Dirk de Bruyn Ouboter, Thomas B. Schuster, Wolfgang Meier

Department of Chemistry, University of Basel, Klingelbergstrasse 80, CH-4056 Basel, Switzerland.
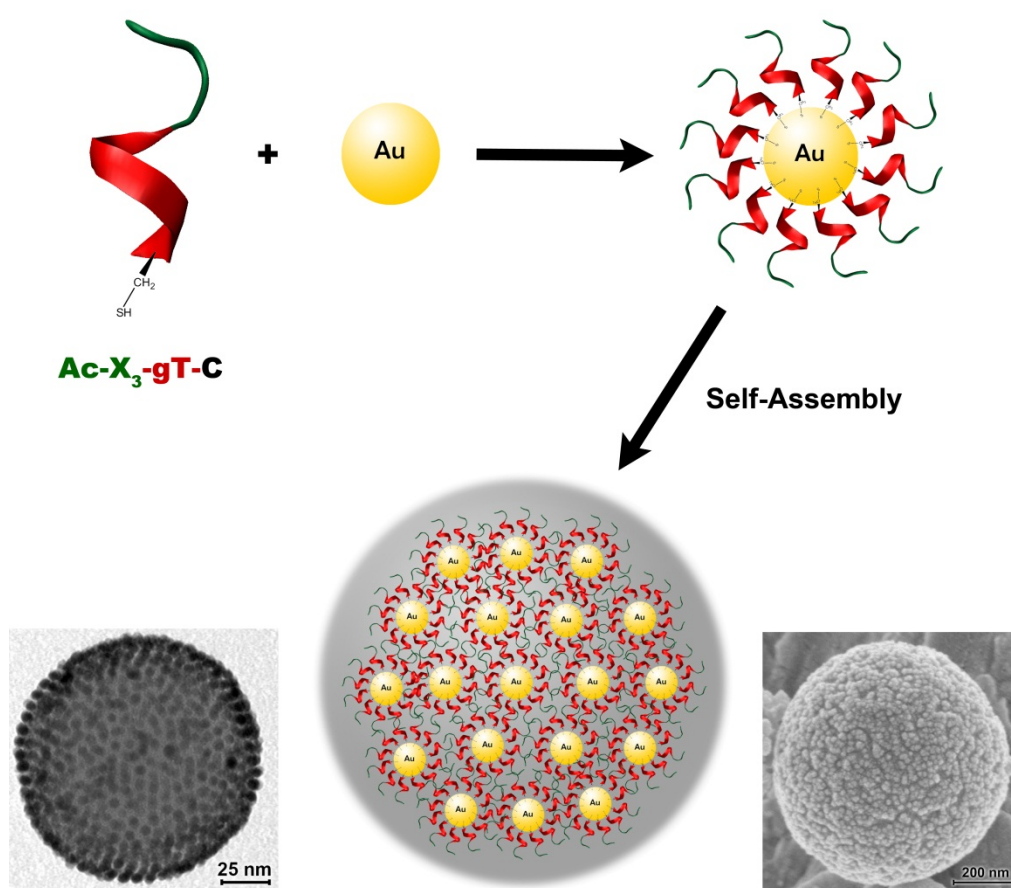
Figure 7-1: Illustration of the formation process, showing the coating of 5 nm gold nanoparticles with the peptide Ac-X_3-gT-C, and the subsequent formation of the composite peptide-gold nanoparticles enabled by the self-assembly features of the peptide. Additionally, transmission- and scanning electron micrographs (TEM & SEM) demonstrate the composite peptide-gold nanoparticles in actuality.

7.1 Abstract

In chapter 7, the use of a self-assembled peptide superstructure as template for nano-patterned objects is presented. The bead-forming peptide Ac-X$_3$-gT was C-terminally modified with a cysteine and linked to gold nanoparticles. Subsequent self-assembly of the peptide-coated gold nanoparticles led to controlled aggregation of the gold core micelles to form composite peptide-gold nanoparticles, in which the individual gold nanoparticles are close together but still separated from one another. Microscopic and spectroscopic examination revealed dense packing of the gold nanoparticles within the peptide beads, offering the opportunity for exceptional optical- and electronic properties as well as the use of the composite material for a potential triggered destruction of the peptide beads by the typical radiation absorption effect of gold nanoparticles.

7.2 Introduction

Colloidal, inorganic nanoparticles have gained ever more attention in recent years due to their exceptional properties: In addition to their total vast surface area, they possess various interesting properties such as fluorescence (quantum dots, e.g. CdTe, CdSe), phosphorescence (e.g. Y$_2$O$_3$), magnetism (e.g. iron oxide, cobalt), high electron density, and strong optical absorption (e.g. Ag, Au). In particular, the exceptional electronic- and optical properties of gold nanoparticles (GNPs)[1] has led to the development of various applications[2]. Similar to mystic Greek hybrid creatures (e.g. centaurs, griffins, etc.), in nanosciences the idea of combining two features into one has also led to composites that reduce limitations of individual materials while expanding their virtues. This fact has given rise to steadily increasing industrial and academic interest in composite materials that exploit the properties of magnetic nanoparticles[3], MRI contrast agents[4], quantum dots[5], and GNPs [2, 6] to improve e.g., medical imaging or diagnostics[7].

An approach taken to reduce the drawbacks of inorganic materials (e.g., toxicity, fast distribution/dilution) while preserving their above mentioned unique features is coating or embedding the inorganic nanoparticles with materials with advantageous properties. As an example, Azzam and Eisenberg[6f] recently coated GNPs with poly(ethylen oxide)-b-poly(caprolactone) to better localize macromolecular assemblies in biological applications. On the other hand, composite materials can generated new features, as is the case with recently presented shell-in-shell multicompartment capsules[8]: The incorporation of near-infrared light (NIR) absorbing GNPs in the membrane of the inner shell allowed membrane degradation by heat, produced by the absorption of near-infrared laser light, leading to mixing of initially separated payloads. These examples show that beneficial new materials might result from expanding the properties of known (nano-sized) materials by incorporation of inorganic nanoparticles. Consequently, we herein show how peptide beads and their self-assembly can be combined with GNPs to allow structural templating of gold nanoparticles, but also to include new functions, as e.g., NIR triggered destruction of the beads in order to speedup payload release.

7.3 Results and discussion

We recently presented the amphiphilic undecapeptide Ac-X$_3$-gT, which – depending on the state of charge – is capable of forming micelles or peptide beads[9] (*cf. chapter 2*). The spherical peptide particles, termed "peptide beads", have controllable radii ranging from 100 to 800 nm and are formed during a self-assembly process that takes place when exchanging the peptide-dissolving ethanol for water. The formation process is a hierarchical self-assembly from micelles to multicompartment micelles (*cf. chapter 2 & 3*).

Peptides exhibiting a cysteine are capable of forming well-known thiol – gold bonds[6d, 10]. In order to transfer self-assembly properties of Ac-X$_3$-gT to GNPs, we attached a thiol functional group (cysteine) to the peptide's hydrophobic part (Table 7-1)Table 7-1 Code and sequence of the use amphiphilic peptide and its precursor [X = LK(*Ac*)].. The thusly obtained Ac-X$_3$-gT-C was then used to coat commercially available GNPs (5 nm and 25 nm) in ethanol solutions, followed by the self-assembly of the so-obtained gold core micelles into composite peptide-gold nanoparticles during dialysis, exchanging ethanol with water (see Figure 7-1).

Table 7-1 Code and sequence of the use amphiphilic peptide and its precursor [X = LK(*Ac*)].

Code	Sequence
Ac-X$_3$-gT	*Ac*-[LK*(Ac)*]$_3$-[LW-DL]$_3$-LW-*NH$_2$*
Ac-X$_3$-gT-**C**	*Ac*-[LK*(Ac)*]$_3$-[LW-DL]$_3$-LW-**LC**-*NH$_2$*

7.3.1 Self-Assembly of the pure Ac-X$_3$-gT-C

As indicated earlier, cysteine functionalization on the hydrophilic part of the peptide did not change the self-assembly behavior with any of the methods used[9] (*cf. chapter 2*). In order to ensure comparable self-assembly behavior of the newly formed peptide, we investigated the impact of cysteine elongation on the hydrophobic part on the self-assembly properties. These investigations revealed that Ac-X$_3$-gT-C similarly self-assembled into peptide beads as AcC-X$_3$-gT and the non-cysteinated analogue Ac-X$_3$-gT (Figure 7-2). The size distribution of the formed beads was relatively large. Nevertheless, the hydrodynamic radius, as determined by dynamic light scattering (DLS), at 256 nm, is consistent with SEM and in the same range as the peptide beads of the other analogues. Although the formed beads exhibit a rougher surface and obviously a looser packing of the micellar subunits – which is presumably caused by additional disulfide stabilization of the micelles (*cf. chapter 3*) – the self-assembly behavior in general is identical to the earlier described peptide beads[9].
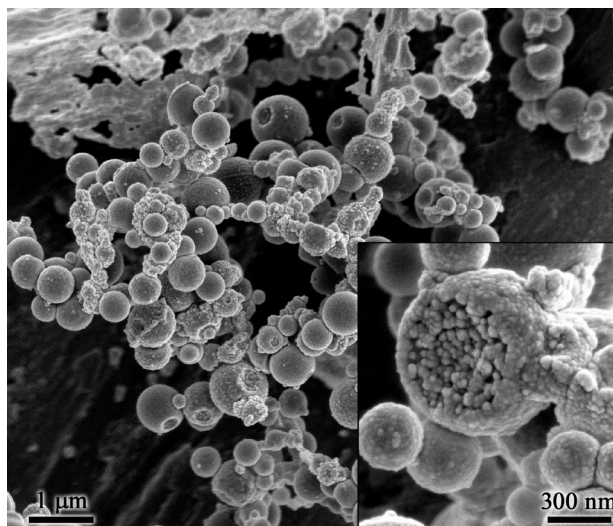
Figure 7-2: SEM of self-assembled peptide beads from Ac-X$_3$-gT-C, showing bead formation comparable to the N-terminally- and non-cysteinated analogues, with a slightly rougher surface, and a looser packing of the micellar subunits.

7.3.2 Self-assembly of the Ac-X$_3$-gT-C–GNP composite material

The coating of the GNPs with the peptide, separation of free peptide by centrifugation, and the subsequent self-assembly into composite peptide-gold nanoparticles (CPGNPs) was successful, as the slow sedimentation of the reddish CPGNPs, resulting from the color of the GNPs, already suggested. DLS showed a hydrodynamic radius of 350 nm for the CPGNPs. Fortunately, the large size distribution provided the small particles that permitted a view by TEM and showed that the newly formed CPGNPs exhibit homogenously distributed GNPs in a dense arrangement (Figure 7-3). The approx. 3 nm thick peptide layer is in agreement with the length of one peptide. SEM showed similar sizes of the particles, further it allowed a closer look to the formation process, since differently matured particles were present in the sample (Figure 7-4). As appearing from the measurements, the particles were formed by aggregation of the gold-cored micelles. Due to the covalent attachment of the peptide to the GNPs, the micelles were hindered to produce a smooth surface by pronounced sintering-like processes (*cf. chapter 3*), which led to better visible individual micelles, but also to gaps between bigger islands in the material. Such bigger islands may have formed first and then aggregated into the final CPGNPs.
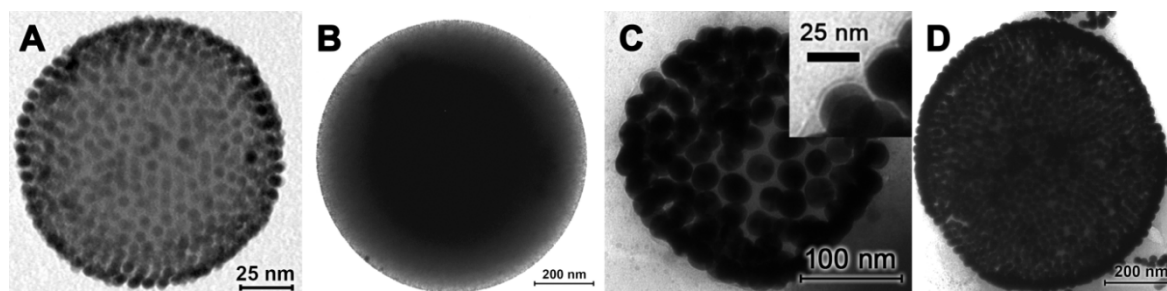
Figure 7-3: TEM micrographs of self-assembled CPGNPs, showing the dense packing of 5 nm GNPs (A,B) and 25 nm GNPs (C,D) within the particles. Small particles reveal a look inside (A, C), in large particles the embedded gold is visible only at the edge due to the high electron density (B, D). The inset in C shows the peptide surrounding the GNP.
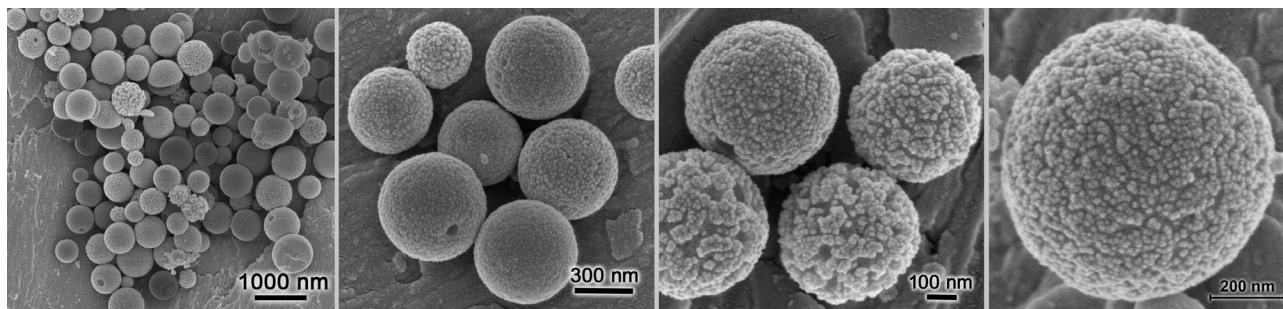
Figure 7-4: CPGNPs in SEM. Produced by aggregation of gold core (5 nm) micelles. The covalent peptide-gold bond prevents the micelles from sintering together in a smooth fashion.

During the first experiments to explore the properties of the composite material we monitored no shift in the size dependent, characteristic gold absorption[11] in UV/Vis (Figure 7-5). This speaks for closely packed but still separated GNPs within the CPGNPs. The close distance of the individual gold nanoparticles lets us assume interesting quantum size effects[1]. However, further experiments are necessary to explore such features.
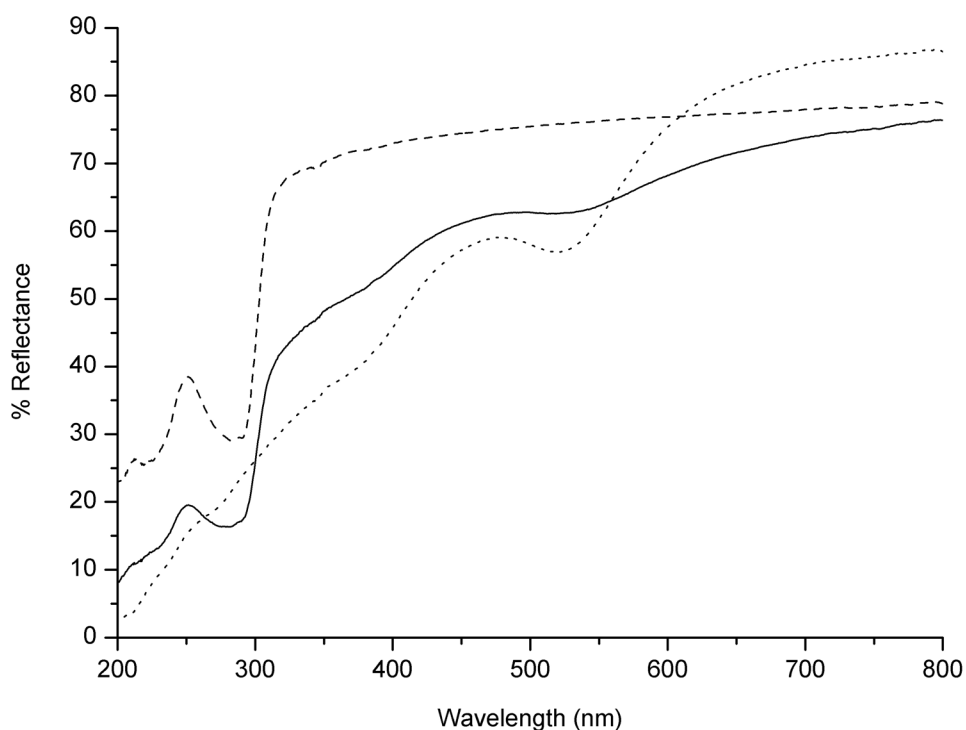
Figure 7-5: Diffuse reflectance UV/Vis spectra of peptide beads (dashed line), gold nanoparticles (dotted line), and composite peptide-gold nanoparticles (solid line) in comparison, showing the characteristic absorption of gold nanoparticles in the range of 500 - 550 nm.

During preliminary experiments we also observed high sensitivity of the material upon irradiation with 532 nm laser light, leading to rapid decomposition of the peptide in a dry state, even at weak laser intensities. This is no surprise, because the incorporation of light absorbing GNPs allows the local production of heat and can be used as a trigger[8]. The earlier reported capacity of the

peptide beads as a drug-delivery system (*cf. chapter 6*) in combination with the light absorbing, heat producing effect could be used to enable an NIR-triggered local release of payload from the peptide beads or simply to adjust the release profile towards a faster release, and therefore release of a higher concentration of the payload. Furthermore, the enhanced contrast of the peptide beads (due to the embedded gold) and the consequently better visibility in optical- and electron microscopes can enhance the study of uptake mechanisms of the beads by cells. The fact that the beads still present the peptide to the outside would make such results particularly interesting for drug delivery applications.

7.4 Conclusion

The introduction of a cysteine to the hydrophobic part of the amphiphilic peptide Ac-X_3-gT led to similar self-assembled peptide beads as with its analogues but with slightly looser packing. The cysteine on the new peptide Ac-X_3-gT-C allowed the linkage of the peptide to gold nanoparticles. In this way, the self-assembly properties of the peptide were transferred to the new composite material, leading to the aggregation of the obtained gold core micelles to form particles with similar sizes as the original peptide beads without gold. We showed that the newly formed composite peptide-gold nanoparticles are a dense package of gold nanoparticles in close association with one another, while the individual gold nanoparticles are still separated by a thin peptide layer.

Preliminary results have shown that the packed gold nanoparticles maintain the properties of the colloidal gold in terms of light absorption. However, energy transferred to the gold by laser light led to local heat production, which may find application as a trigger for the release of payloads embedded in the peptide beads. Since the exceptional optical- and electronic properties of gold nanoparticles[1] have recently led to the development of various concepts for applications[2], the small distance between the individual gold nanoparticles within our particles let us also assume new features that might be explored using our straight forward production process for the new composite material.

7.5 References

[1] M.-C. Daniel and D. Astruc, *Chem. Rev. (Washington, DC, U. S.)* **2004**, *104*, 293-346.

[2] D. A. Giljohann, D. S. Seferos, W. L. Daniel, M. D. Massich, P. C. Patel and C. A. Mirkin, *Angew. Chem., Int. Ed.* **2010**, *49*, 3280-3294.

[3] S. Lecommandoux, O. Sandre, F. Checot, J. Rodriguez-Hernandez and R. Perzynski, *Advanced Materials (Weinheim, Germany)* **2005**, *17*, 712-718.

[4] a) M. Uchida, M. Terashima, C. H. Cunningham, Y. Suzuki, D. A. Willits, A. F. Willis, P. C. Yang, P. S. Tsao, M. V. McConnell, M. J. Young and T. Douglas, *Magn. Reson. Med.* **2008**, *60*, 1073-1081; b) A. Masotti, A. Pitta, G. Ortaggi, M. Corti, C. Innocenti, A. Lascialfari, M. Marinone, P. Marzola, A. Daducci, A. Sbarbati, E. Micotti, F. Orsini, G. Poletti and C. Sangregorio, *Magn. Reson. Mater. Phys., Biol. Med.* **2009**, *22*, 77-87.

[5] I. Willner, B. Basnar and B. Willner, *FEBS Journal* **2007**, *274*, 302-309.

[6] a) N. Higashi, J. Kawahara and M. Niwa, *Journal of Colloid and Interface Science* **2005**, *288*, 83-87; b) R. Sachsenhofer, W. H. Binder, D. Farnik and R. Zirbs, *Macromolecular Symposia* **2007**, *254*, 375-377; c) Y. Li, A. E. Smith, B. S. Lokitz and C. L. McCormick, *Macromolecules (Washington, DC, United States)* **2007**, *40*, 8524-8526; d) R. A. Sperling in *Surface Modification and Functionalization of Colloidal Nanoparticles*, *Vol.* University of Marburg, Marburg, **2008**; e) M. S. Wong, J. N. Cha, K. S. Choi, T. J. Deming and G. D. Stucky, *Nano Letters* **2002**, *2*, 583-587; f) T. Azzam and A. Eisenberg, *Langmuir* **2007**, *23*, 2126-2132.

[7] R. C. Maher, S. A. Maier, L. F. Cohen, L. Koh, A. Laromaine, J. A. G. Dick and M. M. Stevens, *J. Phys. Chem. C* **2010**, *114*, 7231-7235.

[8] O. Kreft, A. G. Skirtach, G. B. Sukhorukov and H. Moehwald, *Advanced Materials (Weinheim, Germany)* **2007**, *19*, 3142-3145.

[9] T. B. Schuster, D. de Bruyn Ouboter, E. Bordignon, G. Jeschke and W. Meier, *Soft Matter* **2010**, *6*, 5596-5604.

[10] a) C. S. Weisbecker, M. V. Merritt and G. M. Whitesides, *Langmuir* **1996**, *12*, 3763-3772; b) L. Fabris, S. Antonello, L. Armelao, R. L. Donkers, F. Polo, C. Toniolo and F. Maran, *Journal of the American Chemical Society* **2005**, *128*, 326-336; c) P. Nativo, I. A. Prior and M. Brust, *ACS Nano* **2008**, *2*, 1639-1644; d) S.-Y. Lin, Y.-T. Tsai, C.-C. Chen, C.-M. Lin and C.-h. Chen, *The Journal of Physical Chemistry B* **2004**, *108*, 2134-2139; e) J. C. Love, L. A. Estroff, J. K. Kriebel, R. G. Nuzzo and G. M. Whitesides, *Chemical Reviews (Washington, DC, United States)* **2005**, *105*, 1103-1169.

[11] G. S. Cleveland Eugene Rayford II, Kevin Shuford, *Nanoscape* **2005**, *2*, 27-33.

8 General conclusion and outlook

This thesis began with the concept of building purely peptidic amphiphiles of small size that are able to self-assemble into supramolecular aggregates. Since potential applications are focused on drug delivery systems, the use of natural amino acids could be a crucial factor, giving the designed materials a high probability of being biocompatible and biodegradable. The general difficulty of producing a purely peptidic, hydrophobic component was overcome by a gramicidin A-inspired peptide sequence. Its β-helical secondary structure permitted hiding the hydrophilic backbone within its interior while presenting hydrophobic residues to the environment. The richness in tryptophan further allowed intermolecular stabilization and alignment of the peptides, while the hydrophilic part can comprise a sequence of variously available hydrophilic amino acids, containing the desired chemical functional group. In the work presented, charged lysine, charged glutamic acid, or the uncharged acetylated lysine served as hydrophilic contributors.

During this research we developed what became an established synthesis and purification procedure, based on Fmoc solid phase peptide synthesis and reversed phase chromatography. The general difficulties that come along with very hydrophobic or amphiphilic sequences –often leading to the rejection of product orders by peptide manufacturers – were overcome by introducing small adaptions to the purification methods and considerable laboratory work. The resulting production process not only produces purely peptidic amphiphiles with a controlled primary structure and purities above 96%, but also allowed the controlled introduction of point mutations, labels, and other modifications. Thus, the process can be used for the production of further amphiphilic peptides to explore the capacity of purely peptidic amphiphiles.

The aspired self-assembly capacity of the new class of peptidic material was demonstrated with the peptides K_3-gT/C-K_3-gT, and Ac-X_3-gT/AcC-X_3-gT (the fully acetylated analogues), which formed micelles and peptide beads in aqueous solution, respectively. Farther-reaching experiments with these structures revealed a detailed view of the formation process and the inner structure of the beads. As a result, we gained not only the understanding that the peptide beads' size is controllable, but also identified the hierarchically self-assembled peptide beads as multicompartment micelles, having the capacity to embed various payloads in their segregated hydrophobic and hydrophilic compartments.

The positive results of exploring the tuneable, purely peptidic amphiphile system encouraged us to produce a library of peptides by inducing point mutations (stepwise acetylation of the lysines) into the hydrophilic part of the sequence. The ten peptides produced in this manner possessed a slightly changing overall hydrophobicity. More importantly, a switch of the peptide's secondary structure was accompanied by a switch in the self-assembled structure, going from micelles to fibers. At maximum degree of acetylation, peptide beads as well as triangular structures were also produced. The synthesized library showed how distinct, small changes in the primary structure (sequence) of the peptide can be used to control the supramolecular output. Therefore, this part

of the work provides direction as to how the self-assembled structures can be controlled by small chemical modifications, and the ease of sequence variations.

With further variations in the sequence we exploited different dimerization effects to stabilize the vesicle formation of purely peptidic amphiphiles. Such additional stabilizing forces are indispensible, due to small molecule size. The drawn conclusions can be converted into a general recipe to form vesicles of a purely peptidic base. In particular for biotechnological and medical applications, the use of amino acid based materials is advantageous, because these possess generally better biocompatibility and biodegradability than competing synthetic macromolecules of polymeric character. As a result, long-term accumulation in a patient's body can be avoided.

The ability of the produced peptide beads to serve as a drug delivery system was evaluated within the scope of this thesis. The nano-sized beads have the great capacity to embed hydrophilic as well as hydrophobic guest molecules with relatively high embedding efficiency. Furthermore, the system was adapted to embed siRNA/DNA material for gene therapy purposes with embedding efficiencies over 99%. The conducted drug delivery tests on human cell models proved effective for both the delivery of hydrophilic and hydrophobic drugs, and siRNA/DNA material for gene silencing. The fact that no toxic effect of the peptide material was observed during testing strongly suggests that the peptidic drug delivery system should be taken to the next level in medical drug development.

Compatibility of the peptide was tested with inorganic nanoparticles. The peptide self-assembly was used to template the dense packing of gold nanoparticles by using a thiol linker (cysteine) on the hydrophobic part of the peptide Ac-X$_3$-gT-C. The thusly formed gold core micelles aggregated into composite peptide-gold nanoparticles. The straightforward production process for the composite material allowed the inclusion of a light trigger that produces heat and might be used to accelerate payload release in drug delivery applications of the peptide beads. Furthermore, the high electron density might allow better visibility of the peptide beads when probing cellular uptake pathways. The latter would be a logical consequence of the drug-delivery related results presented herein, because the knowledge of the uptake mechanisms and the pathways will help optimize the use of the peptide system in drug delivery.

In summary, the presented work offers great potential for purely peptidic amphiphiles in drug delivery applications, while the production methods and the gained knowledge of peptide self-assembly as describe here will hopefully lead to the production of further smart and advanced functional materials.

9   Experimental part

9.1   Materials

Materials and reagents were of the highest commercially available grade and were used without further purification, unless indicated. HCTU, Rink Amide AM resin (0.61 mmol/g) and Fmoc-Trp(Boc)-OH was purchased from IRIS Biotech GmbH. All other amino acids were obtained from Novabiochem. Dichloromethane and ethanol (96%) F15 were provided by Brenntag Schweizerhall AG, DMF by J. T. Baker and acetonitrile (ACN) by Fischer Scientific. Fluorescent dyes were purchased from Invitrogen Inc. DMF was treated with aluminum oxide to reduce free amines prior to application in peptide synthesis. Solvent exchange was carried out in 24-well sitting-drop crystallization plates (HR3-158, Hampton Research) or by dialysis (Spectrum, cellulose ester (CE), MWCO=500-1000 Da) against double-distilled (dd) water. Fluorescently labeled and unlabeled GAPDH-siRNAs (AM4649, AM4624) were purchased from Ambion (Applied Biosystems). The psiSTRIKE-Neomycin vector and MTS-assay were purchased from Promega AG (Switzerland). The used vector was equipped with a hairpin target sequence for PP2Acα to express siRNA against PP2Acα. The sequences of the hairpin oligonucleotide for PP2acα messenger RNA were 5'-ACCGGGATACCGTTTAATTTAA<u>TTCAAGAGA</u>TTAAATTAAACGGTAT   CCCTTTTTC-3'   and   5'-TGCAGAAAAAGGGATACCGTTTAATTTAA<u>TCTCTTGAA</u>TTAAATTAAACGGTATCC-3'   (loop   is underlined). For control, scrambled sequences for the siRNA sequence designed to human PP2Acα were used. The oligonucleotide sequences were 5'-ACCGTTAATGGCTACGAATTAT<u>TTCAAGA</u>GA ATAATTCGTAGCCATTAACTTTTTC-3' and 5'-TGCAGAAAAAGTTAATGGCTACGAATTAT<u>TCTCTTGAA</u>AT AATTCGTAGCCATTAA-3'. Remaining chemicals and buffers were purchased from Sigma-Aldrich.

9.2   Peptide synthesis

All peptides were synthesized on a Syro I Peptide Synthesizer (MulitSynTech GmbH, Witten, Germany) on solid phase using Fmoc-strategy. 2-(6-chloro-1H-benzotriazole-1-yl)-1,1,3,3-tetramethylaminium hexafluorophosphate (HCTU) as the coupling reagent and N-ethyldiisopropylamine (DIPEA) dissolved in N-methyl-2-pyrrolidone (NMP) as the base were used to couple α-N-Fmoc-protected amino acids to the resins (220 mg, Rink Amide AM, 0.61 mmol/g, equals 1 equiv.).

For elongation, Fmoc-Xxx-OH (0.5 mol/L, 4 equiv.), HCTU (0.5 mol/L, 4 equiv.) dissolved in dimethylformamide (DMF), and DIPEA (12 equiv.) were added to the resin. The mixture was agitated for 1 h and washed with DMF (3x3 mL). Fmoc deprotection was performed with 20% piperidine in DMF followed by 3 min agitation, draining, and repetition of deprotection for 10 min. Resin was subsequently washed with DMF (5x3 mL). Acetylation of unreacted amine groups was performed following each coupling using acetic anhydride/DIPEA (3 mol/L, 5 equiv.) in DMF. After synthesis, the peptide resin was washed alternating with DMF (3x6 mL), isopropanol (3x6 mL), and dichloromethane (3x6 mL), and dried under vacuum. For Ac-E$_6$-gA and Ac-K$_6$-gA, N-terminal acetylation was performed after the completed reaction with 30 equivalents of Ac$_2$O/DIPEA for 1

hour. Partially acetylated peptides were produced by using Fmoc-Lys(Ac) and Fmoc-Lys(Boc) during synthesis. Ac-X_8-gA, the precursor for Ac-X_8-gA-OEt, was synthesized by post purification acetylation from K_8-gA.

In a scaled up synthesis using 5 g of Rink Amide AM resin, the same protocol was followed in manual steps. For washing isopropanol was used alternating with DMF. Due to the size, reactions were carried out in a 500 ml glass solid phase reactor using only 3 equiv. of amino acids and coupling reagents for the reaction. The pH was controlled and kept above 9 during reaction, after each amino acid coupling and cleavage of the Fmoc-protection group, the resin was probed for free amine groups using a Kaiser- and TNBS (trinitrobenzene sulfonate)-test. There was no need for NMP as a co-solvent.

Cleavage from the resin and removal of protective groups was performed with a mixture of 95% trifluoroacetic acid (TFA), 2.5% triisopropylsilane (TIS), and 2.5% H_2O. In case of cysteine containing peptides a mixture of 94% TFA, 2.5% TIS, 2.5% ethanedithiol and 1% H_2O was used. The cleavage cocktail was filtered and resin was washed additional two times with cold cleavage cocktail (2 mL) and precipitated in 40 mL cold diisopropylether (IPE). The precipitated crude peptide was washed with cold IPE three times by centrifugation and decantation, before being dried under vacuum.

9.3 Peptide purification, post modification and characterization

Purification and analysis of the peptides were carried out by HPLC (Shimadzu Prominence 20A, Japan) on reverse phase (RP) columns (Merck Chromolith, RP-18e, 100 mm x 10 mm and 100 mm x 4.6 mm; Merck LiChrospher 100, RP-18e, 5 µm, 250 mm x 10 mm and 250 mm x 4.6 mm). The ground crude peptides were dissolved in 2 mL DMF, diluted with H_2O (0.1% TFA, 8 M urea) to a final volume of 20 mL. If necessary, acetonitrile (ACN) was added to dissolve peptide assemblies. The resulting solution was filtered through a 0.45 µm PTFE syringe filter and pumped to the HPLC. Two runs were necessary to yield sample purities higher than 95%. Linear gradients of solvent A (ACN) and solvent B (first run: 0.1% TFA, second run: 2 % AcOH or 0.23% formic acid in dd H_2O) (example given in Figure 9-1). The eluted sample was collected in fixed volume fractions which were subsequently analyzed for purity and molecular weight. Fractions containing more than 80% product (HPLC with 280 nm absorption) were applied to the second purification run. AcC-X_3-gT and C-K_3-gT disulfides were reduced with 1,3-propanedithiol (5 equiv.) in methanol or tris(2-carboxyethyl)phospine (5 equiv.) in water/ACN solution before the second run. Final fractions with purities higher than 95% were combined, neutralised with ammonia and lyophilized until leaving a fluffy, white final product.
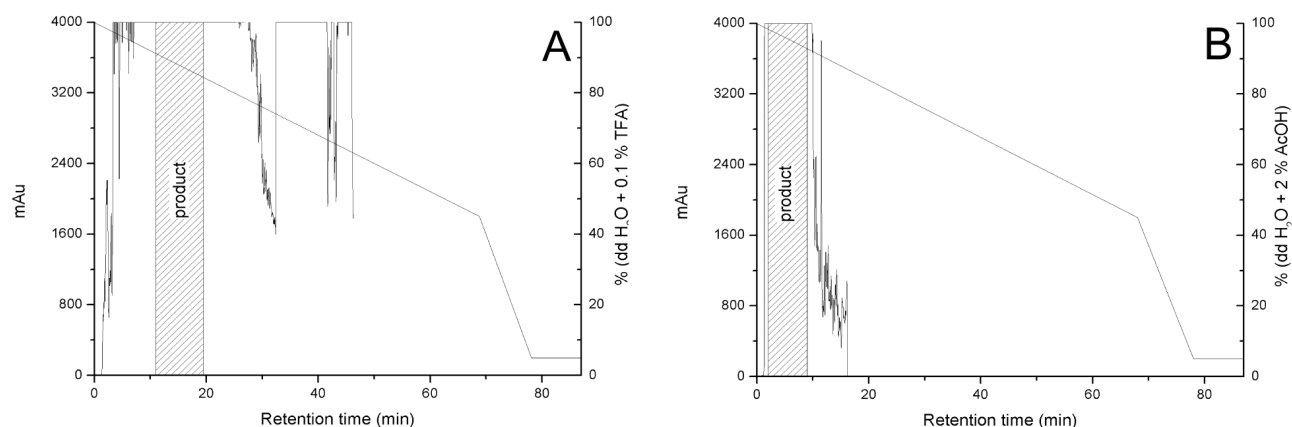
Figure 9-1: Preparative HPLC elution profile of K_3-gT A) first run with ACN/dd H_2O 0.1 % TFA B) second run using ACN/dd H_2O 2 % AcOH. *Published in [1] , Reproduced by permission of the Royal Chemical Society.*

Purification of Ac-E_6-gA was carried out by HPLC on a PRP-3 column (10 μm 300 Å, 4.1 x 250 mm, Hamilton) for peptide/protein/DNA purification. Also here, two runs were necessary and following conditions were used: in run one, ACN/0.5% aqueous TRIS·HCl solution (pH 7), in run two, ACN/50 mM NH_4OAc/HOAc (pH 7).

For verification, final products were again analyzed by HPLC for purity and MALDI-TOF-MS for mass confirmation. Examples are illustrated in Table 9-1 and Figure 9-2. Products were stored under argon at -18 °C.

Table 9-1: Exemplary mass confirmation by MALDI-TOF-MS and HPLC purities of selected peptides.

Code[a]	Mass[b] (g mol^{-1})	Mass (MALDI-TOF-MS)	Purity[c]
Ac-X_8-gA	3328.1	3329.9	>99.5%*
Ac-X_8-gA-OEt	3358.1	3357.1	>99.5%*
Ac-E_6-gA	2684.0	2682.5	95%
Ac-K_6-gA	2678.3	2677.4	96%

[a] one letter code with abbreviations for gramicidin (gA), acetylated lysine (X) and acetylated N-terminus (Ac) [b] calculated with Pinsoft32 [c] Area% on an analytical RP-HPLC [*] HPLC purity from precursor K_8-gA.
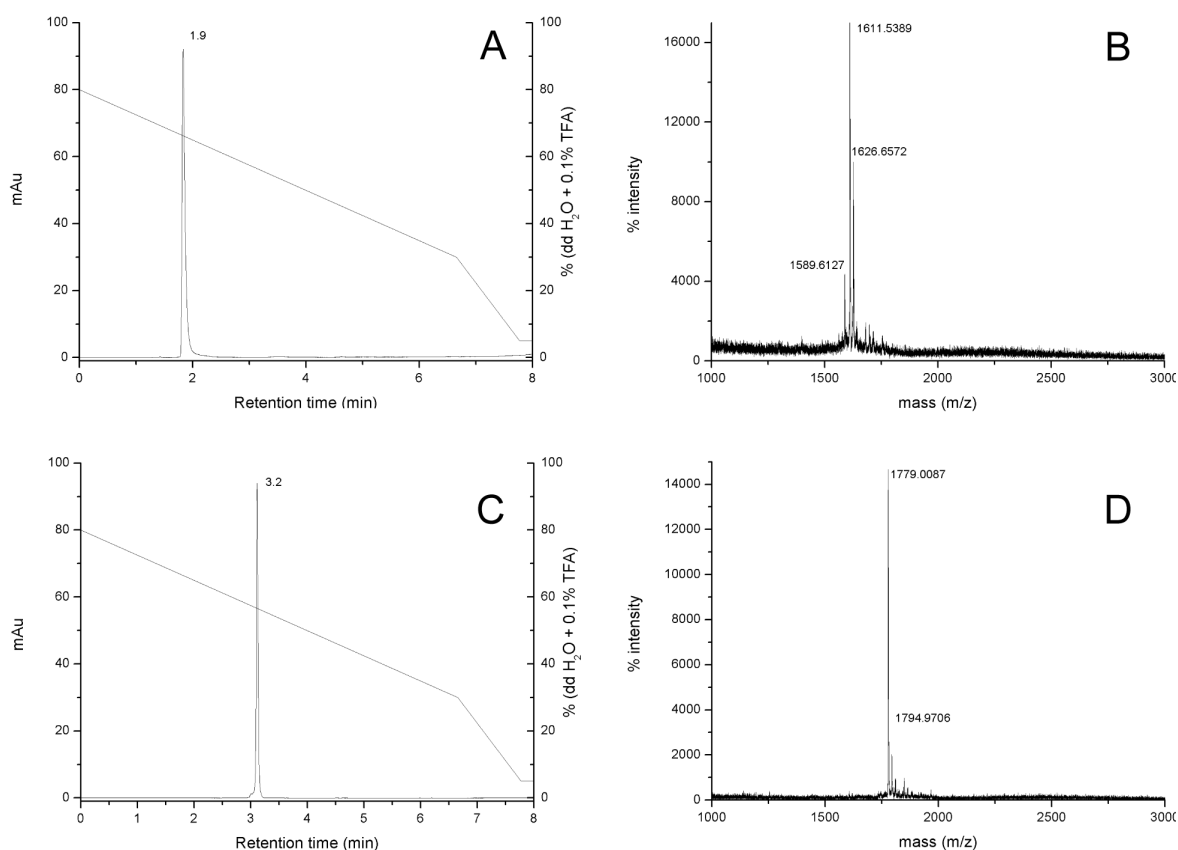
Figure 9-2: Analysis of C-K$_3$-gT A) HPLC profile B) MALDI-TOF-MS and AcC-X$_3$-gT C) HPLC profile D) MALDI-ToF-MS. *Published in* [1] *, reproduced by permission of the Royal Chemical Society.*

Overall yields of the synthesis and purification were generally between 10-15 %, overall yields of the synthesis, purification, post-purification acetylation and end-purification were generally between 6-10 %, and therefore in the normal range for solid phase peptide synthesis and HPLC purification.

Post-purification acetylation of the free N-terminal and lysine amines was performed on the purified peptide dissolved in DMF using a 40-fold excess of acetic anhydride and DIPEA. Completeness of the reaction was controlled by MALDI-TOF-MS. The reaction mixture was repurified according to the procedure described above.

Transesterification of the Ac-X$_8$-gA amide to the Ac-X$_8$-gA-OEt was performed in ethanol/0.1M HCl at 70°C for 3 x 10 min and intermediate ultrasonic treatment for 3 x 30 s at 70°C.

MALDI-TOF-MS was performed on Voyager-DE[TM] System (Applied Biosystems, USA) with α-cyano-4-hydroxycinnamic acid as the matrix in positive ion reflector mode for lysine-rich peptides and negative ion reflector mode for glutamate-rich peptides, respectively, an accelerating voltage of 25 kV, grid voltage of 75% and 300 ns extraction delay time. These standard values were optimized according to the sample. A 100-well stainless steel or gold plate was used.

Hydrophobicity was calculated using Pinsoft32 (Chiron Technologies Pty Ltd., Australia) which uses the hydrophobicity algorithm from Fauchere & Pliska[2] (for X = Lys(Ac) a value of - 0.55 was used[3]).

9.4   Nanostructure formation

Either the peptide or the corresponding mixtures (*e.g.* AcC-X$_3$-gT / AcC(sl)-X$_3$-gT, Ac-X$_3$-gT / K$_3$-gT) were dissolved in ethanol at the appropriate concentration and filtered through a 0.2 μm hydrophilic PTFE filter. The self-assembly process was initiated by solvent exchange from the organic solvent to dd H$_2$O, the corresponding dd H$_2$O/ethanol mixture, or buffer [NaCl (140 mM), EDTA (0.5 mM), TRIS (10 mM), NaN$_3$ (0.003 mM) adjusted to pH 7.4 with HCl and filtered through a 0.2 μm hydrophilic PTFE filter)]. A change in polarity was usually accompanied by opalescence. Solvent exchange (in dialysis tubes or on crystallization plates) was performed within 24 h with dd H$_2$O exchanged three times. Since K$_3$X$_5$-gA to K$_8$-gA are water soluble, they were dissolved directly in water or buffer for surface tension measurements. Composite gold nanoparticles were produced by dissolving the cysteinated peptide in ethanol at 1 mg/ml and filtered through a 0.2 μm hydrophilic PTFE filter. Aqueous dispersions of gold nanoparticles (5 nm or 25 nm, Sigma-Aldrich) were mixed added to the peptide solution 1:1 and shaken during reaction for one week. The remaining non-reacted peptide was removed by centrifugation and decantation, and refilled with fresh ethanol. Self-assembly was induced by solvent exchange as described above.

9.5   Nanostructure characterization

9.5.1   Microscopic methods

Transmission electron microscopy (TEM) images were taken on an FEI Morgani 268D operated at 80 keV. 5 μL of the sample was deposited on carbon-coated, parlodion (2% in n-butyl acetate)-covered copper grids, blotted after 2 min with a filter paper and dried in air. If necessary, staining was performed with uranylacetat (2%) for 10 s before drying.

For *cryo-transmission electron microscopy* (CryoTEM) a holey carbon-coated grid (Quantifol, Germany) was used to adsorb 4 μL of an aqueous Ac-E$_6$-gA solution (~5 mg mL^{-1}) which was blotted with Whatman 1 filter paper and vitrified in liquid ethane at -178°C using a Vitrobot (FEI company, Netherlands). After transferring the frozen grids onto a Philips CM200-FEG electron microscope using a Gatan 626 cryo-holder, measurements were performed at an acceleration voltage of 200 kV and a 20k magnification. Micrographs were recorded on a 2K x 2K CCD camera (Gatan, USA) using a low-dose system (10 e$^-$/Å^2) while keeping the sample at -172°C.

Scanning Electron Microscopy (SEM) was performed on a Philips XL 30 ESEM operating between 2 and 5 kV. The aqueous peptide samples were frozen with liquid nitrogen and lyophilized directly on the SEM grid, or lyophilized powder was put on a double-sided carbon sticker before being sputtered with gold or platinum (2-5 nm).

Atomic force microscopy (AFM) measurements were carried out using a 5100 Agilent system (formerly PicoLE Molecular Imaging) equipped with a multi-purpose scanner. Images were acquired using a silicon cantilever (type-NCHR PointProbe® Plus, force constant 42 N/m) as indicated by the manufacturer for acoustic mode images. Samples were prepared by exposing

aqueous peptide sample to a freshly cleaved mica surface for 5 min, removing the supernatant solution, and drying.

Confocal laser scanning microscopy measurements were performed on a Zeiss Confocor 2 LSM equipment. For the peptide vesicles, BODIPY 650/665 and Alexa488 solutions were added to an ethanol solution with Ac-E_6-gA (0.5 mg mL^{-1}) to reach a concentration of 0.2 µmol L^{-1} and 0.5 µmol L^{-1} respectively before vesicle formation and dialysis (MWCO=100 kDa). For peptide beads and cell imaging, the appropriate filter/channel settings were applied and combined to fit the demands of the fluorophores: tryptophan (ex. 405 nm, em. 420 nm), Cy3-labeled siRNA (Ex. 543 nm, Em. 573 nm), Hoechst 33342 (Ex. 350 nm, Em. 461 nm), CellMask DeepRed (Ex. 649 nm, Em. 666 nm), Lystotracker DND-99 (Ex. 577 nm, Em. 590 nm), and transmission channel (DIC). Cell staining was performed directly before the microscopy measurements according to the manufacturer's protocol. Shortly, the tempered dye solutions were added simultaneously to the cells in 2 ml PBS buffer and incubated for the needed time at 37 °C (Hoechst 33342: 6 µl 16.2 mM 30 min, Lysotracker: 2 µl 1 mM 30 min, DeepRed: 2 µl 5 mg/ml 5 min). The cells were rinsed with fresh PBS buffer and instantly used for microscopy at room temperature.

9.5.2 Scattering methods

Dynamic and static light scattering (DLS and SLS) measurements were performed with an ALV/CGS-8F platform-based goniometer system equipped with an ALV/-5000/E correlator and a HeNe-laser with a wavelength of 633 nm (35 mW). Measurements were made at 20 °C and at a scattering angle θ from 30° – 150° in steps of 10°.

DLS correlation functions were fitted with the 2nd cumulant function or the CONTIN algorithm. The resulting hydrodynamic radii (mass weighted) were extrapolated to zero wave vector (q = ($4\pi n_0/\lambda_0$) sin (θ/2)) and to zero concentration. The Stokes-Einstein equation was used to calculate the hydrodynamic radius. To determine the size dependence of the peptide beads, 2nd cumulant fit analysis at 90° with measurement times of 300 s was used. For the pH dependent size evolution of the peptide vesicles, the initial peptide concentration was 0.34 mg mL^{-1}. Here, also the 2nd cumulant function (90°, 300 s) was used. Aliquots of 2-10 µL of corresponding molarities (10^{-3} to 1 mol L^{-1}) NaOH or HCl were used to adjust the pH of the 800 µL peptide solution.

SLS data analysis was done with ALVStat 4.31 software (ALV, Langen, Germany) by constructing a Guinier plot (second order in q and linear concentration dependency)

$$ln\left(\frac{K \cdot c}{R_\theta}\right) = ln\left(\frac{1}{M_W \cdot e^{-\frac{1}{3}R_g \cdot q^2}} + 2A_2 c\right) \tag{1}$$

with the optical constant (K), concentration (c), Rayleigh ratio (R_θ), molar mass (M_W), radius of gyration (R_g) and 2nd virial coefficient (A_2). The refractive increment (dn/dc) was set to 0.185 mL/g (commonly used for peptides[4]). The deviation in dn/dc, caused by the different ethanol concentrations[5], provided negligibly different results.

The scattering intensity $i(\theta)$ was normalized to zero angle, yielding the particle scattering factor P.

$$P(\theta) = \frac{i(\theta)}{i(\theta=0)} \qquad (2)$$

This provided information on the shape and internal structure of the particles in solution. Structural differences become apparent by plotting P versus $u = q \cdot R_g$. For analysis, the experimental data from the present system were compared to well-known particle scattering factors for hard spheres and monodispersed coils, given in eq. 3 and 4 respectively.

$$P(\theta) = \left(\frac{3}{x^3} \big(sin(x) - x cos(x) \big) \right)^2 \qquad (3)$$

$$x = \sqrt{\frac{5}{3}} u$$

$$P(\theta) = \left(\frac{2}{u^4} \big(e^{-u^2} - 1 + u^2 \big) \right)^2 \qquad (4)$$

More detail on theoretical background and SLS data analysis can be found in the literature[6].

ζ-potential measurements of peptide solutions in dd H_2O were performed with a Malvern Instruments Zetasizer Nano ZS, using the identical samples as for DLS measurements. The pHs of the solutions were determined in advance to range from 7.0 to 7.8 using a Mettler Toledo MP 220 pH meter with an InLab micro electrode.

Small-Angle X-ray scattering (SAXS) was performed using the µSpot Beamline at BESSY[7], using a wavelength of λ = 1.0000 Å. Samples were measured using an ultrasonic levitator. The scattering pattern of silver behenate served as an external calibration standard, and 2D data were converted using the program FIT2D[8]. Bidistilled water was used as blank, and data were analyzed using a two level Beaucage method[9] as implemented in the Irena SANS package[10] and Igor Pro 6.11 (Wavemetrics). IPG-TNNLS[11] (Internal Point Gradient - Total Non-Negative Least Square) analysis was performed as implemented in the Irena Package[10] version 2.38 using Igor Pro 6.11 (Wavemetrics). Data were fitted for a nanoparticle population with sizes starting from 3 nm to 50 nm and a logarithmic binning. The NNLS approach parameter was set to 0.5 and the maximum number of iterations was set to 400, which proved to be satisfactory to obtain a convergence.

9.5.3 Spectroscopic methods

Fluorescence spectroscopy was carried out at room temperature (293 K) on a Perkin Elmer LS55 Luminescence Spectrometer with a 1 mm quartz glass cuvette in a 90° arrangement. The quencher acrylamide (c = 2.26 mol/L) was added stepwise to the peptide solutions (c = 0.04 to 0.31 mol/L) in 2 to 40 µL quantities and intensity was corrected for dilution. High tryptophan and peptide concentrations required the use of a built-in 1% filter to prevent detector saturation. Data analysis was performed by plotting F_0/F (fluorescence intensities without and with the presence of quencher) vs. the concentration of the quencher [Q] according to the modified Stern-Volmer law[12]. It can be divided into collisional and static components characterized by K_{SV} (Stern-Volmer constant) and V (active volume)[13]. For encapsulation efficiency measurements, the cy3-payload

filled beads were centrifuged and the supernatant separated from the beads. The peptide beads were dissolved in ethanol (50%) to release the payload. The supernatant was filled up with the same amount of ethanol (50%). Fluorescence of both samples was measured at maximum emission/excitation and taken to calculate the encapsulation efficiency.

UV-VIS absorbance spectroscopy was performed on a Perkin Elmer Lambda 35 UV/VIS Spectrometer, equipped with a Peltier temperature control element and a 1 mm quartz glass cuvette. For temperature dependent peptide bead formation, detection at 280 nm was used to monitor the onset of scattering due to bead formation. Diffuse reflection was measured on a Varian Cary 5000 UV-VIS-NIR spectrophotometer equipped with an integrating sphere and PTFE as white standard and a 1 mm quartz glass cuvette in front of the standard.

Circular Dichroism (CD) was measured using a Chirascan CD Spectrometer (Applied Biophysics Ltd., Leatherhead, UK) using 1 mm path length quartz glass cuvettes. The peptide concentration was adjusted according to an HT voltage between 300 and 600 V in the far UV and subsequently determined by analytical HPLC to be in the range of 0.1 to 0.25 mg mL^{-1}. Spectra were acquired at 22°C from 190 – 320 nm in 0.2 nm steps, with a bandwidth of 1 nm, and averaged over five points and two scans. Measurements of assembled structures in dd H_2O are excluded due to scattering.

9.5.4 Electron paramagnetic resonance

To measure *electron paramagnetic resonance* (EPR), a spin label (sl) was attached to the amphiphilic peptide by dissolving AcC-X$_3$-gT and 3-(2-iodoacetamido)-2,2,5,5-tetramethyl-1-pyrrolidinyloxy in a mixture of 58% ethanol in TRIS buffer (25 mM) and 12 h reaction time. The spin labeled peptide was separated from the reaction mixture by using solid phase extraction cartridges (Whatman Inc., ODS-5 Octadecyl; 18%; EC), leading to a purity of 97% (HPLC).

All *continuous wave (cw) EPR* experiments were performed at X-band frequencies (9.3 – 9.4 GHz) with a Bruker Elexsys 500 spectrometer equipped with a Bruker Elexsys Super High Sensitive probe head equipped with a continuous flow N_2 cryostat controlled by a Bruker Er 4111 VT temperature controller. Samples were loaded into EPR glass capillaries (0.9 mm inner diameter, sample volume 15 μL) and recorded with 100-kHz field modulation, 2 mW microwave power, 0.15 mT modulation amplitude. For low temperature (160 K) cw EPR spectra, samples were loaded into EPR quartz capillaries (3.8 mm inner diameter, sample volume 30 μL) and recorded with 100-kHz field modulation, 0.08 mW microwave power, 0.2 mT modulation amplitude.

Pulse EPR experiments were performed at X-band frequencies (9.3 – 9.4 GHz) at 50 K with a Bruker Elexsys 580 spectrometer equipped with a Bruker Flexline split-ring resonator ER 4118X-MS3 that included a continuous flow He cryostat (ESR900; Oxford Instruments) controlled by an Oxford Instruments temperature controller ITC 503S.

Dipolar time evolution data were recorded using a four-pulse DEER (double electron-electron resonance) experiment[14]. The measurements were performed at 50 K with observer pulse lengths of 32 ns for π/2 and π pulses, with the ELDOR π pulse set to 12 ns. Deuterium nuclear

modulations were averaged (50 volume % (v %) of deuterated glycerol was added to the ethanol sample to increase the signal to noise ratio). Traces were accumulated for 24 hours. Data analysis of the DEER traces was performed with DeerAnalysis 2009 software[15].

The following parameters were used to calculate micelle rotational time so as to compare DLS with EPR: R = 5.65 nm, T = 293 K and n = 1.3583, η = 2.84 10^3 $kgs^{-1}m^{-1}$ for 40 weight % (wt %) ethanol.

9.5.5 Gel permeation chromatography (GPC)

Measurements of gramicidin A (gA) and Ac-X$_3$-gT (c = 1 mg/mL) were performed on a Shimadzu Prominence HPLC, using an Agilent PLgel column (5 μm, 10^3 Å, 2 x 250 mm) and isocratic elution with THF/10% H$_2$O. Stabilizer-free solvent improved detection at the tryptophan adsorption maximum of 280 nm. For the comparison of gA, Ac-X$_8$-gA, and Ac-X$_8$-gA-OEt two GPC-columns were mounted in series (1. CATSEC-100, 5μm, 250 x4.6 mm, 2. GPCPEP 5μm, 250 x 4.6 mm, Eprogen Inc.). Isocratic elution (1mL min^{-1}) was performed with 95% THF (without stabilizer for UV detection at 220 nm, T=295K) and 5% dd H$_2$O.

9.5.6 Tensiometry

Surface tension was measured on a Sigma 703D Tensiometer (KSV Instruments, Finland) with a platinum Wilhelmy plate, pre-cleaned with ethanol and water, followed by flame annealing. Solutions were prepared 24 h prior to measurements by dissolving the peptides in dd H$_2$O or buffer and subsequent dilution. All measurements were performed at room temperature.

9.6 Biological experiments

9.6.1 Cell viability tests on THP-1 cells (MTS assay)

Peptide beads were produced by using filtered (0.2 μm hydrophilic PTFE) ethanol solutions of the peptide and the payloads to produce the mixtures in ethanol with Ac-X$_3$-gT (0.25mg/ml), Ac-X$_3$-gT (0.25mg/ml) / paclitaxel (150 μM), Ac-X$_3$-gT (0.25mg/ml) / doxorubicin (275 μM), and Ac-X$_3$-gT (0.25mg/ml) / doxorubicin (138 μM) / paclitaxel (75 μM). Self-assembly was induced according to *chapter 9.4 (Nanostructure formation).* The payload filled peptide beads were separated from potentially free payload by triple centrifugation in Amicon Ultra 15 Centrifugal Filter Units (15 ml, 100'000 Da MWCO, Millipore), and refilling with dd H$_2$O.

Cell viability tests for payload filled and unfilled peptide beads were performed using THP-1 monocytes and macrophages. Monocytes were split and prepared in complete RPMI medium (2 ml well, 20'000 cells/well). Peptide bead samples were added to the medium according to the experimental setup in 1:10 and 1:100 dilutions and incubated at 37 °C for 3 days. Experiment was performed in triplicate. For THP-1 macrophages, the same procedure was performed with 50'000 cells/well after differentiation of the THP-1 monocytes to macrophages in the presence of 100 nM

PMA (phorbol 12-myristate 13-acetate, Sigma-Aldrich 79346). After incubation, MTS was added (20 µl/well, MTS kit CellTiter 96 Aqueous One Solution Cell Proliferation Assay, PROMEGA G3580). After incubation for 1 h at 37 °C, the absorbance at 490 nm was measured according to the manufacturer and compared corrected using a blank sample (medium without cells).

9.6.2 Gene silencing

Peptide beads were produced by using filtered (0.2 µm hydrophilic PTFE) ethanol solutions of the peptides and aqueous solutions of the payloads to produce mixtures in ethanol with Ac-X_3-gT (0.25mg/ml), siRNA (250 nM) or same mass of plasmid, K_3-gT to neutralize the basepairs (3.57 µg/ml for 1:1 charge compensation according to the amount of siRNA/plasmid). Self-assembly was induced according to *chapter 9.4 (Nanostructure formation).* Encapsulation efficiency was measured according to the fluorescence method described above.

The translucent peptide beads were added to the growth media of the HuH-7 cells in the appropriate concentrations and incubated for the indicated times at 37 °C and 5% CO_2.

RNA isolation, reverse transcription, and SYBR-PCR: Cells were washed twice with PBS. The total RNA was isolated from the cells using Trizol according to the manufacturer instructions (Invitrogen, USA). RNA was reverse transcribed by M-MLV reverse transcriptase (Promega, Switzerland) in presence of random hexamers (Promega) and dNTPs. After incubation for 5 min at 70 °C and 1 h at 37 °C, the reaction was stopped by heating at 95 °C for 5 min. SYBR-PCR was performed based on SYBR-Green Fluorescence (Applied Biosystems). To prevent influence from genomic DNA amplification, the primers were designed across exon-exon junctions. The forward and reverse primers for GAPDH were 5'-CTCCTCCTGTTCGACAGTCA-3' and 5'-ACCTTCCCCATGGTGTCTGA-3', respectively. The forward and reverse primers for PP2Acα were 5`-CCACAGCAAGTCACACATTGG-3` and 5`-CAGAGCACTTGA TCGCCTACAA-3`, respectively. The ΔCT value was derived by subtracting the threshold cycle (CT) value for GAPDH, which served as an internal control, from the CT values for PP2Acα. For GAPDH, only arbitrary values were used. All reactions were run in duplicate using the ABI 7000 Sequence Detection System (Applied Biosystems). The mRNA expression level of PP2Acα was expressed as a fold increase or fold decrease according to the formula $2^{\Delta CT(PBS)-\Delta CT(Treatment)}$.

9.7 References

[1] T. B. Schuster, D. de Bruyn Ouboter, E. Bordignon, G. Jeschke and W. Meier, *Soft Matter* **2010**, *6*, 5596-5604.

[2] J. L. Fauchere and V. Pliska, *Eur. J. Med. Chem.* **1983**, *18*, 369-375.

[3] E. Casero, M. Darder, D. J. Diaz, F. Pariente, J. A. Martin-Gago, H. Abruna and E. Lorenzo, *Langmuir* **2003**, *19*, 6230-6235.

[4] a) J. Wen, T. Arakawa and J. S. Philo, *Analytical biochemistry* **1996**, *240*, 155-166; b) A. Oliva, J. B. Farina and M. Llabres, *Analytica Chimica Acta* **2004**, *512*, 103-110.

[5] W. Liu, D. Bratko, J. M. Prausnitz and H. W. Blanch, *Biophysical Chemistry* **2004**, *107*, 289-298.

[6] a) J. Pencer and F. R. Hallett, *Langmuir* **2003**, *19*, 7488-7497; b) O. Stauch, R. Schubert, G. Savin and W. Burchard, *Biomacromolecules* **2002**, *3*, 565-578; c) W. Burchard, *Advances in Polymer Science* **1983**, *48*, 1-124.

[7] O. Paris, C. Li, S. Siegel, G. Weseloh, F. Emmerling, H. Riesemeier, A. Erko and P. Fratzl, *J. Appl. Crystallogr.* **2007**, *40*, s466-s470.

[8] A. P. Hammersley, S. O. Svensson, M. Hanfland, A. N. Fitch and D. Hausermann, *High Pressure Research: An International Journal* **1996**, *14*, 235 - 248.

[9] G. Beaucage, *J. Appl. Crystallogr.* **1995**, *28*, 717-728.

[10] J. Ilavsky and P. R. Jemian, *J. Appl. Crystallogr.* **2009**, *42*, 347-353.

[11] a) J. A. Potton, G. J. Daniell and B. D. Rainford, *Journal of Applied Crystallography* **1988**, *21*, 663-668; b) J. A. Potton, G. J. Daniell and B. D. Rainford, *Journal of Applied Crystallography* **1988**, *21*, 891-897.

[12] B. Valeur and Editor, *Molecular Fluorescence - An Introduction: Principles and Applications, 1st Edition 2000*, **2000**, p. 250 pp. (approx.).

[13] M. R. Eftink and C. A. Ghiron, *Biochemistry* **1976**, *15*, 672-680.

[14] M. Pannier, S. Veit, A. Godt, G. Jeschke and H. W. Spiess, *Journal of Magnetic Resonance* **2000**, *142*, 331-340.

[15] G. Jeschke, V. Chechik, P. Ionita, A. Godt, H. Zimmermann, J. Banham, C. R. Timmel, D. Hilger and H. Jung, *Applied Magnetic Resonance* **2006**, *30*, 473-498.

10 Acknowledgements

I would like to thank *Prof. Dr. Wolfgang Meier* for giving me the opportunity and the freedom to perform this thesis, but also for crucial input and inspiring discussions that were always exactly at the time necessary. I also would like to thank *PD Dr. Cornelia Palivan* for the time during which she was in charge of the group and for the drive she contributed, not only concerning the ongoing research but also in caring for our careers. Together, they can be proud of maintaining such a great, open minded research atmosphere that is a perfect base for inspiration.

Further, I would like to thank *Dr. Nico Bruns* for a lot of useful discussion, manuscript corrections, and for sharing his experience as to how science works best. *Dr. Ramona Enea* for having an "open ear" concerning the delivery related research, and her help in this topic.

The wide scope of this thesis would also not have been possible without external collaboration, therefore, thanks go to: *Dr. Michael Kümin* and *Roman Erdmann* from the group of *Prof. H. Wennemers* for access to the peptide synthesizer and help in issues related to syntheses, *Dr. Barbara Fischer* from University Hospital for her cell viability tests in a "stormy" atmosphere, *Dr. Alexandre Mantion* and the BAMline-team for access to the synchrotron and related work, *Vijay Shanker* from the University Hospital (group of *Prof. Markus Heim)* for the cancer cell experiments and his biological expertise, *Theo Bühler* and *Helmut Fally* for access to the IR-microscope and the Zetasizer/laser diffractometer, respectively, *Dr. Mohamed Chami* for CryoEM (C-CINA), *Prof. Dr. Thomas Pfohl* for his help with the first SAXS measurements in Göttingen, and the ZMB, namely *Vesna*, *Ursula*, *Marcel*, *Daniel*, *Eva*, and *Gianni*.

Then there are a lot of in house people and group members and former group members. In particular I want to thank "The Scatterers" *Jörg* & *Olivier*, "Miss Biolab" *Ozana*, *Alessandro* – "okay, they are really not hollow", *Per* for teaching me FCS and the confocal microscope, *Corinne* for the introduction to light scattering, *Vimal* for cell staining and microscopy help, *Lucy*, *Mariusz*, *Caro*, *Serena*, and *Fabsi*, "the spirit makers". *Gaby* for GPC and TEM. My office mates, *Stefan*, *Nico*, *Thomas*, *Diana*, *Francisco*, *Christian*, *Smahan*, *Gergely*, *Xiaoyan* and *Philipp* for good discussions, good working breaks and the "emergency chocolate box". *Kasia* for good scientific input and inspirational help. *Christian*, who really inspired me with lots of great discussions in the beginning of the thesis and who finally showed me how publishing can be handled. The 11:30 lunch group. *Sven*, who really understands the lab stuff. *Mark* for the linguistic correction of the manuscripts but also for tickling my brain every other day. And all those who helped with ideas and maintaining a good spirit.

I also want to thank my "block-course students" *Patric Baumann*, *Sebastian Suter*, *Luzian Michel*, *Patrick Hofer*, *Karim Nerouz*, and *Divya*, as well as my BNF collaborators *Louis John* and *Irène Mühlemann*.

A special word goes to *Thomas* who worked with me on the peptide self-assembly project hand-in-hand, being a friend and partner in studies. I also want to thank my parents *Elke* and *Ulli* for their

support and care during all these years, my fiancée *Eva* for support even in stressful situations, as well as my friend *Michel* for providing a solid backup over the last 24 years.

11 Curriculum Vitae and list of publications

Name:	Dirk C. de Bruyn Ouboter
Date and place of birth:	21.9.1980, Basel, Switzerland
Nationality:	Swiss
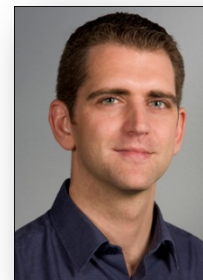
Profession

Chemist

Qualifications

August 1999   Lab Technician in chemistry with Professional Baccalaureate (Berufsmatura)
February 2004   Dipl. Chemiker FH (Bachelor Honours of Science, University of Applied Sciences)
November 2006   Master of Science in chemistry
May 2011   PhD in physical chemistry

Basic Education

Apr. 1987 – Aug. 1992:   Elementary school in Ettingen, Switzerland
Aug. 1992 – Aug. 1996:   Secondary school in Therwil, Switzerland
Aug. 1996 – Aug. 1999:   Berufsmaturitätsschule Novartis (Professional Baccalaureate
                            School) in Muttenz, Switzerland

Professional Education

Aug. 1996 – Aug. 1999:   Ciba Spezialitäten Chemie AG, Basel, Switzerland
                            Apprenticeship as lab technician in chemistry
Oct. 2000 – Feb. 2004:   University of Applied Sciences (FHBB), Muttenz, Switzerland
                            Studies in chemistry
Oct. 2005 – Oct. 2006 :   University of Basel, Master student in chemistry
Oct. 2006 – Apr. 2011:   University of Basel, PhD student in physical chemistry,
                            Prof. Dr. W. Meier, *„Rational design of purely peptidic amphiphiles
                            for drug delivery applications"*, synthesis and characterization

Practical Experience

02.05.1997 - 20.10.1997	**Ciba Spezialitäten Chemie AG, Basel, Switzerland** Internship, Pigments, analytical development
20.10.1997 - 30.11.1997	**Ciba Spezialitäten Chemie GMBH, Grenzach, Germany** Internship, Consumer Care, research
30.11.1997 - 10.10.1998	**Ciba Spezialitäten Chemie AG, Basel, Switzerland** Internship, Pigments, analytical development
02.02.1998 - 23.03.1998	**Ciba Spezialitäten Chemie AG, Basel, Switzerland** Internship, Pigments, development (BANCH-scale/pilot)
20.05.1999 - 15.08.1999	**Ciba Spezialitäten Chemie AG, Basel, Switzerland** Internship, Pigments, analytical research
15.08.1999 – 15.08.2000	**Ciba Specialty Chemicals Inc., McIntosh, Alabama, USA** Lab technician, Additives, AOFF-plant assistance
18.08.2000 – 20.10.2000	**Ciba Spezialitäten Chemie AG, Basel, Switzerland** Lab technician, Colors, Colors-Analytics

16.09.2002 – 20.10.2002	**SynphaBase AG, Muttenz, Switzerland**
	Lab technician; medicinal chemistry, R&D
13.10.2003 – 09.02.2004	**Kühni AG, Allschwil, Switzerland**
	Diploma thesis, Chemist FH, membrane technologies
02.03.2004 – 15.07.2004	**SynphaBase AG, Muttenz, Switzerland**
	Chemist FH; medicinal chemistry, scale-up/development
12.07.2004 – 31.08.2005	**Bachem AG, Bubendorf, Switzerland**
	Chemist FH; group leader, GMP-production of peptides (API)

Patents & Publications

W. Riedl, U. Buehlmann, D. de Bruyn Ouboter; *Aqueous two-phase extraction of biological material using a porous membrane*; EP1609800

V. Malinova, S. Belegrinou, D. de Bruyn Ouboter, W. Meier; *Biomimetic Block Copolymer Membranes*; Advances in Polymer Science; Springer Berlin (**2009**)

Th. B. Schuster, D. de Bruyn Ouboter, E. Bordignon, G. Jeschke, W. Meier; *Reversible peptide particle formation using a mini amino acid sequence*; Soft Matter, **2010**, 6, 5596-5604

D. de Bruyn Ouboter, Th. B. Schuster, Ch. Dittrich, W. Meier; *Self-Assembled Peptide Microspheres*; eCells & Materials Journal, **2010**, 20, 3, 51

T. Schuster, D. de Bruyn Ouboter, W. Meier, *Vesicular Structures Using Short Amphiphilic Peptides*; eCells & Materials Journal; **2010**, 20, 3, 232

T. Schuster, D. de Bruyn Ouboter, W. Meier; *Access to Controlled Self-Assembly form Fibers to Micelles of a Lysine Rich Amphiphilic Peptide via Point Mutation*. Chimia, **2010,** 64, (7/8), 594

T. Schuster, D. de Bruyn Ouboter, C. G. Palivan, W. Meier; *From fibers to micelles using point mutated amphiphilic peptides*, Langmuir, **2011**, 10.1021/la200443p

T. Schuster, D. de Bruyn Ouboter, N. Bruns, W. Meier; *Exploiting dimerization of amphiphilic peptides to form vesicles*; Small, **2011**, 10.1002/smll.201100701

D. de Bruyn Ouboter, T. Schuster, A. Mantion, W. Meier; *Hierarchical organization of purely peptidic amphiphiles into peptide beads*; The Journal of Physical Chemistry C, **2011**, 10.1021/jp203048h

D. de Bruyn Ouboter, T. Schuster, V. Shanker, M. Heim, W. Meier; *Multicompartmentized peptide beads as biocompatible drug delivery tool*; **2011**, in preparation

T. Schuster, D. de Bruyn Ouboter, W. Meier; *Molecular thin films produced by short amphiphilic peptides*; **2011**, in preparation

Pat. Pend. USPPA 61328198 *"Self-Assembly of Short Peptides to Supramolecular Aggregates"*

European patent application EP11172558 *"Peptide Beads"*

Languages

German   (native)
English   (fluently)
French   (basic)

12 List of synthesized and remaining peptides

Short name	Full sequence (3 letter code)	Molecular weight	Lot number	Purity
(CAc-X₃-gT)₂	(Ac-Cys-Lys(Ac)-Lys(Ac)-Trp-leu-Trp-leu-Trp-leu-Trp-NH2)₂	3513.80 Da	TSC3/11e	
(CAc-X₃-gT)₂	(Ac-Cys-Lys(Ac)-Lys(Ac)-Trp-leu-Trp-leu-Trp-leu-Trp-NH2)₂	3513.80 Da	TSC3/12e	
(K₃-gT-Cl)₂	(Ac-Lys(Ac)-Lys(Ac)-Trp-leu-Trp-leu-Trp-leu-Trp-Cys-NH2)2	3177.80 Da	TSC6/1e	
[K(Ac)]ₓ	Ac-[K(Ac)]ₓ-NH2	4000-8000	Acetylated polylysine	
AcC(sl)-X₃-gT	Ac-Cys(Proxyl)-Lys(Ac)-Lys(Ac)-Trp-leu-Trp-leu-Trp-leu-Trp-NH2	1947.00 Da	TSC3ac-sl	95 %
AcC-X₃-gT	Ac-Cys-Lys(Ac)-Lys(Ac)-Trp-leu-Trp-leu-Trp-leu-Trp-NH2	1757.90 Da	TSC3/11f	95 %
AcC-X₃-gT	Ac-Cys-Lys(Ac)-Lys(Ac)-Trp-leu-Trp-leu-Trp-leu-Trp-NH2	1757.90 Da	TSC3/12f	
AcC-X₃-gT	Ac-Cys-Lys(Ac)-Lys(Ac)-Trp-leu-Trp-leu-Trp-leu-Trp-NH2	1757.90 Da	TSC3/12f	
AcC-X₃-gT	Ac-Cys-Lys(Ac)-Lys(Ac)-Trp-leu-Trp-leu-Trp-leu-Trp-NH2	1757.90 Da	TSC3/13f	
Ac-E₆gA	Ac-Glu-Glu-Gly-Glu-Glu-Gly-Glu-Glu-Gly-Ala-leu-Ala-val-Val-val-Val-val-Trp-leu-Trp-leu-Trp-NH2	2684.00 Da	Ac-DdB-7/1d	80 %, Rt 1.46
Ac-E₆gA	Ac-Glu-Glu-Gly-Glu-Glu-Gly-Glu-Glu-Gly-Ala-leu-Ala-val-Val-val-Val-val-Trp-leu-Trp-leu-Trp-NH2	2684.00 Da	Ac-DdB-7/1d	82 %, Rt 1.6
Ac-E₆gA	Ac-Glu-Glu-Gly-Glu-Glu-Gly-Glu-Glu-Gly-Ala-leu-Ala-val-Val-val-Val-val-Trp-leu-Trp-leu-Trp-NH2	2684.00 Da	Ac-DdB-7/2d	90 %
Ac-E₆gA	Ac-Glu-Glu-Gly-Glu-Glu-Gly-Glu-Glu-Gly-Ala-leu-Ala-val-Val-val-Val-val-Trp-leu-Trp-leu-Trp-NH2	2684.00 Da	Ac-DdB-7/2d	95 %
Ac-gA	Ac-Val-Gly-Ala-leu-Ala-val-Val-val-Trp-leu-Trp-leu-Trp-NH2	1754.10 Da		crude material
Ac-gA-E₆	Ac-Gly-Ala-leu-Ala-val-Val-val-Trp-leu-Trp-leu-Trp-Glu-Glu-Gly-Glu-Glu-Gly-NH2	2684.10 Da	DdB5/1d	
Ac-gA-K₆	Ac-Gly-Ala-leu-Ala-val-Val-val-Trp-leu-Trp-leu-Trp-Lys-Lys-Gly-Lys-Lys-NH2	2678.00 Da	DdB4/1d	
Ac-gT	Ac-Trp-leu-Trp-leu-Trp-leu-Trp-NH2	1143.30 Da		crude material
Ac-K₆gA	Ac-Lys-Lys-Gly-Lys-Lys-Val-Gly-Ala-leu-Ala-val-Val-val-Val-val-Trp-leu-Trp-leu-Trp-NH2	2678.30 Da	Ac-DdB-6/1d	
Ac-K₆gA	Ac-Lys-Lys-Gly-Lys-Lys-Val-Gly-Ala-leu-Ala-val-Val-val-Val-val-Trp-leu-Trp-leu-Trp-NH2	2678.30 Da	Ac-DdB6/2b	crude material
Ac-X₂-gT	Ac-Lys(Ac)-Lys(Ac)-Trp-leu-Trp-leu-Trp-leu-Trp-NH2	1483.80 Da	CD2ac/2f	
Ac-X₃-gT	Ac-Lys(Ac)-Lys(Ac)-Lys(Ac)-Trp-leu-Trp-leu-Trp-leu-Trp-NH2	1653.90 Da	CD3ac/6f	
Ac-X₃-gT	Ac-Lys(Ac)-Lys(Ac)-Lys(Ac)-Trp-leu-Trp-leu-Trp-leu-Trp-NH2	1653.90 Da	CD3ac recycled	
Ac-X₃-gT	Ac-Lys(Ac)-Lys(Ac)-Lys(Ac)-Trp-leu-Trp-leu-Trp-leu-Trp-NH2	1653.90 Da	CD3ac recycled	
Ac-X₃-gT	Ac-Lys(Ac)-Lys(Ac)-Lys(Ac)-Trp-leu-Trp-leu-Trp-leu-Trp-NH2	1696.00 Da	CD3ac/7g superacetylated	
Ac-X₃-gT	Ac-Lys(Ac)-Lys(Ac)-Lys(Ac)-Trp-leu-Trp-leu-Trp-leu-Trp-NH2	1653.90 Da	CD3ac/7f	
Ac-X₃-gT-C	Ac-Lys(Ac)-Lys(Ac)-Lys(Ac)-Trp-leu-Trp-leu-Trp-leu-Trp-Cys-NH2	1757.90 Da	TSC6/2f	
Ac-X₃-LgT	H-Lys-Lys-Lys-Lys(Ac)-Lys(Ac)-Lys(Ac)-Trp-leu-Trp-leu-Trp-leu-Trp-NH2	1654.00 Da	I-CD3ac/2d	
Ac-X₈gA	Ac-Lys(Ac)-Lys(Ac)-Gly-Lys(Ac)-Lys(Ac)-Lys(Ac)-Gly-Lys(Ac)-Lys(Ac)-Val-Gly-Ala-val-Val-val-Val-val-Trp-leu-Trp-leu-Trp-NH2	3328.00 Da	DdB80/3f	
Ac-Y₁₀K₂	Ac-Tyr-Tyr-Tyr-Tyr-Tyr-Tyr-Tyr-Tyr-Tyr-Tyr-Lys-Lys-NH₂	1947.20 Da	Y10K2Ac/1d	< 90 %
Ac-Y₁₀K₂	Ac-Tyr-Tyr-Tyr-Tyr-Tyr-Tyr-Tyr-Tyr-Tyr-Tyr-Lys-Lys-NH₂	1947.20 Da	Y10K2Ac/1d	< 90 %
Biotin-K₆gA	Biotin-Lys-Lys-Lys-Gly-Lys-Lys-Lys-Val-Gly-Ala-leu-Ala-val-Val-val-Val-val-Trp-leu-Trp-leu-Trp-NH2	3386.30 Da	DdB6-Biotin	≥ 50 %
BODIPY-K₈-gA	BOPDOPY650/665-Lys-Lys-Gly-Lys-Lys-Lys-Gly-Lys-Lys-Lys-Val-Gly-Ala-leu-Ala-val-Val-val-Val-val-Trp-leu-Trp-leu-Trp-NH2	3478.17 Da	DdB-F2-13/4d	
C-gT	H-Cys-Trp-leu-Trp-leu-Trp-leu-Trp-NH2	1204.51 Da	TSC2/2d	
C-gT	H-Cys-Trp-leu-Trp-leu-Trp-leu-Trp-NH2	1204.51 Da	TSC2/3d	
C-K₂-gA	H-Cys-Lys-Lys-Val-Gly-Ala-leu-Ala-val-Val-val-Trp-leu-Trp-leu-Trp-NH2	2169.70 Da	TSC9/1d	≥ 95 %
C-K₂-gA	H-Cys-Lys-Lys-Val-Gly-Ala-leu-Ala-val-Val-val-Trp-leu-Trp-leu-Trp-NH2	2169.70 Da	TSC9/1d	< 90 %
C-K₂-LgT	H-Cys-Lys-Lys-Trp-leu-Trp-leu-Trp-leu-Trp-NH2	1460.90 Da	TSC8/1d	95 %
C-K₃-gT	H-Cys-Lys-Lys-Lys-Trp-leu-Trp-leu-Trp-leu-Trp-NH2	1589.90 Da	TSC3/3d	
C-K₃-gT	H-Cys-Lys-Lys-Lys-Trp-leu-Trp-leu-Trp-leu-Trp-NH2	1589.90 Da	TSC3/6d	
C-K₃-gT	H-Cys-Lys-Lys-Lys-Trp-leu-Trp-leu-Trp-leu-Trp-NH2	1589.90 Da	TSC3/7d	
C-K₃-gT	H-Cys-Lys-Lys-Lys-Trp-leu-Trp-leu-Trp-leu-Trp-NH2	1589.90 Da	TSC3/14b	crude material
C-K₃-LgT	H-Cys-Lys-Lys-Lys-Trp-leu-Trp-leu-Trp-leu-Trp-NH2	1589.90 Da	TSC7/1d	98 %

Short name	Full sequence (3 letter code)	Molecular weight	Lot number	Purity
C-K$_6$-gA	H-Cys-Lys-Lys-Lys-Gly-Lys-Lys-Val-Gly-Lys-Ala-leu-Ala-val-Val-Trp-leu-leu-leu-Trp-NH2	2740.49 Da	TSC4/1d V4-14	67 %
C-K$_6$-gA	H-Cys-Lys-Lys-Lys-Gly-Lys-Lys-Val-Gly-Lys-Ala-leu-Ala-val-Val-Trp-leu-leu-leu-Trp-NH2	2740.49 Da	TSC4/1d V15-25	67 %
C-K$_6$-gT$_2$	H-Cys-Lys-Lys-Lys-Gly-Lys-Lys-Gly-Lys-Lys-Trp-leu-leu-Trp-leu-Trp-leu-Trp-leu-Trp-NH2	2640.00 Da	TSC5/4d	95 %
C-K$_6$-gT$_2$	H-Cys-Lys-Lys-Lys-Gly-Lys-Lys-Gly-Lys-Lys-Trp-leu-leu-Trp-leu-Trp-leu-Trp-leu-Trp-NH2	2640.00 Da	TSC5 V0-10	
E-gT-K	H-Glu-Trp-leu-Trp-leu-Trp-leu-Trp-leu-Trp-Lys-NH2	1358.60 Da	CD14/1d	crude material
E-gT-K	H-Glu-Trp-leu-Trp-leu-Trp-leu-Trp-leu-Trp-Lys-NH2	1358.00 Da	CD14/3d	
gA	H-Val-Gly-Ala-leu-Ala-val-Val-Trp-leu-leu-leu-Trp-NH2	1712.10 Da		crude material
gT	H-Trp-leu-Trp-leu-Trp-leu-Trp-leu-Trp-NH2	1101.30 Da		crude material
H$_6$-gA	H-His-His-His-His-His-Val-Gly-Ala-leu-Ala-val-Val-Trp-leu-leu-leu-Trp-NH2	2690.10 Da	DdB18/2b	crude material
K$_{10}$-gA	H-Lys-Gly-Lys-Lys-Lys-Gly-Lys-Lys-Val-Gly-Lys-Ala-leu-Ala-val-Val-Trp-leu-leu-leu-Trp-NH2	3263.10 Da	DdB10/2d	
K$_1$-gT	H-Lys-Trp-leu-Trp-leu-Trp-leu-Trp-leu-Trp-NH2	1229.50 Da	CD1/2d	
K$_2$-gA	H-Lys-Val-Gly-Ala-leu-Ala-val-Val-Trp-leu-leu-leu-Trp-NH2	2066.60 Da	DdB9/4d	
K$_2$-gA-E$_2$	H-Lys-Val-Gly-Ala-leu-Ala-val-Val-Trp-leu-leu-leu-Trp-Glu-Glu-NH2	2324.80 Da	DdB22/2b V5	crude material
K$_2$-gA-E$_2$	H-Lys-Val-Gly-Ala-leu-Ala-val-Val-Trp-leu-leu-leu-Trp-Glu-Glu-NH2	2324.80 Da	DdB22/2b V6-V13	crude material
K$_2$-gT	H-Lys-Lys-Trp-leu-Trp-leu-Trp-leu-Trp-leu-Trp-NH2	1357.70 Da	CD2/1d	
K$_2$-gT	H-Lys-Lys-Trp-leu-Trp-leu-Trp-leu-Trp-leu-Trp-NH2	1357.70 Da	CD2/2d	
K$_2$-gT$_{1.3}$	H-Lys-Lys-Lys-Trp-leu-Trp-leu-Trp-leu-Trp-leu-Trp-NH2	1657.10 Da	CD11/1d	
K$_3$	H-Lys-Lys-Lys-NH2	401.50 Da	K3 Rink Amid	peptide resin
K$_3$	H-Lys-Lys-Lys-NH2	401.50 Da	K3 Rink Amid	peptide resin
K$_3$-gT	H-Lys-Lys-Lys-Trp-leu-Trp-leu-Trp-leu-Trp-leu-Trp-NH2	1485.90 Da	CD3	
K$_3$-gT	H-Lys-Lys-Lys-Trp-leu-Trp-leu-Trp-leu-Trp-leu-Trp-NH2	1485.90 Da	CD3/4d	
K$_3$-gT	H-Lys-Lys-Lys-Trp-leu-Trp-leu-Trp-leu-Trp-leu-Trp-NH2	1485.90 Da	CD3/7d	
K$_3$-gT	H-Lys-Lys-Lys-Trp-leu-Trp-leu-Trp-leu-Trp-leu-Trp-NH2	1485.90 Da	CD3 Rink Amid	peptide resin
K$_3$-gT-C	H -Lys-Lys-Lys-Trp-leu-Trp-leu-Trp-leu-Trp-leu-Cys-NH2	1589.90 Da	TSC6/2d	
K$_3$-LgT	H-Lys-Lys-Lys-Trp-Leu-Trp-Leu-Trp-Leu-Trp-Leu-Trp-NH2	1485.90 Da	I-CD3/1d	
K$_3$-LgT	H-Lys-Lys-Lys-Trp-Leu-Trp-Leu-Trp-Leu-Trp-Leu-Trp-NH2	1485.90 Da	I-CD3/2d	
K$_4$-gA	H-Lys-Gly-Lys-Lys-Lys-Val-Gly-Ala-leu-Ala-val-Val-Trp-leu-leu-leu-Trp-NH2	2380.00 Da	DdB11/1d	
K$_4$-gT	H-Lys-Lys-Lys-Lys-Trp-leu-Trp-leu-Trp-leu-Trp-leu-Trp-NH2	1614.05 Da	CD4/2d	
K$_6$	H-Lys-Lys-Lys-Gly-Lys-Lys-Lys-NH2	843.10 Da	K3GK3 Rink Amid	peptide resin
K$_{6-12}$-gA	H-[Lys-Lys-Lys-Gly]$_{1-4}$-Val-Gly-Ala-leu-Ala-val-Val-Gly-Ala-leu-Ala-val-Val-Trp-leu-leu-Trp-Glu-Glu-NH2	mixture	gA-K8-12	crude material
K$_6$-gA	H-Lys-Lys-Lys-Gly-Lys-Lys-Lys-Val-Gly-Ala-leu-Ala-val-Val-Trp-leu-leu-leu-Trp-NH2	2636.30 Da	DdB6/2d	
K$_6$-gA	H-Lys-Lys-Lys-Gly-Lys-Lys-Lys-Val-Gly-Ala-leu-Ala-val-Val-Trp-leu-leu-leu-Trp-NH2	2636.30 Da	DdB6/4d	
K$_6$-gA	H-Lys-Lys-Lys-Gly-Lys-Lys-Lys-Val-Gly-Ala-leu-Ala-val-Val-Trp-leu-leu-leu-Trp-NH2	2636.30 Da	DdB6 Rink Amid	peptide resin
K$_6$H$_6$-gA	H-Lys-Lys-Lys-Gly-Lys-Lys-His-His-His-His-His-His-Gly-Ala-leu-Ala-val-Val-Trp-leu-leu-leu-Trp-NH2	3573.20 Da	DdB19/1b	crude material
K$_8$-gA	H-Lys-Gly-Lys-Lys-Lys-Gly-Lys-Lys-Val-Gly-Ala-leu-Ala-val-Val-Trp-leu-leu-leu-Trp-NH2	2949.00 Da	DdB89/3d	
K$_8$-gA	H-Lys-Gly-Lys-Lys-Lys-Gly-Lys-Lys-Val-Gly-Ala-leu-Ala-val-Val-Trp-leu-leu-leu-Trp-NH2	2949.80 Da	DdB13/2d	
K$_8$-gT$_{1.86}$	H-Lys-Gly-Lys-Lys-Lys-Gly-Lys-Lys-Lys-Gly-Lys-Lys-Lys-Trp-leu-Trp-leu-Trp-leu-Trp-leu-Trp-NH2	3138.90 Da	CD6/1b	crude material
K-gT-K	H-Lys-Trp-leu-Trp-leu-Trp-leu-Trp-leu-Trp-Lys-NH2	1357.70 Da	CD13/1d	
K-gT-K	H-Lys-Trp-leu-Trp-leu-Trp-leu-Trp-leu-Trp-Lys-NH2	1357.70 Da	CD13/2d	crude material
OG488-K$_8$-gA	OregonGreen488-Lys-Gly-Lys-Lys-Lys-Gly-Lys-Lys-Val-Gly-Ala-leu-Ala-val-Val-Trp-leu-leu-leu-Trp-NH2	3344.10 Da	DdB-F1-13/3e	
S$_4$-gT	H-Ser-Ser-Ser-Ser-Gly-Lys-Lys-Lys-Lys-Lys-Trp-leu-Trp-leu-Trp-leu-Trp-leu-Trp-NH2	1229.00 Da	CD9/1d	
S$_5$-gA	H-Ser-Ser-Gly-Ser-Ser-Gly-Lys-Lys-Lys-Lys-Lys-Trp-leu-Trp-leu-Trp-leu-Trp-leu-Trp-NH2	2302.70 Da	DdB16/1d	greenish

Short name	Full sequence (3 letter code)	Molecular weight	Lot number	Purity
SNP-C-K$_3$-gT	H -Cys (SNP)-Lys-Lys-Lys-Trp-leu-Trp-leu-Trp-leu-Trp-NH2	Silver aggregate	SNP-TSC3/12d	
V-gT	H-val-Trp-leu-Trp-leu-Trp-leu-Trp-leu-Trp-NH2	1199.00 Da	Kettenabbruch	crude material
X$_1$K$_7$-gA	H-Lys-Lys-Gly-Lys-Lys-Lys-Gly-Lys-Lys-Lys(Ac)-Gly-Ala-leu-Ala-val-Ala-val-Ala-val-Ala-val-Ala-val-Ala-val-Trp-NH2	2992.00 Da	DdB88/3d	
X$_2$K$_6$-gA	H-Lys-Lys-Gly-Lys-Lys-Lys-Gly-Lys-Lys-Lys(Ac)-Lys(Ac)-Gly-Ala-leu-Ala-val-Ala-val-Ala-val-Ala-val-Ala-val-Trp-NH2	3034.00 Da	DdB87/3d	
X$_2$K$_6$-gA	H-Lys-Lys-Gly-Lys-Lys-Lys-Gly-Lys-Lys-Lys(Ac)-Lys(Ac)-Gly-Ala-leu-Ala-val-Ala-val-Ala-val-Ala-val-Ala-val-Trp-NH2	3034.00 Da	DdB87/3d recycled	99.0 %
X$_3$K$_5$-gA	H-Lys-Lys-Gly-Lys-Lys-Lys-Gly-Lys-Lys(Ac)-Lys(Ac)-Lys(Ac)-Gly-Ala-leu-Ala-val-Ala-val-Ala-val-Ala-val-Trp-NH2	3076.00 Da	DdB86/3d	
X$_3$K$_5$-gA	H-Lys-Lys-Gly-Lys-Lys-Lys-Gly-Lys-Lys(Ac)-Lys(Ac)-Lys(Ac)-Gly-Ala-leu-Ala-val-Ala-val-Ala-val-Ala-val-Trp-NH2	3076.00 Da	DdB86/3d recycled	99.0 %
X$_4$K$_4$-gA	H-Lys-Lys-Gly-Lys-Lys-Lys-Gly-Lys(Ac)-Lys(Ac)-Lys(Ac)-Lys(Ac)-Gly-Ala-leu-Ala-val-Ala-val-Ala-val-Trp-NH2	3118.00 Da	DdB85/3d	
X$_4$K$_4$-gA	H-Lys-Lys-Gly-Lys-Lys-Lys-Gly-Lys(Ac)-Lys(Ac)-Lys(Ac)-Lys(Ac)-Gly-Ala-leu-Ala-val-Ala-val-Ala-val-Trp-NH2	3118.00 Da	DdB85/3d recycled	96.0 %
X$_5$K$_3$-gA	H-Lys-Lys-Gly-Lys-Lys-Lys(Ac)-Lys(Ac)-Lys(Ac)-Lys(Ac)-Lys(Ac)-Gly-Ala-leu-Ala-val-Ala-val-Trp-NH2	3160.00 Da	DdB84/3d	
X$_5$K$_3$-gA	H-Lys-Lys-Gly-Lys-Lys-Lys(Ac)-Lys(Ac)-Lys(Ac)-Lys(Ac)-Lys(Ac)-Gly-Ala-leu-Ala-val-Ala-val-Trp-NH2	3160.00 Da	DdB84/3d recycled	93.5 %
X$_6$K$_2$-gA	H-Lys-Lys-Gly-Lys(Ac)-Lys(Ac)-Lys(Ac)-Lys(Ac)-Lys(Ac)-Lys(Ac)-Gly-Ala-leu-Ala-val-Trp-NH2	3202.00 Da	DdB83/3d	
X$_6$K$_2$-gA	H-Lys-Lys-Gly-Lys(Ac)-Lys(Ac)-Lys(Ac)-Lys(Ac)-Lys(Ac)-Lys(Ac)-Gly-Ala-leu-Ala-val-Trp-NH2	3202.00 Da	DdB83/3d recycled	88.0 %
X$_7$K$_1$-gA	H-Lys(Ac)-Lys(Ac)-Gly-Lys(Ac)-Lys(Ac)-Lys(Ac)-Lys(Ac)-Lys(Ac)-Gly-Ala-leu-Ala-val-Trp-NH2	3244.00 Da	DdB82/3d	
X$_8$-gA	H-Lys(Ac)-Lys(Ac)-Gly-Lys(Ac)-Lys(Ac)-Lys(Ac)-Lys(Ac)-Lys(Ac)-Lys(Ac)-Gly-Ala-leu-Ala-val-Trp-NH2	3286.00 Da	DdB81/3d	
Y$_8$	H -Tyr-tyr-tyr-Tyr-tyr-Tyr-tyr-tyr-NH$_2$	1364.50 Da	Y8/1d Vial a	> 93 %
Y$_8$	H -Tyr-tyr-Tyr-tyr-Tyr-tyr-Tyr-tyr-NH$_2$	1364.50 Da	Y8/1d Vial b	< 93 %
Y$_8$K$_1$	H -Tyr-tyr-Tyr-tyr-tyr-Tyr-tyr-Tyr-tyr-Lys-NH$_2$	1492.70 Da	Y8K1/1d	
Y$_8$K$_2$	H -Tyr-tyr-Tyr-tyr-tyr-Tyr-tyr-Tyr-tyr-Lys-Lys-NH$_2$	1620.80 Da	Y8K2/1d	97 %

13 Abbreviations

AA	amino acid
ACN	acetonitrile
AFM	atom force microscope
Alox	aluminium oxide
API	active pharmaceutical ingredient
Boc	tert-butyloxycarbonyl
CCA	α-cyano-4-hydroxycinnamic acid
CD	circular dichroism
CLSM	confocal laser scanning microscope
cmc	critical micelle concentration
CPGNPs	composite peptide-gold nanoparticles
cw	continuous wave
Da	Dalton, molecular weight
DA	degree of acetylation
DCC	N,N'-dicyclohexylcarbodiimide
DCM	dichloro methane
dd H_2O	double distilled water
DDS(s)	drug delivery system(s)
DEER	double electron-electron resonance
DIPEA	*N,N*-diisopropylethylamine
DLS	dynamic light scattering
DMF	*N,N*-dimethylformamide
DMPC	dimyristoylphosphatidylcholine
DNA	deoxyribonucleic acid
DQC	double-quantum coherence
EDT	ethanedithiol
EPR	electron paramagnetic resonance
Eq	equivalent
EtOH	ethanol
FDA	Food and Drug Administration (U.S. Department of Health & Human Services)
Fmoc	9-fluorenylmethyloxycarbonyl
gA	gramicidin A
GAPDH	glyceraldehyde-3-phosphate dehydrogenase
GNP	gold nano particle
GPC	gel permeation chromatography
HCTU	2-(6-chloro-1H-benzotriazole-1-yl)-1,1,3,3-tetramethylaminium hexafluorophosphate
HOBt	N-hydroxybenzotriazole
HPLC	high pressure (performance) liquid chromatography
IPE	diisopropylether
IR	infrared spectroscopy
K_{sv}	Stern-Volmer constant
LCM	large compound micelle
LCST	low critical solution temperature

MALDI-TOF-MS	matrix assisted laser desorption/ionization - time of flight – mass spectroscopy
MCM	multicompartment micelle
M_w	molecular weight
NCA	N-carboxy anhydride
NIR	near infrared
NMP	N-methyl-2-pyrrolidone
PAA	poly(acrylic acid)
PD.I.	polydispersity index
PDDF	pair distance distribution function
PDMS	poly(dimethylsiloxane)
PEG	see PEO
PEO	poly(ethylene oxide)
PGA	poly glutamic acid
PLGA	poly(L glutamic acid)
PLL	poly(L lysine)
PMOXA	poly(2-methyloxazoline)
PNIPAM	poly (N-isopropylacrylamide)
PS	polystyrene
PyBOP	benzotriazol-1-yloxy) tripyrrolidinophosphonium hexafluorophosphate
qRT-PCR	quantitative real time polymerase chain reaction
R_g	radius of gyration
R_h	hydrodynamic radius
RNA	ribonucleic acid
RP	reversed phase
R_s	spherical radius
RT	room temperature
SAXS	small angle X-ray scattering
SEM	scanning electron microscope
shRNA	small hairpin RNA / short hairpin RNA
siRNA	short interfering RNA / small interfering RNA / silencing RNA
SLS	static light scattering
SPPS	solid-phase peptide synthesis
TBTU	O-(benzotriazol-1-yl)-N,N,N',N'-tetramethyluronium tetrafluoroborate
TEAP	triethyl ammonium phosphate
TEM	transmission electron microscope
TES	triethylsilane
TFA	trifluoroacetic acid
TFE	trifluoro ethanol
THF	tetrahydrofuran
TIS	triisopropylsilane
TNBS	2,4,6-trinitrobenzenesulphonic acid
TNNLS	Total Non-Negative Least Square analysis
Tris	tris-(hydroxymethyl)aminomethan

Amino acids (one letter code) and sequences:

Ac	Acetylated
DL	D-leucine
LC	L-cysteine
LK	L-lysine
LE	L-glutamic acid
LV	L-valine
LW	L-tryptophan
LX	acetylated L-lysine
G	glycine
-gA	gramicidin A inspired hydrophobic part of the amphiphile
-gT	truncated version of gA